Implications of Radiosonde Data for Sub-Millimeter Array Site Selection

J. A. Biretta (CFA)

MEMO #6

21 August 1989

Contents

I. Introduction

The optimum selection of a site for a sub-millimeter array depends on consideration of many factors. Here we consider only the effects of atmospheric opacity. We attempt to use measurements of atmospheric pressure, temperature, and humidity from weather balloons to compare the long term opacity variations above Mauna Kea and Mt. Graham. This method of opacity estimation was developed by R. Martin and collaborators at Steward Observatory, and further improved by F. Schwab and collaborators at NRAO.

The use of weather balloon data to compute opacities has several clear advantages over other methods of opacity measurement. These are:

1) Long term data are available for the last 25 years or more near both sites.

2) The data are sampled with extreme regularity. There are two balloon launches each day; only a few percent of the balloon flights fail to yield acceptable data.

3) The cost to us is very small compared with other methods.

This method also has several severe limitations:

1) The radiosonde relative humidity sensor gives only upper limits at low humidities. This upper limit corresponds roughly to a precipitable water vapor (PWV) of about 3 mm, and opacities of 0.2, 0.7, 3, 4, and 6, at 230, 345, 461, 691, and 808 GHz, respectively. Hence it is not possible to evaluate site quality for the highest sub-millimeter frequencies.

2) The radiosondes are launched only twice at day (0 and 12 UT), so it is impossible to measure any variations on shorter timescales. This also makes it difficult to evaluate diurnal effects.

3) We use data from nearby weather stations to infer atmospheric conditions over prospective telescope site. Hence, it is impossible to evaluate any effects local to the site.

II. The Radiosonde System

Radiosondes are launched twice a day (0 and 12 U.T.) from several hundred locations around the globe. Their purpose is to provide an "snap shot" of global atmospheric conditions from ground level to about 30 km altitude. During their flight they measure (directly or indirectly) pressure, temperature, relative humidity, and wind speed and direction. They are sometimes referred to as "rawindsondes" to denote the capability of measuring wind speed and direction.

There are several models of radiosondes; for illustrative purposes we will describe the model VIZ radiosonde. It is not certain that this was the exact model used for all the data we will analyze, but it appears to have been in wide use during the period of interest (Spackman 1978; Richner and Phillips 1981), and will give a general picture of how they operate. It is important to bare in mind that these are essentially "disposable" or "throw away" devices, so that they must be made as cheaply as possible.

The VIZ radiosonde consists of an aneroid barometer driven selector switch, a thermistor, a humidity sensor, 1680 MHz transmitter, battery, and rubber balloon (Ference 1951, McElroy 1985). Upon release, the system ascends at 5 to 10 m/s until the balloon ruptures (typically at ~30 km altitude). As the atmospheric pressure decreases, the aneroid selector switch connects the transmitter alternately to the thermistor, a reference resistor, the humidity sensor, a second reference resistor, then again to the thermistor, and so on. The resistance of each device is telemetered as the frequency of an amplitude modulation imposed on the 1680 MHz carrier. Since the humidity sensor does not work at low temperatures there are no connections to it at altitudes greater than about 10 km. The action of the selector switch is logarithmic; at low altitudes it cycles through a set of measurements every ~100m, while at high altitudes it cycles every ~1000m. The

transmitted signals are received by a ground station consisting of an ~2.5 m parabola, an automatic direction finder / tracking system, and recording equipment.

The atmospheric parameters are then estimated from the transmitted data. The temperature is obtained from the thermistor resistances and a calibration curve. The humidity is derived from the resistance of the humidity transducer and the temperature. The occurrence of pre-designated pressures is indicated by the changing pattern of the resistance data, with the aid of the reference resistances. The altitude is not measured directly, but is computed from the other measurements and a model atmosphere. The wind speed and direction are estimated from the balloon's elevation and azimuth as measured by the ground antenna, and from the computed altitude.

A typical set of radiosonde data is tabulated in Table 1, and plotted in Figure 1. Apparently the raw temperature, pressure, and humidity data have been interpolated onto a single set of altitudes. Pressure and temperature readings continue to 32km, while the humidity measurements stop at 9km altitude. No humidity data are recorded at higher altitudes since the humidity sensor does not work well there (see below). There are also no humidity values much below ~15 percent, since the device cannot respond to low humidities. Apparently there was a change around 1973 in the data handling procedures of the National Climatic Data Center. In data after 1973 all humidity readings less than 19 percent have been reset to 19 percent. This reflects their unwillingness to communicate unreliable readings at low humidities (R. Martin, private communication).

Both the pressure and temperature readings are reasonably accurate. The error of the pressure measurement is typically in the range of ± 1 to 3 mBar; the temperature is typically accurate to $\pm 0.5^{\circ}$C (Schmidlin, Olivero, and Nestler 1982).

Since the opacity is strongly dependent on the amount of water vapor in the air, we now discuss the humidity transducer and its limitations in some detail. It appears that two basic types of humidity transducer were used with the VIZ radiosonde during the period of interest.

The first is the "Dunmore" type lithium chloride hygrometer. It appears to have been the standard hygrometer since the 1940's (Mathews 1965), and was gradually phased out during the late 1960's (Finger and McInturff 1978). It operates on the fact that lithium chloride is an insulating powder at low humidities, but at high humidities it absorbs moisture and becomes a conducting electrolyte. The device consists of a 4" by 2" rectangle made of thin plastic which has been coated with a thin electrolytic film of lithium chloride dissolved in polyvinyl acetate or alcohol. Electrodes are placed along the two long edges. The resistance decreases with increasing humidity from ~10M Ohms at 15% relative humidity (RH), to ~5000 Ohms near saturation (Mathews 1965). Figure 2a shows a typical set of lithium chloride hygrometer calibration curves as a function of radiosonde recorder output (inverse resistance) and temperature.

The lithium chloride hygrometer is subject to a number of uncertainties and errors. For the range 15 to 96% RH and temperature $> -10°C$, Ference (1951) gives the accuracy as 2.5% RH. For our purposes the most important error is the lack of response at low humidities. Below 12% RH (at room temperature) lithium chloride is an insulating powder (Mathews 1965), so that the device reads ~10M Ohms for all humidities less than this. Hence, at low humidities the measured value is only an upper limit. This lower humidity limit varies with temperature. Figure 2a provides an example of this; the lowest humidity readings are ~15% at room temperature , and increase to ~25% at -15°C. (We note that these exact values are somewhat at odds with the limits quoted by Ference (1951). He states the accuracy is 2.5% to 15% RH and -10°, whereas Figure 2a suggests a response lower limit of 24% RH at -10°.)

Other sources of error are: 1) Time lag. At low temperatures the response has a significant time lag. For example, the time to respond within 1-1/e of a change is ~15 sec. at 0°C, and ~120 sec. at -30°C (Mathews 1965). 2) "Washing out." After prolonged exposure to high humidities, the lithium chloride electrolyte begins to migrate on the plastic strip, and the calibration is altered. The effect appears to be <1% RH (Ference 1951). 3) Lack of response to humidity changes at very low temperatures. 4) Lack of

response to humidity changes at very high humidities. 5) Inability to measure humidity at very low atmospheric pressure. These five errors tend to be less important for our work, since they occur for high humidities (very high opacity) or high altitudes, where the volume density of water molecules is low.

One final error could have some impact on our results. Direct exposure to moisture can wash away some of the lithium chloride, thus increasing the resistance, and causing humidity readings which are too low. While some effort is made to shield the hygrometer from mist and rain, complete protection is impossible since air must circulate freely across the detector. The magnitude of this error is very difficult to assess. Tests by Handegord, Hedlin, and Trofimenkoff (1965) found that condensation on the device caused readings up to 6% relative humidity too low after exposure; but it is not clear whether this test would be applicable to actual flight data. This error could have some impact on our results, since the calibration is permanently altered after exposure. As will we see, Hilo often has a very humid inversion layer below the observatory. Hence it is possible that water in the inversion layer could damage the calibration, hence causing the device to read low when it reaches altitudes above Mauna Kea. Fortunately, this error affects only the lithium chloride hygrometer. In section IV.C. we show that the results are the same when we avoid data taken with the lithium chloride hygrometer.

A second hygrometer, the carbon hygristor, came into operational use in 1963 (Mathews 1965), and appears to have become the standard device by the late 1960's (Finger and McInturff 1978). In one version, it consists of a 2.5" x 11/16" x 0.04" flat acrylic plastic strip with the long edges metalized. The strip is coated with gelatinous cellulose containing fine carbon particles in suspension (Stine 1965). It is basically a variable resistor; as the humidity increases the cellulose adsorbs moisture and expands, thus decreasing the volume density of the carbon particles, and hence increasing the resistance. Figure 2b shows a typical calibration curve, where the curves for different temperatures have been normalized to unit resistance at 33.3% RH. For a temperature of +25°C, the resistance is typically 14k Ohms at 10% RH, and 2.9M Ohms at 100% RH. (This range is similar

to the lithium chloride hygrometer, and hence it can be used interchangeably in the VIZ radiosonde, provided the correct calibration table is used.) The primary advantages of the carbon element, are that it has less time lag and is more resistant to "washing out," than the lithium chloride hygrometer.

The carbon hygristor is also subject to various errors. Richner and Phillips (1981) give the accuracy as 5% RH for the range 10 to 100% RH and -60 to $+40$°C temperature. The device also appears to have a lower response limit similar to the lithium chloride hygrometer (although the exact cause does not appear to be explained in the literature). *Radiosonde Observations* (1968, 1975) states that the "lower limit of measurable relative humidity is about 10% throughout the temperature range of the carbon hygristor, and the upper limit is 100%." It further specifies that any humidity readings significantly below 10% are to be taken as bad, and treated as missing data. Hence it appears that, as with the lithium chloride hygrometer, the device gives only upper limits at low humidities.

Other sources of error, which are less important for our work because they occur at high humidities, are: 1) Diurnal effect. Solar heating of the element caused readings to be 15% too low near 70% humidity, while humidities below 20% and 100% are unaffected (Ostapoff, Shinners, Augstein 1970). This defect appears to have been largely corrected by the late 1970's (Finger and McInturff 1978; Richner and Phillips 1981). 2) Error in calibration table. Apparently there was an error in the calibration table which caused low readings near 100% humidity (Phillips *et al.* 1981; Richner and Phillips 1981). This appears to have been corrected in 1980.

To further examine the lower limit of the humidity sensor, we have plotted histograms of all the raw humidity data for the period 1965-1971 (Figure 2.1). Since the limit may depend on temperature, we plot a separate histogram for each 5°C temperature range. The effect of the hygrometer response lower limit is readily apparent. The histograms peak between 15 and 20% RH, and there are very few points below 10%. The widths of the peaks are consistent with the 3 to 5% RH uncertainty in the measurements. There

appears to be only a slight temperature dependence, with the histogram peaks shifting about 2% RH toward higher values at low temperatures. (The Hilo data show a large number points at high humidity and high temperatures; these are caused by the warm inversion layer at low altitudes, and not by any limit in the hygrometer.)

III. Calculation of Opacities

For much of our comparisons, we will rely on opacities which are computed from the radiosonde data. The radiosonde data for the period 1 January 1965 to 30 October 1986 were obtained from F. Schwab (NRAO). These data were originally obtained from the National Climatic Data Center by R. Martin and collaborators at Steward Observatory.

For each radiosonde flight we compute the zenith opacity (τ) which would occur above the nearby telescope site. For Mauna Kea, we use radiosonde data from the station at Hilo (weather station 21504) 41 km to the ESE. For Mt. Graham we use data from Tucson (weather station 23160) which is 115 km to the WSW.

We first test the data of each balloon flight for various problems, before computing opacities. We discard balloon flights which do not reach at least 15km altitude, and those with implausible temperature ($> 55°$C) or humidity values (>100 percent). We also discard flights where $> 1/3$ of the humidity readings below 10km are flagged as bad in the raw data (set to -999.), or if there are less than 12 valid humidity readings.

It is unlikely that our results are biased by rejecting this data. First, the fraction of missing or discarded data is quite small. Of the ~15950 radiosonde flights we would expect during the period of the data, only 2 percent are missing or discarded as "bad" at Hilo, and only 3 percent at Tucson. And secondly, the bad data are most likely due to problems with the instrumentation, rather than severe weather. The most common cause for rejecting data is that the balloon fails to reach the 20km lower limit we impose; this is probably caused by defects in the rubber balloon which cause it to burst prematurely.

The greatest source of uncertainty in the opacity calculation comes from the lower limit in the humidity sensor response; at low humidities the radiosonde reports only an upper limit. In order to allow for this uncertainty we compute two opacities, a minimum and a maximum, for each flight. These correspond roughly to the lowest and highest humidities, respectively, which would be consistent with the observed data.

The minimum is computed by resetting all humidity values below 20 percent, to 0.1 percent. We chose 20 percent as the threshold, since humidity measurements after 1973 have an "artificial" lower limit of 19 percent imposed by the Climatic Data Center. This 20% limit is well above the response limit of the carbon hygristor, and the limit for the lithium chloride hygrometer at temperatures $> 0°C$ (Ference 1951; Figure 2a). It is also well above the peaks seen in the histograms in Figure 2.1. This assumed minimum humidity profile is displayed in Figure 3a, for the data of Figure 1.

The maximum is computed by using the actual measurements where there is data, and a value of 90 percent where the is no data, such as at altitudes above 10 km (Figure 3b). This latter assumption is probably an over-estimate, since there is evidence for extremely low humidities above 16 km (<60% for 10 to 16 km, <3% above 16km; *U.S. Standard Atmosphere 1976*, Ellsaesser, *et al.* 1980, Liebe 1985). In terms of opacity, however, any over-estimate is extremely small; for a typical range of conditions the over-estimate is 0.004 ± 0.004 in 230.5 GHz opacity.

(In section IV.C. below we present minimum and maximum opacities derived using more conservative assumptions about the hygrometer response at low humidities. As we will see, the results are nearly identical.)

We have not included in any way, an allowance for the 3 to 5% RH uncertainty on individual data points. This was judged as unnecessary, since we are only concerned with the statistical properties of the entire data set, which are not biased by random errors on individual data points.

The actual calculation of opacity begins by interpolating the data on to a uniform grid with a spacing of 250m altitude. This spacing is adequate, since the raw data are sampled every >500m at the altitudes of interest. At each grid point the opacity per unit path length is computed from the atmospheric parameters. Once this is done, we simply integrate the opacity from the altitude of the observatory on upwards to the highest altitude measured by the radiosonde (>20km). For Mauna Kea we started the integrations at 13300' (4054m), for Mt. Graham at 10500' (3200m). The precipitable water vapor (PWV) is also computed in a similar manner.

At each grid point the opacity per unit length is computed using the Millimeter Propagation Model of Liebe (1985). The implementation we use was originally programmed by H. Lehto, (U.Va.). This model takes into account line, continuum, and hydrosol opacities. The line opacity is estimated from empirical spectroscopic data for ~80 oxygen and water lines in the range 22 to 1000 GHz. The empirical line parameters we use are not those originally published by Liebe (1985), but rather are an updated set privately communicated by H. Liebe via F. Schwab (NRAO). A rough estimate of hydrosol (haze and cloud) opacity is included when the local humidity exceeds 95 percent.

Since the computations are very lengthy (2.5 CPU days on microVAX per frequency per site) opacity calculations for all 22 years of data were done only at one frequency, 230.5 GHz. We chose this frequency since it is astrophysically interesting (CO J=2 to 1 line), and because it is close the frequency of the 225 GHz water vapor radiometers. Calculations were also done at 345.8 GHz (CO J=3 to 2), 461 GHz (CO J=4 to 3), 691 GHz (CO J=6 to 5), and 808 GHz (CO J=7 to 6) for only the 1985 data.

IV. Results

A. Comparison of Raw Humidity Data.

We first examine the raw humidity data for the two sites, without calculation of opacities. This will elucidate some of the properties of the two sites.

First we will look at the vertical structure of the humidity data. Figure 4a shows the 22 year mean humidity at 1km altitude intervals for Hilo; each season is plotted separately. The structure for each season is nearly identical; there is a marine inversion layer with high humidity up to 2.5 km, above which the humidity is relatively low. Examination of individual balloon flights shows that the boundary of inversion layer is extremely sharp (*e.g.* Figure 4c). Mean humidities for Tucson are shown in Figure 4b. Here the mean humidity is nearly independent of altitude, except during the summer when there is a large increase in the humidity below 5.5km.

Its is also interesting to ask how often the "best" possible conditions occur. Such conditions would be indicated by low humidity readings at all altitudes above the observatory. To quantify this, we chose a threshold humidity, and then computed the fraction of balloon flights where the measure humidity was below this threshold at all altitudes above the observatory. In choosing the threshold, it is necessary choose a value sufficiently high to avoid bias caused by the hygrometer response lower limit. Using Figure 2a for the lithium chloride hygrometer, we chose a threshold of 22% relative humidity (RH) below 5000m altitude ($> 0°$C), and 25% RH above 5000m ($< 0°$C). This threshold is also valid for the carbon hygristor, since its response lower limit is $\sim$10% RH.

The results for both sites are shown in Figure 5 plotted against month of year. At Hilo about 40 percent of the flights were below this threshold independent of month. At Tucson only about 25 percent of flights were below the threshold during the best months; the months July through September only a very small fraction of flights below the threshold. From this simple criterion, it appears that Mauna Kea would be a better site than Mount

Graham. However, this criterion does not indicate the magnitude of the resulting opacity difference, or any information about periods of extremely low (<10 percent) humidity.

B. Raw Opacity Results for Year 1985.

To give an example of the temporal structure of the computed opacities, we examine the 230.5 GHz opacity values computed for each balloon flight during 1985. Figure 6a shows the results for Hilo. The "maximum" opacity values were computed using the maximum humidity values consistent with the data (see above). They are mostly between 0.1 to 0.15, which corresponds to the lower limit of the hygrometer range. Interspersed among these are occasional periods of high opacities (storms?) lasting up to a few days. The "minimum" opacity values were computed using the minimum humidity consistent with the data. Many of these values are near zero opacity, indicating many balloon flights where the humidity readings were below 20 percent for all altitudes.

Figure 6b shows the results for Tucson. Here there is a much smaller incidence of the minimum opacity being near zero, indicating a smaller fraction of flights where all humidity readings were below 20 percent. There is also a large seasonal effect; during the summer months the opacity is almost always greater than 0.4.

C. Probability Distribution for All 22 Years of Data.

Results for the entire period 1 Jan. 1965 to 30 Oct. 1986 are shown in Figure 7 for both sites. For each opacity value, the curves give the fraction of "good" radiosonde flights where the computed opacity is less than the specified value. This is essentially the cumulative probability distribution of the opacity.

The solid curves give the maximum opacity value consistent with the humidity readings. The lower limit of the hygrometer response causes the probability to drop off sharply between opacities of 0.1 and 0.15. Below an opacity of 0.1 the curves fall smoothly to zero probability. One might naively expect the drop off to be extremely sudden, but this

is not so for several reasons. The density of water molecules in the air depends on the temperature, as well as on the relative humidity, so that the lower limit of the hygrometer maps into a range of opacity values. Secondly, the hygrometer lower limit itself is not fixed, but varies from depending on temperature, and is different for the lithium chloride and carbon hygrometers. The humidity values have a dispersion of 3 to 5% RH about the true value, which contributes a large fractional error at low humidities. And finally, the post-1973 data are truncated at 19 percent relative humidity, which further smooths the fall-off at low opacities.

The dashed curves give the minimum opacity consistent with the humidity readings. These curves fall off slowly with decreasing opacity, until the dry opacity is reached; then there is a sudden drop-off to zero probability. At opacities greater than ~ 0.2 the maximum and minimum curves are nearly identical, since the opacity is dominated by humidities well above the $\sim$15 percent relative humidity limit of the hygrometer.

Several conclusions can be drawn from this plot:

1) At opacity values greater than 0.12, Hilo is clearly superior to Tucson. This is because the occurrence rate derived from the maximum possible humidity values at Hilo, exceeds the rate derived from the minimum possible humidity values at Tucson.

2) At opacities less than 0.1, it is impossible to clearly distinguish which site is best. This is essentially because of the 15 to 20 percent humidity lower limit in the hygrometer response.

3) While a superior site cannot be clearly distinguished at low opacities, we note that opacity values < 0.012 never occur at Tucson, and yet *could* occur as much as 40 percent of the time at Hilo. Similar statements can be made for a range in opacities up to $\tau \sim 0.1$; the probability of a certain opacity *could* be several times larger at Mauna Kea, than at Mt. Graham.

In section III, we described the criteria used to select the minimum and maximum humidities consistent with the data, which were then used to compute the minimum and maximum opacities, respectively. We now consider how Figure 7 would change, if we were to use more conservative criteria in selecting the minimum and maximum humidities. Figure 7.1 shows the result obtained if we set all humidities below 19% equal to 19%, as the Climatic Data Center had done for the post-1973 data. This has the effect of shifting the maximum opacity curve slightly to the right at low opacities. We now find that Hilo is superior to Tucson at $\tau > 0.121$, instead of $\tau > 0.116$ as we found in Figure 7. Figure 7.2 shows the result if we use a more complex lower limit when computing minimum opacities, to allow for variation in the lithium chloride hygrometer lower limit caused by temperature. For example, at temperature T$< -40°$C we set all humidities to 0.1%; for $-40°$C$<$T$< -35°$C we set all humidities below 31% to 0.1%; *etc.* in a manner which follows Figure 2a. We do this only for the 1965-1968 data, where the lithium chloride hygrometer may have been used (Finger and McInturff 1978). This has the affect of shifting the minimum opacity curves slightly to the left. For Figure 7.2 Hilo is superior to Tucson at $\tau > 0.122$. Hence using more conservative minimum and maximum humidities has very little effect on the results. Hereinafter we use only opacities computed using the minimum and maximum humidities described in section III.

In section II we discussed a possible error caused by water coming in contact with the lithium chloride hygrometer. This could, in principal, cause low humidity readings for Hilo at altitudes above Mauna Kea. In Figure 7.3 we show the results obtained when only the carbon hygristor data are used (data from 1969 onwards) for which this error does not occur. The results are nearly identical to those in Figure 7; Hilo is superior to Tucson for $\tau > 0.116$.

D. Year to Year Variations.

It is useful to have an estimate of the magnitude of year to year variations, since it gives some indication of the validity of using of short term data, to assess long term

and future trends. Figure 8a and b shows the cumulative probability distribution plotted separately for each of the 22 years. The year to year variations appear to be relatively small. To quantify this we measured the mean, dispersion, and range of probabilities for a "maximum" opacity of 0.2, where the hygrometer lower limit has a small effect. For Hilo the mean was 0.86 with a dispersion of 0.05, and a range of 0.80 to 0.97. At Tucson the mean was 0.52, the dispersion was 0.06, and the range was 0.47 to 0.70. We note for opacities of 0.16 to >0.5, the probability was *always* higher at Hilo, than at Tucson.

To give a more detailed picture of the year to year variations, we have plotted several statistics against calendar year. Figures 8.1 (a-f) show the zenith opacity at the 10^{th}, 50^{th} (median), and 90^{th} percentiles, and the probability of zenith opacities <0.1, <0.2, and <0.4, for each calendar year at Hilo. It is difficult to clearly discern any long term trends. The opacities at the 90^{th} percentile show slight evidence of an 11 to 12 year period, but the evidence is weak, and 1982 does not fit the pattern. Figure 8.2 (a-f) shows the same information for Tucson. Here there is a fairly linear decrease in the probability of opacity <0.4 from ~0.80 to ~0.75 from 1965 to 1986. At low opacities both sites show an increase in the difference (range) between the maximum and minimum opacities after 1973; this is an artifact caused by the 19% RH cutoff imposed on the data after 1973.

E. Seasonal and Monthly Effects.

We now examine the opacity results for variations which depend on time of year. Figure 9 shows the fraction of time the opacity is below 0.15 for each month of the year. As discussed above, the conditions at Tucson are relatively poor during the summer months. During July, August, and September the probability of low opacity is very small at Tucson. While the strongest effect occurs during these three months, some degradation in conditions is evident as early as May and lasting into November. The best months at Tucson are from December through April. The opacity at Hilo, on the other hand, shows almost no seasonal dependence. It is also evident that Hilo almost always has a higher probability of opacity <0.15, even when compared to the best months at Tucson.

Figures 10a and 10b show similar plots for opacity 0.2, but with a separate curve plotted for each calendar year. It is evident that July through September are *always* very poor at Tucson. The onset of poor conditions is sometimes as early as May, and sometimes lasts until October.

Huge year to year variations are also evident for both sites. The probability of opacities < 0.2 can vary from 50 to 100 percent depending on the year.

Figure 11 presents the monthly variations in a different way. Here we plot the opacity which has a 10, 50, and 90 percent probability of exceeding the measured opacity. From Figure 11a (10th percentile) we cannot distinguish between the two sites, except during July and August when the conditions at Tucson are clearly inferior. For the other months, both sites show possible opacities in the range $\sim$0.01 to 0.1. This large range is due to uncertainty caused by the hygrometer response lower limit.

Figure 11b shows the results for the 50th percentile (median). Here the conditions at Tucson appear to be inferior to those at Hilo from May through October. For the other months there is still a large overlap of the possible opacity values, so we cannot distinguish between the sites.

Opacities at the 90th percentile are shown in Figure 11c. Here the opacity values are large enough so that the hygrometer lower limit contributes only a small uncertainty. The opacities at Tucson are larger than those at Hilo for all months, except for November.

It is interesting to compare the best months at Tucson with the average conditions at Hilo. From Figure 9 the best months at Tucson appear to be December through April. The probability distribution for these months at Tucson are plotted against the distribution for all months at Hilo in Figure 12. Apparently at opacities of 0.15 or greater, the average conditions at Hilo are better than the best months at Tucson. At lower opacities the hygrometer lower limit contributes a large uncertainty, and it is not possible to distinguish between the sites.

F. Diurnal Effects

We now examine the data for any effects which depend on time of day, and also consider the possibility of effects undetectable in the 12 hour sampling of the radiosonde data.

The cumulative probability distributions for the 0 and 12 UT radiosonde data are shown in Figures 13a and b, for Hilo and Tucson, respectively. For both sites the 0 and 12 UT probabilities are essentially identical at low opacity values; no diurnal effect is evident. At higher opacities, Hilo tends to be slightly better at 2 PM than 2 AM. (This is opposite the effect seen in Mauna Kea radiometer data, see below.)

In order to investigate diurnal effects on shorter timescales, we must rely on other sources of information, such as radiometer data. The 22 GHz radiometer data at Mt. Graham for Jan. and Feb. 1986 (Martin, private communication, 1989; see Figure 20) shows only slight evidence for diurnal effects. Visual inspection of these data suggest a slight trend for a ~50 percent decrease in opacity near noon of about half the days. A larger body of 225 GHz data (Nov. 86 to Dec. 87) is readily available for South Baldy Mountain in New Mexico, which is geographically similar to Mt. Graham (Hogg, Owen, and McKinnon 1988). Their plots of median hourly opacity often show a minimum opacity in early morning, followed by a broad maximum extending from ~11 AM to ~7 PM local time. The amplitude of the variation seems to depend on the time of year. During the Nov. to April the amplitude is small and varies from 0.02 to 0.07 in opacity, about a mean opacity of ~0.14. From May to July amplitude of the effect is much larger, being >0.14 about a mean of >0.44. The available data for August to October show only that the median opacity is >0.5, and do not provide any information on diurnal effects. From this rather scanty information, it appears that diurnal effects at Mt. Graham would, at most, give a ~30% variation in opacity, with the maximum lasting ~8 hours per day.

Some information on diurnal effects at Mauna Kea can be extracted from the 270 GHz radiometry of de Zafra, *et al.* (1983) and Parrish, *et al.* (1987). Together they provide

data for about 110 days between 1982 and 1986; they typically sample the opacity every 20 minutes for several weeks at a time. Both of these papers note somewhat poorer conditions "for a few hours shortly after noon" on some days. They attribute this effect to warm updrafts which carry moist air from the inversion layer to the top of the mountain.

From examination of their data the diurnal effect, when present, appears to begin between 10 AM and 12 noon, peaks in the early afternoon, and dissipates by 6 PM. This would appear to coincide with the the period of poor millimeter seeing at Mauna Kea noted by Church and Hills (1989).

To further quantify the diurnal opacity variation, we examined de Zafra's and Parrish's plots of PWV vs. time, and classified each day in one of four categories: clearly no diurnal effect (35 days), some evidence of diurnal increase near noon (37), days containing the notation "bad weather" so as to make judgement of a diurnal effect impossible (26), and days with no data due to equipment troubles (12). Of the days with a diurnal effect near noon, the median duration was 7 hours with a dispersion of 3 hours; the (maximum) fractional opacity increase had a median value of 80% and a dispersion of 40%. A simple estimate of the average time per day suffering from the diurnal increase, when averaged over all days, would be 4.5 hours, where we assume the 26 "bad weather" days all had a diurnal effect.

This simple analysis in terms of the fractional increase in opacity tends to exaggerate the severity of the diurnal effect, since the opacity is small, so that the opacity increase is also small. We examined their data for days where the maximum opacity during the diurnal maximum exceeded 2mm PWV. Of the 110 days, there were 2 which showed a diurnal peak >2mm PWV, 65 which clearly did not, 31 where some notation such as "bad weather" or "unstable" prevented evaluation, and 12 with equipment problems. Hence, the fraction of time with a noontime peak exceeding 2 mm PWV (~0.1 in 230.5 GHz opacity) must be <34%. The average duration for the two periods exceeding 2 mm PWV was 6 hours.

From the foregoing discussion it is apparent that there is some diurnal increase at Mauna Kea, but only the possibility of one at Mt. Graham. Earlier in section C we saw that the comparison of the Hilo and Tucson radiosonde data indicated that Mauna Kea was clearly a superior at opacities >0.12. We now consider how a diurnal effect at Mauna Kea would affect that comparison. The diurnal effect must be considered separately from the radiosonde data, since it is not seen in the 2 PM Hilo radiosonde, and hence must be local to Mauna Kea.

We consider two scenarios. In both we assume the Hilo radiosonde correctly represents daily "good" hours at Mauna Kea, and that no observations are conducted during the noontime diurnal increase. At Mt. Graham we consider two different assumptions: 1) the Tucson radiosonde results correctly represents the Mt. Graham conditions, with observations conducted year round, and 2) the same but assuming an observatory at Mt. Graham would shut down from July to September, when conditions are very poor.

We then ask how many hours of Mauna Kea data must be discarded each day, in order to degrade the Mauna Kea cumulative probability distribution so that it overlaps that for Mt. Graham, over as wide a range of low opacities as possible. Figure 14a illustrates the first scenario. Here 7.8 hours per day must be discarded at Mauna Kea (Hilo) to cause the two probabilities to overlap. (For a smaller number of hours discarded, there would be a region near 0.16 opacity where Mauna Kea is significantly better; the "max" opacity curve for Hilo would lie above the "min" curve for Tucson.) For the second scenario (Figure 14b) the probabilities overlap when 8.4 hours are discarded at Mauna Kea.

From the above analysis of the observed diurnal effect at Mauna Kea, we estimated that the noontime opacity increase affected *on average* only ~4.5 hours per day. This is roughly half the amount of time which must be discarded at Mauna Kea to equilibrate the probability distributions for the two sites. Hence, Mauna Kea appears to be a superior site at opacities >0.12, even when we consider diurnal effects. This conclusion is further strengthened when we consider: 1) that there might also be some diurnal affect at Mt.

Graham, 2) that we have assumed all the time during the diurnal increase must be discarded, whereas a noontime diurnal peak exceeding 0.1 opacity (2 mm PWV) seems to occur <34% of the time, and 3) we assumed all the "bad weather" days had a diurnal effect.

G. Local Effects

Since the radiosonde samples conditions at some distance from the prospective telescope site, it is important to test for any effects local to the site. Of the atmospheric parameters used in the opacity calculation, local variations in humidity would have the largest on the opacities.

Merrill, *et al.* (1987) have published monthly mean humidities measured at both Mauna Kea and Mt. Graham. The precise times of the measurements have not been published, but they were made predominantly at night, roughly three times per night, sometime during the period March 1984 to March 1986 (Merrill, private communication, 1989). At Mauna Kea the measurements were made by manually recording the output of a humidity sensor on the catwalk of the 88" University Hawaii Telescope. At Mt. Graham measurements were made manually with a sling-psychrometer ~1 m above the ground.

In Figure 15 we compare their humidity data with the radiosonde measurements for the same altitude and time period. The 0 and 12 UT radiosonde measurements are plotted separately to facilitate better comparison with the night time local measurements. From Figure 15a it appears that the Hilo radiosonde and the nighttime Mauna Kea data are in very good agreement. The difference between the local values and radiosonde averages about ~0 percent humidity, with a range of about ± 9% percent humidity. (In the previous section we discussed a local diurnal effect near noon at Mauna Kea. This is not inconsistent with Merrill's humidity measurements, since they were made primarily at night.)

At Mount Graham, however, there appears to be large local excess (Figure 15b). The local values average ~33 percent relative humidity greater than the Tucson radiosonde, with the difference ranging from +17 to +40 percent humidity.

The opacity contributed by this excess humidity at Mount Graham depends upon the vertical thickness of this moist air layer. A likely source of this moisture is outgassing from the dense vegetation atop Mt. Graham. Echosonde measurements (Forbes, *et al.* 1985; Forbes, Morse, and Poczulp 1986; Forbes, private communication 1989) give evidence for a turbulent boundary layer above Mt. Graham. The height of this layer above the local surface varies from ~50m during the night, to ~300m during the day. If the moist air extends to the top of this boundary layer, the excess 230.5 GHz opacity is very small, being roughly 0.007 and 0.033, respectively, for night and day.

(We note that Mauna Kea is relatively devoid of vegetation, that Echosonde measurements there find no evidence for such a boundary layer, and that there is no nighttime local humidity enhancement. This gives some support for associating the the humidity enhancement with the boundary layer at Mt. Graham.)

It is also possible that the local humidity excess at Mt. Graham could involve a very thick layer. Some support for this comes from the broad trend for climatic conditions to degrade with distance from Yuma, Arizona. For example, the mean total hours of sunshine is ~3900 at Tucson, but only ~3650 in the vicinity of Mt. Graham (Lynds and Goad 1984). For a 2 km and 10 km moist layer above Mt. Graham, the excess opacity would be ~0.16 and ~0.21 (3.1 and 4.5 mm PWV), respectively. The continuous presence of such a large excess PWV, however, appears to be ruled out by 22 GHz radiometer measurements during several months in 1986 and 1987, which show a majority of days having PWV<3 mm (Martin, private communication, 1989). Further, there is good agreement between simultaneous radiosonde and radiometer data (see below) which would be lost if as much as 2 mm PWV were added to the radiosonde data. We conclude that the 33% humidity

excess at Mt. Graham probably involves a thin layer, and contributes only slightly to the opacity.

H. Latitude and Declination Effects

So far we have compared the sites only in terms of zenith opacity. For a celestial object, however, the opacity also depends on the range of zenith angles through which the source passes, which is a function of the site latitude and source declination.

To examine this effect we computed the cumulative distribution of opacities for sources at several declinations. This was done by convolving the differential probability distribution for the zenith opacities (derivative of Figure 7) with the distribution function of source $sec(z)$, and then summing to obtain the cumulative distribution. Figure 16 shows the results for source declinations $\delta = 90°$, $60°$, $30°$, $0°$, and $-30°$ expressed in terms of hours per year vs. opacity. We assumed 4.5 hours per day were lost at Mauna Kea due to diurnal effects (see section IV.F.).

At declinations $\delta > 10°$ and opacities < 0.5 the two sites are very similar (see Figure 16 a-c). This is because of two effects which tend to counteract each other: at Mt. Graham the sources are higher in the sky, and up for more hours; while at Mauna Kea low zenith opacities are more probable. However, at high opacities ($0.5 < \tau$) Mt. Graham has more hours per year, since the sources are "up" more hours per day due to its higher latitude.

At southerly declinations Mauna Kea has a clear advantage (Figures 16 d-e). This is because the sources are higher in the sky, up for more hours, and Mauna Kea has a higher probability of low zenith opacities.

Figure 17 shows the hours per year plotted against source declination, for opacities 0.2 and 0.5. At opacity 0.2 it is difficult to clearly select the better site, because of the radiosonde hygrometer response lower limit. At opacity 0.5 the hygrometer limit contributes less uncertainty. Here the sites appear to be similar from $10° < \delta < 90°$, but

below 10° declination, Mauna Kea has a clear advantage. For declinations $\sim -40°$ Mauna Kea has roughly twice the number of hours with $\tau < 0.5$ as Mt. Graham.

I. Relationship of 230.5 GHz Opacity to PWV and Other Opacities

From integration of the radiosonde data at Hilo, we find PWV and opacities at other frequencies are related to the 230.5 GHz opacity by:

$$\mathrm{PWV} \approx 27.6\ \tau(230.5\mathrm{GHz}) - 0.25 \ \ \mathrm{mm}$$

$$\tau(345.8\mathrm{GHz}) \approx 3.78\ \tau(230.5\mathrm{GHz}) - 0.02$$

$$\tau(461\mathrm{GHz}) \approx 18.6\ \tau(230.5\mathrm{GHz}) - 0.17$$

$$\tau(691\mathrm{GHz}) \approx 20.3\ \tau(230.5\mathrm{GHz}) - 0.16$$

$$\tau(808\mathrm{GHz}) \approx 28.9\ \tau(230.5\mathrm{GHz}) - 0.22$$

These relations were determined by fitting lines to the low opacity data ($\tau(230.5\mathrm{GHZ}) < 0.15$) in Figure 18. The PWV relation is based on data for all 22 years, while the others use only the 1985 data. All of these plots show a number of points to the right of the main distribution; these are points where aerosols contribute most of the opacity. These points were ignored in fitting the data.

As a rough check of our opacity calculations, we compare these relations with the empirical results of Zammit and Ade (1981). They give relations between PWV, $\tau(230\mathrm{GHz})$,

and τ(344GHz) based on data obtained on Izana (altitude 2.4km) in Tenerife during conditions of PWV between 4.3 and 14mm. They measure PWV with an IR hygrometer which was calibrated against radiosonde ascents; the opacities are measured with a radiometer. For PWV they find PWV $\propto$ 17.8 τ(230GHz) which we have drawn as a dashed line in Figure 18a. This slope appears to be in reasonable agreement with our calculations for PWV>4mm, which is the range over which their their measurements were made. For τ(345GHz) they find τ(344GHz) $\propto$ 3.33 τ(230GHz), whereas we find a proportionality constant of 3.47 for PWV>4mm; again in reasonable agreement. Since opacity depends pressure as well as PWV, and Izana and Mauna Kea have very different altitudes, we should probably not expect better agreement.

J. Detailed Comparison of Radiosonde and Radiometer Data.

As a further check of the radiosonde calculations, we compare simultaneous radiosonde and radiometer measurements. Figure 19 shows Hilo radiosonde measurements of PWV plotted on top of Mauna Kea 270 GHz radiometer measurements from de Zafra, *et al.* (1983). The radiosonde results are indicated by vertical bars with 12 hour spacing; arrows indicate values which are off the top of the plot. The undulating horizontal line shows the radiometer data. In nearly all cases the radiometer measurements are within the range allowed by the radiosonde data. The large uncertainty in the radiosonde PWV is caused by the lower limit in the hygrometer response.

Figure 20 compares Mt. Graham 22 GHz radiometer PWV measurements with the Tucson radiosonde results. The radiometer data are from Martin (private communication, 1989) and are shown by the continuous, erratic line. The radiosonde results are shown by vertical bars spaced 12 hours apart. The length of each vertical bar indicates the range of PWV consistent with the radiosonde data.

In most cases the agreement between the radiosonde and radiometer is excellent. During this time there are ~74 points with simultaneous data. Of these, only ~8 show the

radiometer value lying outside the radiosonde range, and in most of these cases the error is <0.5 mm PWV.

It is also interesting to note that the Mt. Graham radiometer data contain many gaps, and these gaps often occur when the radiosonde indicates a large PWV. This probably reflects the difficulties of operating a radiometer on a remote mountain site during adverse weather conditions. It seems likely that some correlation between bad weather and missing data would occur for all radiometers, so that one must be cautions when drawing conclusions from radiometer data with incomplete coverage.

V. Conclusions

Mauna Kea appears to be a superior site in the following important respects:

1) Ignoring local and diurnal effects, Mauna Kea has a higher probability of 230.5 GHz opacity <0.12, than Mt. Graham.

2) If one considers only the best months of the year at Mt. Graham, Mauna Kea still has a higher probability of 230.5 GHz opacity <0.15.

3) Radiometer data in the literature suggest <4.5 hours per day *on average* would be lost at Mauna Kea due to local and diurnal effects. We find at least 7.8 hours per day must be lost at Mauna Kea, before it looses its advantage over Mt. Graham. Hence, Mauna Kea would appear to be superior, even when local and diurnal effects are included.

4) For sources at southerly declinations, Mauna Kea has a much higher number of hours per year of 230.5 GHz opacity < 0.5 than Mt. Graham. For $\delta \sim -40°$ the number of hours per year is nearly twice as high at Mauna Kea.

We did not find any important respects where Mt. Graham appeared superior to Mauna Kea.

Mauna Kea often has a local diurnal opacity increase. It typically begins between 10AM and noon, peaks in the early afternoon, and dissipates by 6PM. On average the opacity increase is 80%, and lasts 7 hours. There is a substantial fraction of days ($\sim$ 35%) where no diurnal increase occurs.

Mt. Graham appears to have a local humidity excess of $\sim$33% relative humidity. This excess probably involves a layer only a few hundred meters thick, and contributes only a small opacity increase. A small diurnal opacity increase is seen at South Baldy, which is geographically similar to Mt. Graham and has more complete radiometer data available; the variation is $\sim$30% or less, and last $\sim$8 hours per day. During the summer months conditions are nearly always bad; for July and August the probability of 230.5 GHz opacity $<$0.15 is less than 5%.

The radiosonde hygrometer response lower limit makes results at PWV$<$3mm highly uncertain. More complete radiometer data are needed to study and compare the probability of very low PWV at the sites. The additional data would also improve our understanding of the local and diurnal effects.

VI. Future Work

It may be useful to obtain radiosonde data from the National Climatic Data Center for 1972 to present, where actual humidity values below 19% are reported, instead of being set to 19%. The actual readings below 19% probably contain some useful information, and better reflect the true humidity, than the arbitrary value 19%.

Radiometer data are need for Mauna Kea to assess the diurnal and local effects there, and to study the probability of low opacities (PWV$<$3mm). Further efforts should be made to obtain detailed radiometer data (PWV vs. time) for Mt. Graham from R. Martin. It is necessary to have the actual data, rather that statistical plots, since the same analysis procedure must be applied to data from both sites. There is also a tendency for gaps to

appear in radiometer during bad conditions, and one cannot correct for this without the actual PWV vs. time history.

When more radiometer data are available, they should be used together with the radiosonde data to form a more complete picture of the two sites. There are several ways to combine the data sets: (A) Use radiosonde derived PWV to fill in gaps in the radiometer data, keeping track of both the minimum and maximum PWV consistent with the radiosonde. This would minimize uncertainties caused by missing radiometer data. (B) Study the statistical properties of the radiometer data at low PWV, and use these results to extrapolate the radiosonde data to very low PWV for all 22 years.

We have compared the two sites only in terms of opacity. However, for an interferometer, seeing and phase stability must also be considered. Some effort should be made to understand the relationship between opacity and phase stability.

Acknowledgements

We extend our deepest gratitude to F. Schwab for providing a tape of the radiosonde data, portions of the opacity computation code, and for helpful discussions. We also thank R. Martin for providing radiometer data for Mt. Graham; and F. Forbes, D. Hogg, R. Martin, and M. Merrill for interesting discussions.

References

Church, J., and Hills, R. 1989, "Measurements of Daytime Atmospheric 'Seeing' on Mauna Kea Made with the James Clerk Maxwell Telescope," in *Proc. IAU Symposium on Radio Astronomical Seeing*, in preparation.

de Zafra, R., Parrish, A., Solomon, P., and Barrett, J. 1983, "A Quasi-Continuous Record of Atmospheric Opacity at $\lambda = 1.1$mm Over 34 Days at Mauna Kea Observatory," *Int. J. Infrared and Millimeter Waves*, **4**, 757.

Ellsaesser, H. W., Harries, J. E., Kley, D., and Penndorf, R. 1980, "Stratospheric H20," *Planet. Space Sci.*, **28**, 827.

Ference, M., 1951, "Instruments and Techniques for Meteorological Measurements," in *Compendium of Meteorology*, ed. T. F. Malone (American Meteorological Society, Boston), p. 1207.

Finger, F. G. and McInturff, R. M. 1978, "Part I: Research on Compatibility of Data from Radiosondes, Rocketsondes, and Satellites," in *World Meteorological Organization - No. 512 Technical Note No. 163: The Compatibility of Upper-Air Data*, (World Meteorological Organization: Geneva, Switzerland).

Forbes, F., Barker, E., Peterman, K., Cudaback, D., and Morse, D. 1985, "High Altitude Acoustic Soundings," *S.P.I.E.*, **551**, 60.

Forbes, F., Morse, D., and Poczulp, G. 1986, "Planning the National New Technology Telescope (NNTT): VI. Site Survey Instrumentation," *S.P.I.E.*, **628**, 118.

Handegord, G. O., Hedlin, C. P., and Trofimenkoff, F. N. 1965, "A Study of the Accuracy of Dunmore Type Humidity Sensors," in *Humidity and Moisture*, ed. A. Wexler (Reinhold Publishing, N.Y.), p. 265.

Hogg, D., Owen, F., and McKinnon, M. 1988, "First Results from the Site Testing Program of the Millimeter-Wave Array," (*Millimeter Array Memo 45*).

Liebe, H. J. 1985, "An Updated Model for Millimeter Wave Propagation in Moist Air," *Radio Science* , **20**, 1069.

Lynds, R., and Goad, J. 1984, "Observatory-Site Reconnaissance," *P.A.S.P.*, **96**, 750.

Mathews, D. A. 1965, "Review of the Lithium Chloride Radiosonde Hygrometer," in *Humidity and Moisture*, ed. A. Wexler (Reinhold Publishing, N.Y.), p. 219.

McElroy, T. 1985, "The Measurement of Temperature, Ozone, and Water Vapor," in *Middle Atmosphere Program, Vol. 15, Balloon Techniques*, ed. D. G. Murcray (International Council of Scientific Unions), p. 1.

Merrill, K., Forbes, F., *et al.* 1987, "Comparison Study of Astronomical Site Quality of Mount Graham and Mauna Kea," (*Millimeter Array Memo 39*).

Ostapoff, F., Shinners, W., and Augstein, E. 1970, "Some Tests in the Radiosonde Humidity Element," *N.O.A.A. Technical Report ERL194-AOML4* .

Parrish, A., de Zafra, R., Barrett, J., Solomon, P., and Connor, B. 1987, "Additional Atmospheric Opacity Measurements at $\lambda = 1.1$mm Over 34 Days at Mauna Kea Observatory, Hawaii," *Int. J. Infrared and Millimeter Waves*, **8**, 431.

Phillips, P. D., Richner, H., Joss, J., and Ohmura, A. 1981, "ASOND-78: An Intercomparison of Vaisala, VIZ, and Swiss Radiosondes," *Pure and Applied Geophysics*, **119**, 259.

Radiosonde Observations - Effective January 1,1969 (Federal Meteorological Handbook No. 3), 1968, (U. S. Department of Commerce, U. S. Department of Defense; U. S. Government Printing Office: Washington, D.C.).

Radiosonde Observations - Effective January 1,1969 (Federal Meteorological Handbook No. 3), 1975, (U. S. Department of Commerce, U. S. Department of Defense; U. S. Government Printing Office: Washington, D.C.).

Richner, H. and Phillips, P. D. 1981, "Reproducibility of VIZ Radiosonde Data and Some Sources of Error," *Journal of Applied Meteorology*, **20**, 954.

Schmidlin, F. J., Olivero, J. J., and Nestler, M. S. 1982, "Can the Standard Radiosonde Meet Special Atmospheric Research Needs?" *Geophys. Res. Lett.*, **9**, 1109.

Spackman, E. A. 1978, "Part II: The Compatibility and Performance of Radiosonde Measurements of Geopotential Height in the Lower Stratosphere for 1975-76," in *World Meteorological Organization - No. 512 Technical Note No. 163: The Compatibility of Upper-Air Data*, (World Meteorological Organization: Geneva, Switzerland).

Stine, S. L. 1965, "Carbon Humidity Elements - Manufacture, Performance, and Theory," in *Humidity and Moisture*, ed. A. Wexler (Reinhold Publishing, N.Y.), p. 316.

U.S. Standard Atmosphere 1976, (National Oceanic and Atmospheric Administration, N.A.S.A., U.S. Air Force; Washington, D.C.), p. 44.

Zammit, C., and Ade, P. 1981, "Zenith Atmospheric Attenuation Measurements at Millimetre and Sub-Millimetre Wavelengths," *Nature*, **293**, 550.

Altitude (m)	Pressure (mBar)	Temperature (°C)	Relative Humidity (%)
789.00	927.00	3.90	79.00
1032.00	900.00	10.00	57.00
1080.00	896.00	11.00	52.00
1507.00	850.00	9.20	41.00
2005.00	800.00	4.90	42.00
2310.00	769.00	2.10	42.00
2520.00	750.00	1.40	34.00
3082.00	700.00	-0.30	14.00
3670.00	650.00	-2.30	14.00
3840.00	636.00	-2.90	14.00
4305.00	600.00	-6.20	15.00
4970.00	550.00	-11.30	16.00
5704.00	500.00	-16.90	17.00
6480.00	450.00	-22.90	45.00
7341.00	400.00	-28.00	45.00
8284.00	350.00	-35.50	45.00
9337.00	300.00	-43.50	-999.00
10539.00	250.00	-52.30	-999.00
11650.00	210.00	-60.90	-999.00
11947.00	200.00	-61.80	-999.00
12510.00	183.00	-63.50	-999.00
12771.00	175.00	-61.10	-999.00
13728.00	150.00	-61.90	-999.00
14849.00	125.00	-64.10	-999.00
15160.00	119.00	-64.80	-999.00
16214.00	100.00	-63.40	-999.00
17590.00	80.00	-61.70	-999.00
18415.00	70.00	-61.80	-999.00
19369.00	60.00	-62.50	-999.00
20504.00	50.00	-59.00	-999.00
21905.00	40.00	-58.40	-999.00
23714.00	30.00	-59.40	-999.00
24855.00	25.00	-58.50	-999.00
26270.00	20.00	-54.70	-999.00
27300.00	17.00	-55.50	-999.00
28110.00	15.00	-52.90	-999.00
30775.00	10.00	-44.90	-999.00
32268.00	8.00	-43.90	-999.00

Table 1. A typical set of radiosonde data. (Tucson, 12 UT on 3 January 1965.)

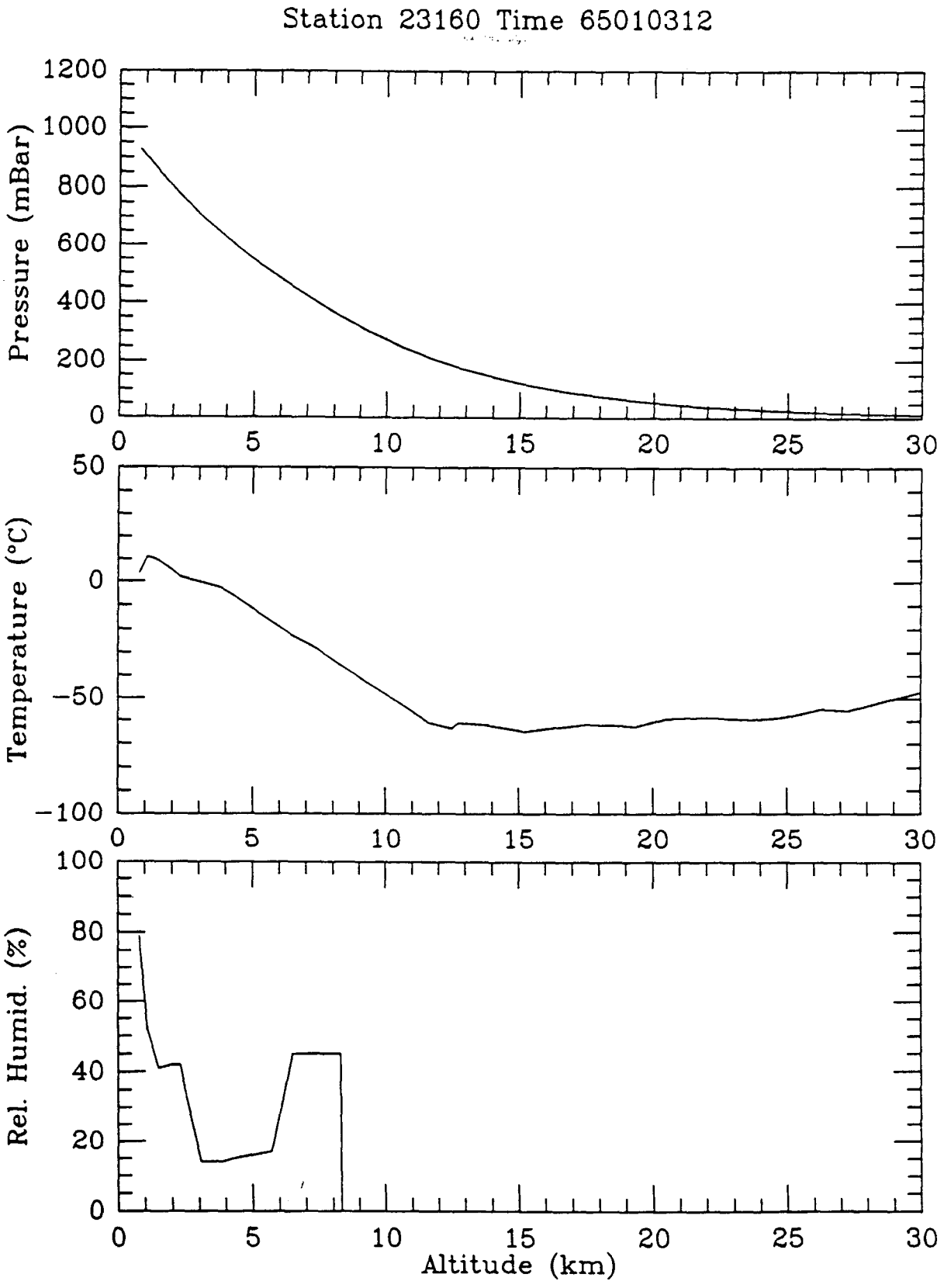

Figure 1. A typical set of radiosonde data. The humidity readings stop at 8.4km. (Tucson, 12 UT on 3 January 1965.)

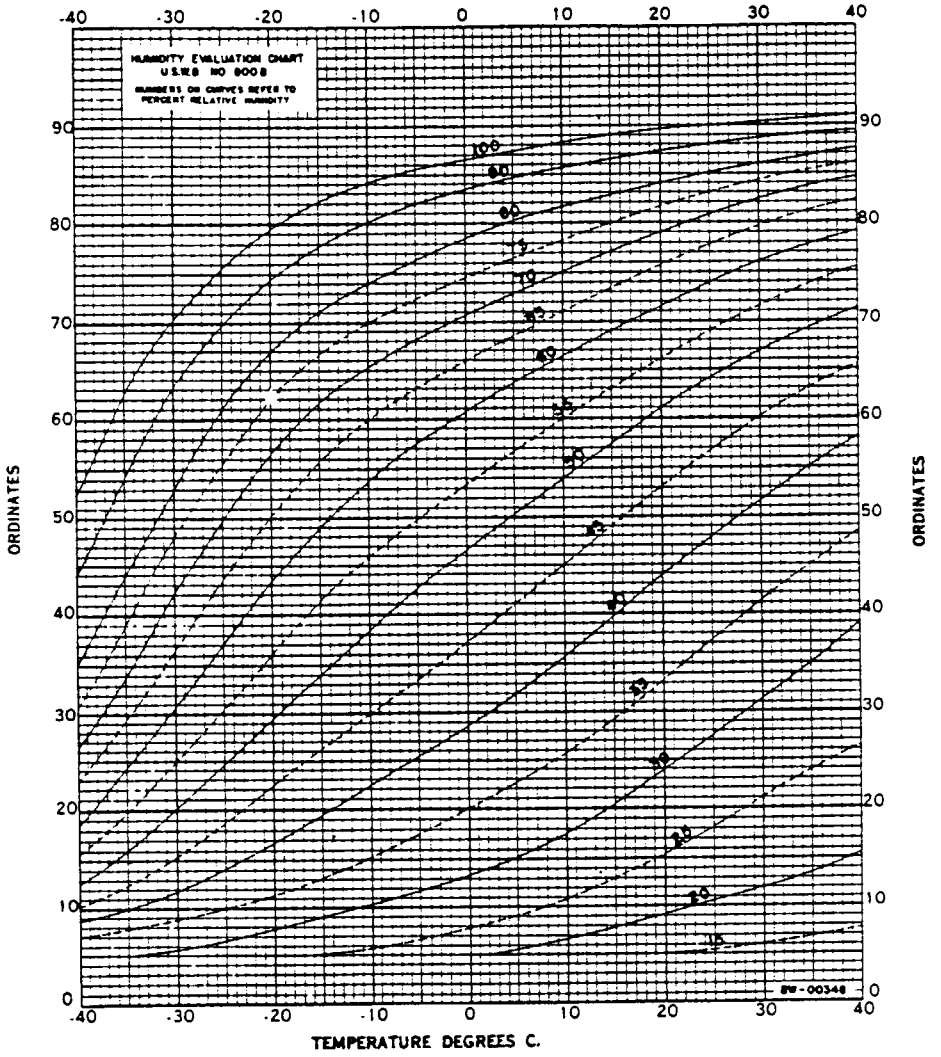

Figure 2(a). Lithium chloride radiosonde hygrometer calibration chart 800B. Vertical axis (ordinates) are in radiosonde output units. Numbers on curves give percent relative humidity. From Mathews (1965).

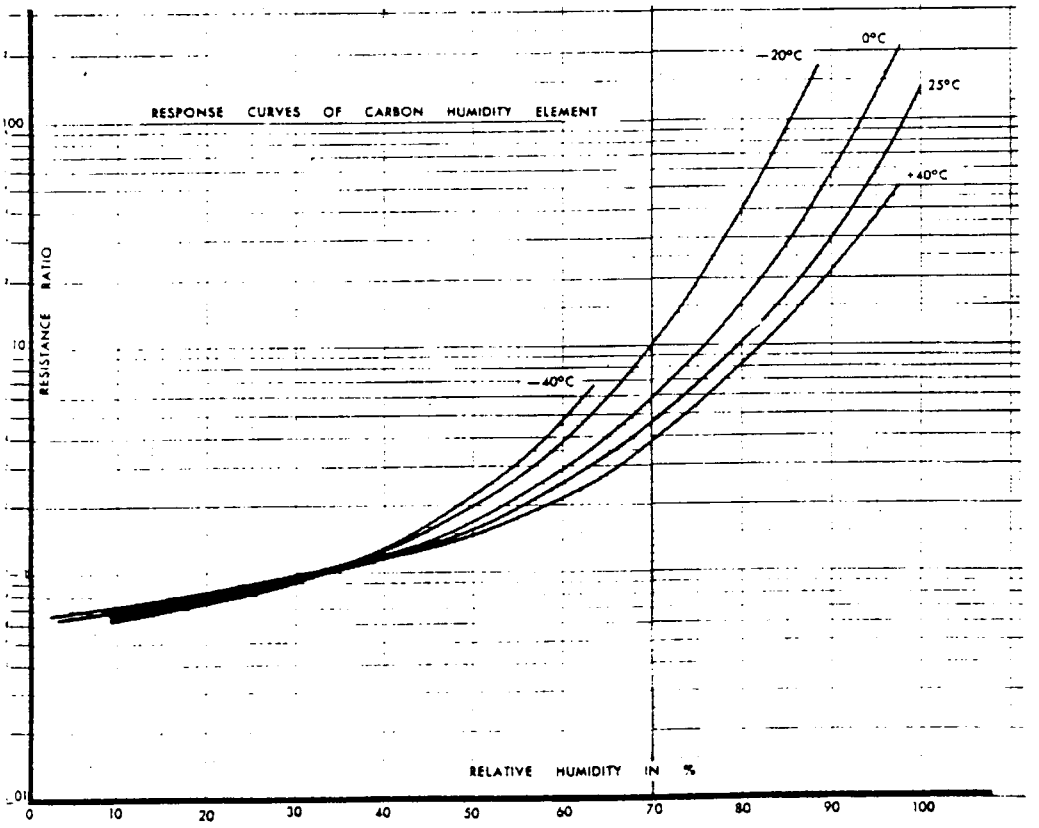

Figure 2(b). Carbon hygristor calibration chart. Curves for different temperatures have been normalized to unit resistance at 33.3% relative humidity. Typical resistances at 33.3% humidity are 20.0K Ohms at 25°C, 21.6K Ohms at 0°C, 24.5K Ohms at -20°C, and 29.0K Ohms at -30°C. From Stine (1965).

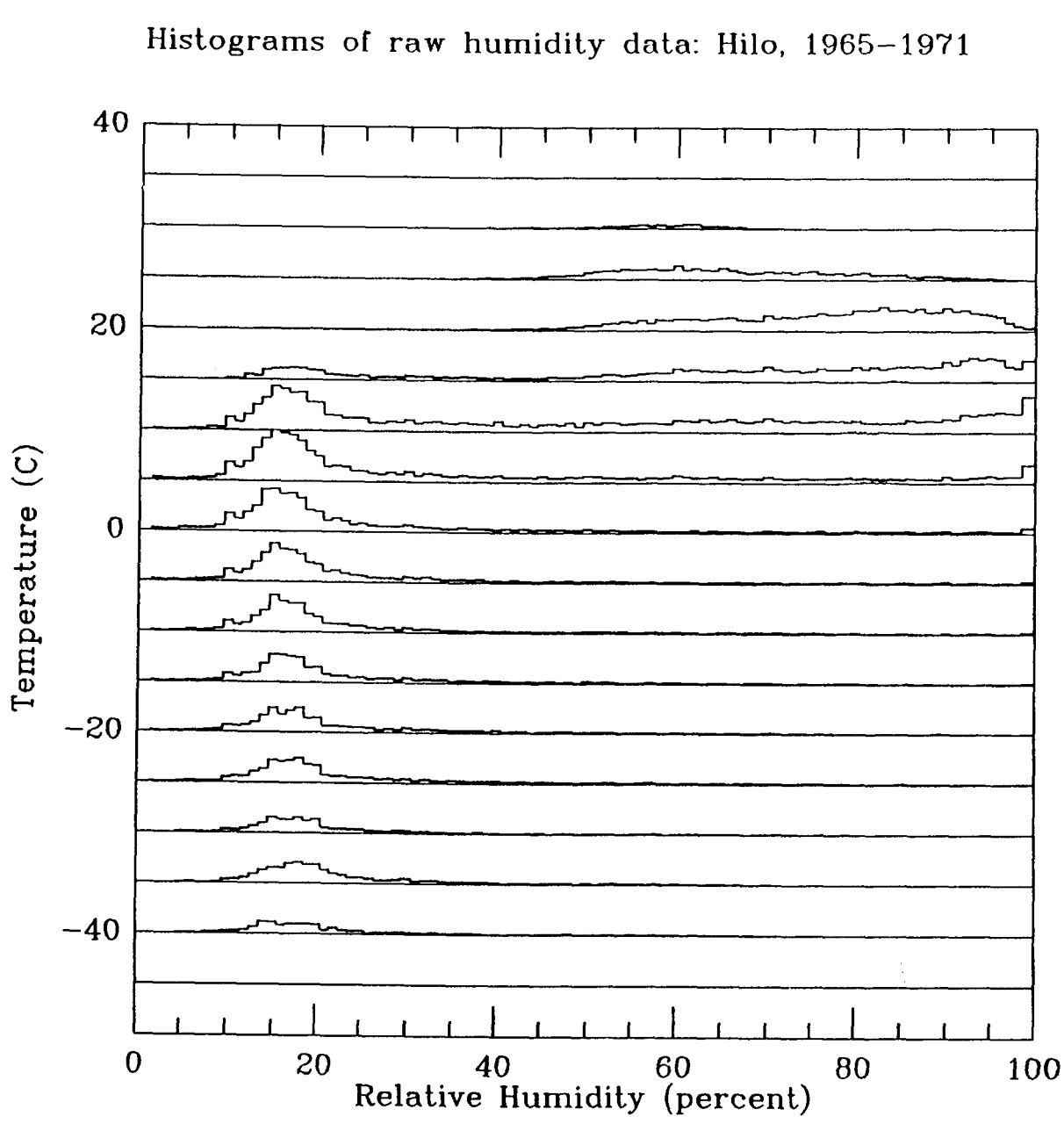

Figure 2.1(a-b). Histogram of raw humidity data for 1965-1971. A separate histogram is plotted for each 5°C range in temperature. (a) Hilo. A vertical distance equaling 5°C corresponds to 797 humidity measurements.

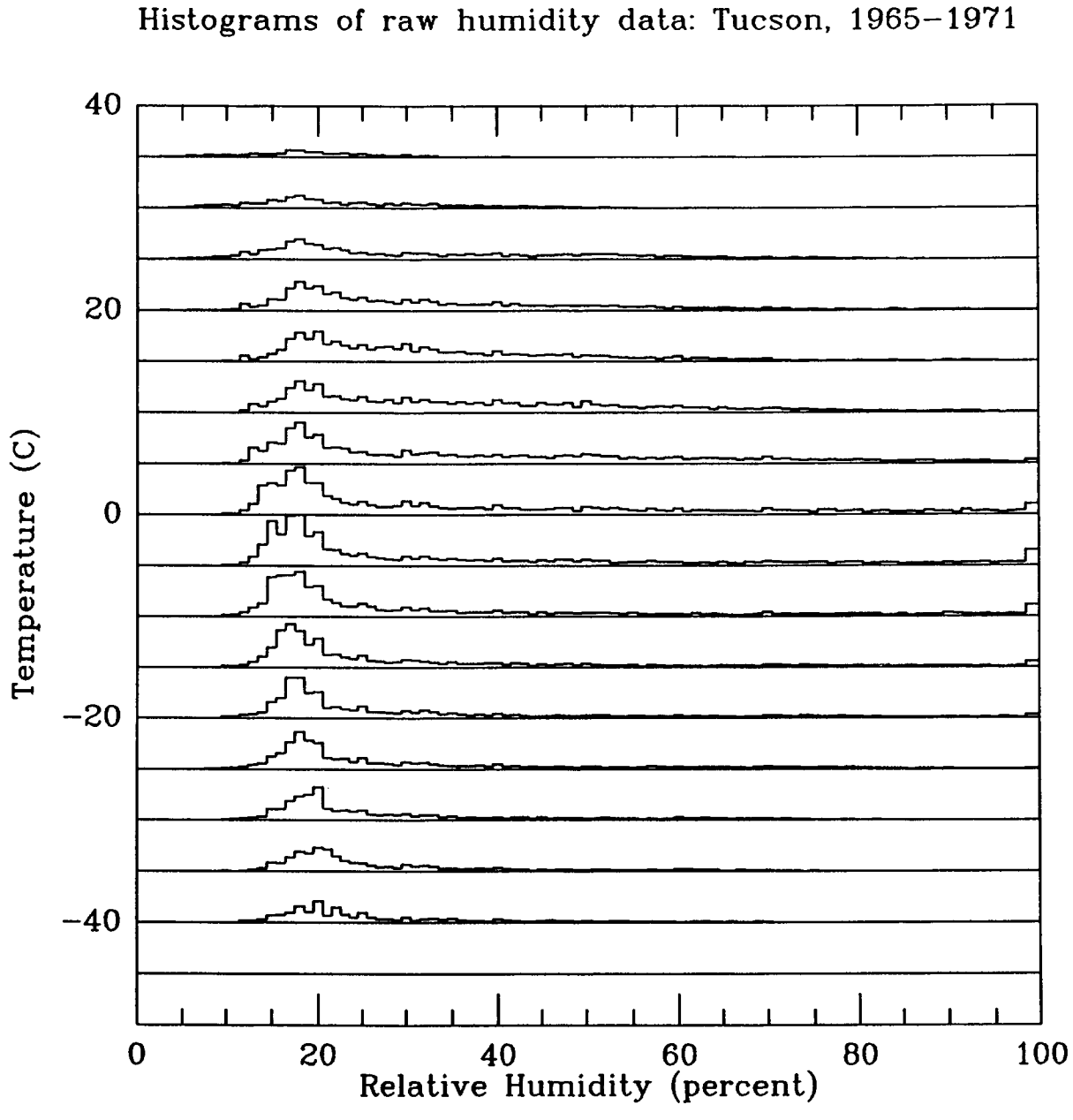

Figure 2.1(b) Tucson. A vertical distance equaling 5°C corresponds to 650 humidity measurements.

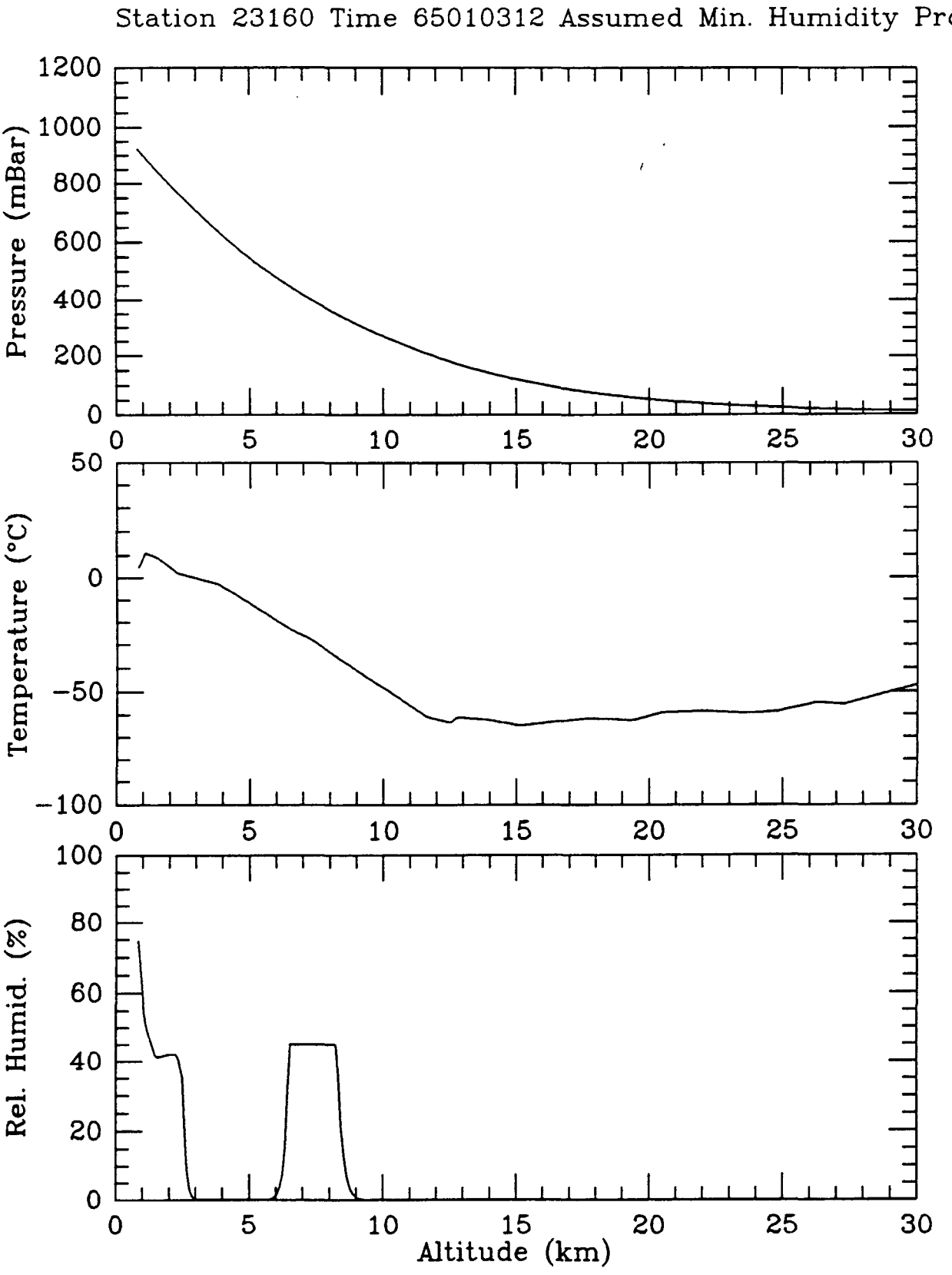

Figure 3(a-b). Humidities assumed during opacity calculation for raw data of Figure 2. (a.) Minimum profile; unknown values and those below 20% have been set to 0.1%.

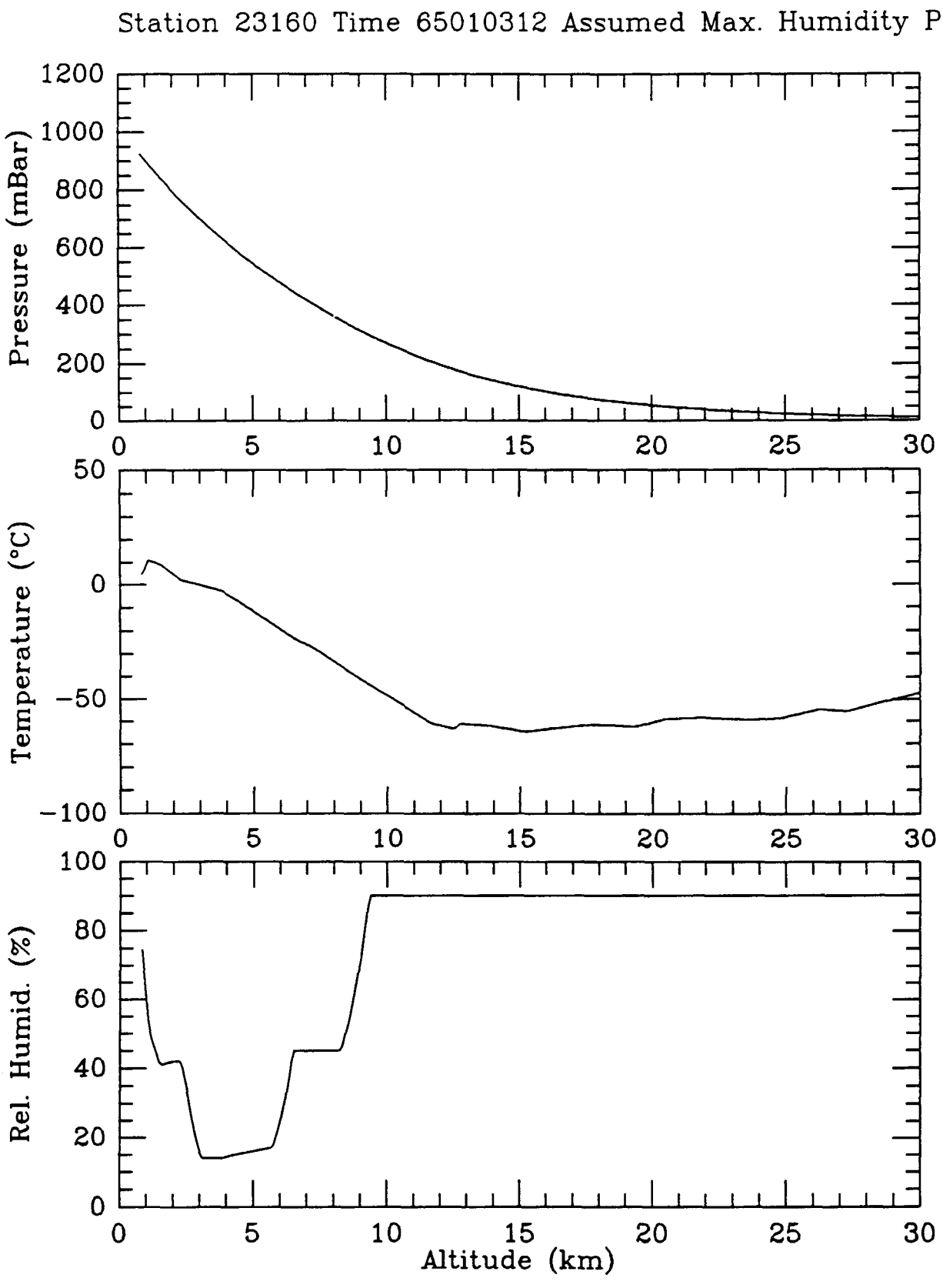

Figure 3(b). Maximum profile; unknown values have been set to 90%.

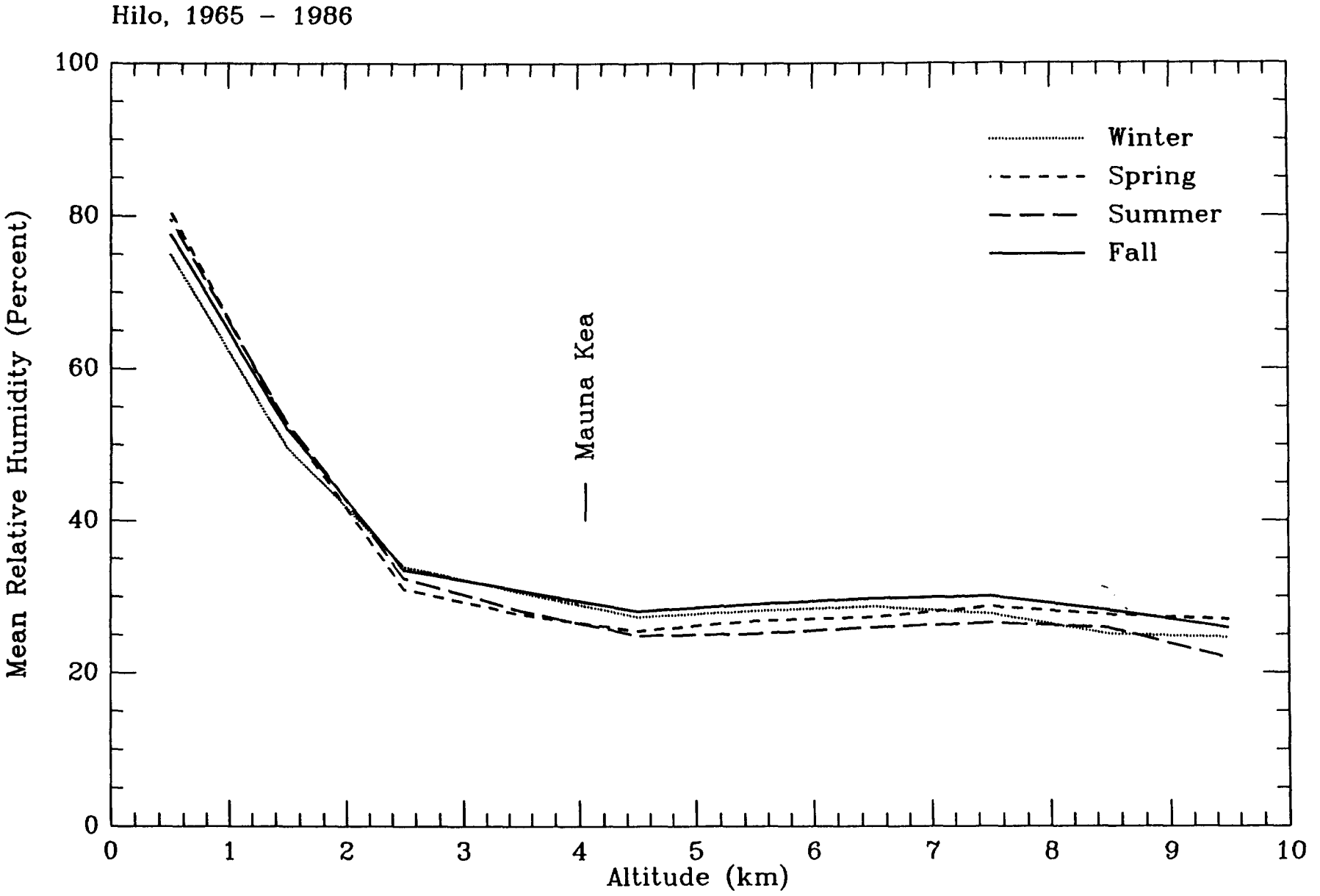

Figure 4(a-b). Mean humidity vs. altitude plotted separately for each season. (a.) Hilo; altitude of Mauna Kea indicated.

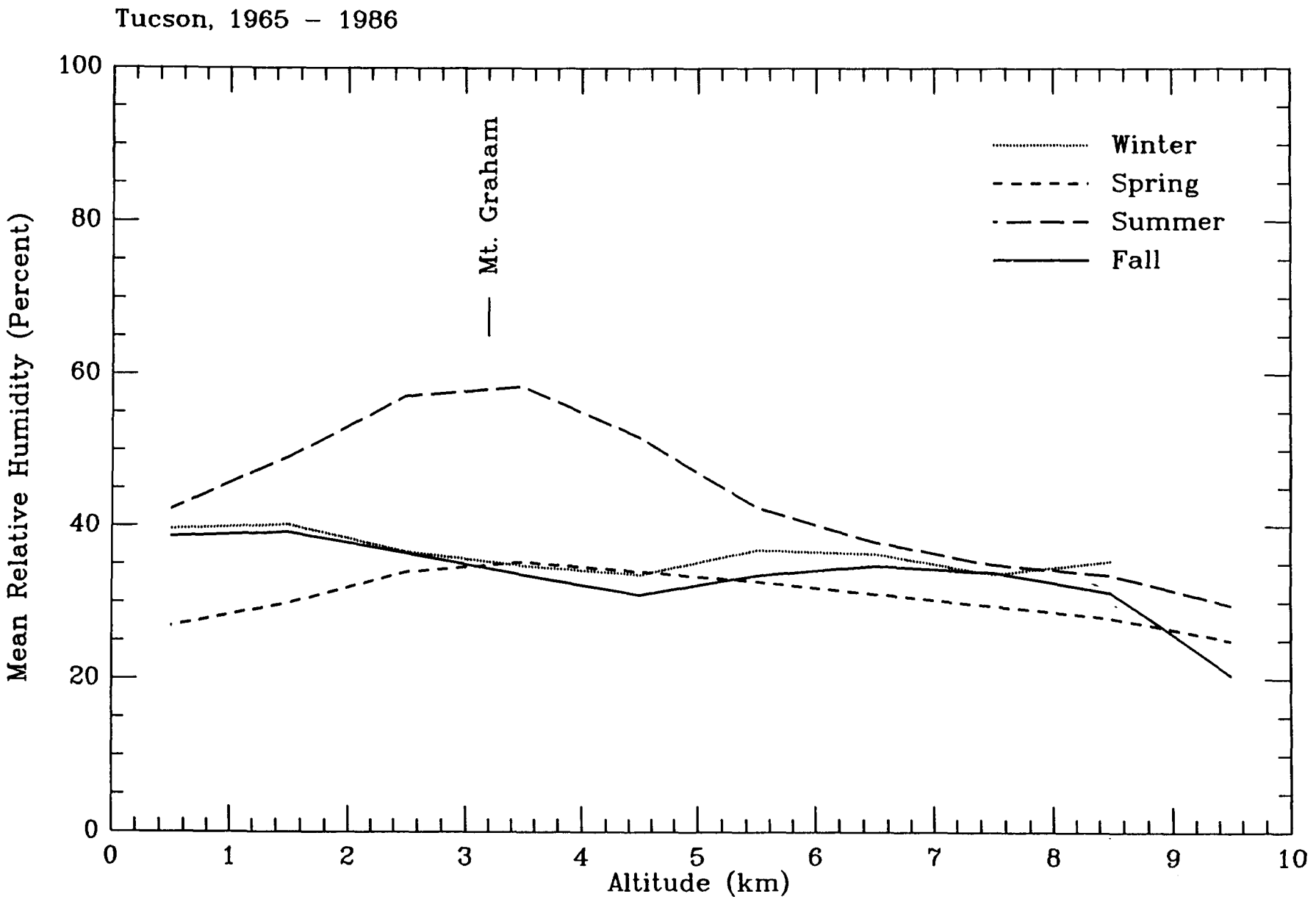

Figure 4(b). Tucson; altitude of Mt. Graham indicated.

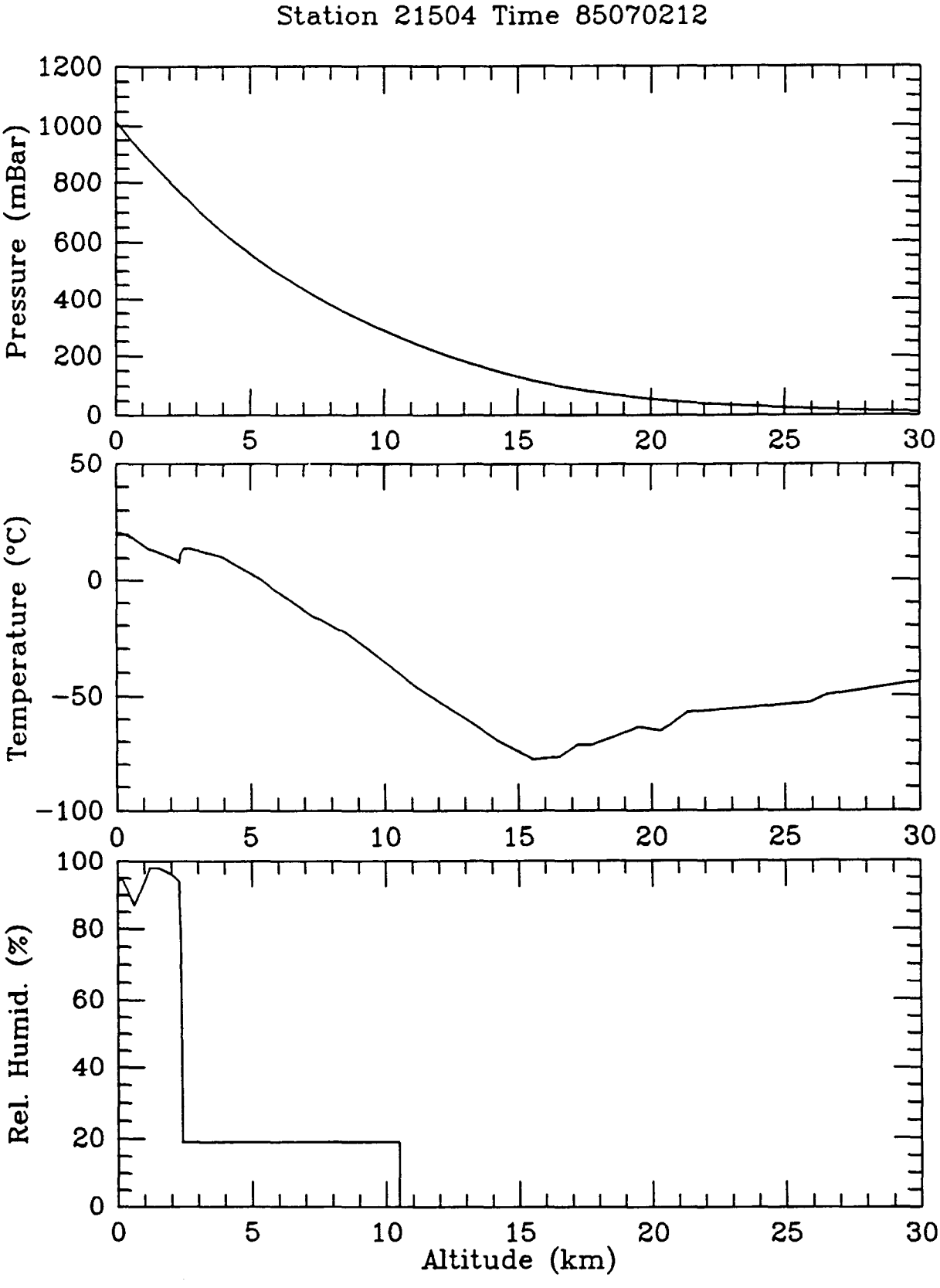

Figure 4(c). Radiosonde data for Hilo showing typical inversion layer structure. Inversion layer has sharp boundary at 2.2km altitude. Note that humidity values below 19% have been reset to 19% by weather service; no humidities are reported above 10.5km altitude. Data for 12 UT on 2 July 1985.

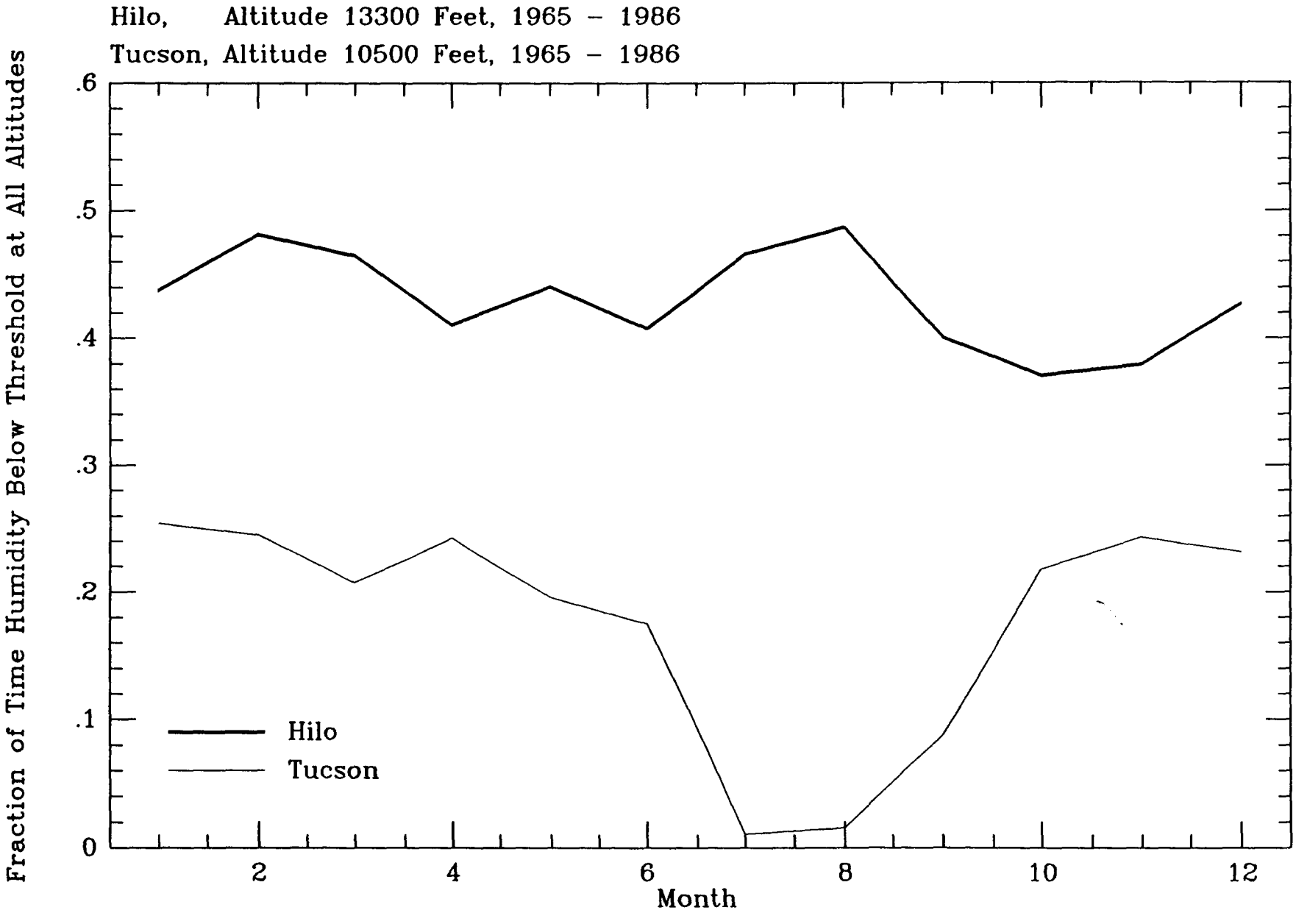

Figure 5. Probability of "best" humidity conditions vs. month of year. "Best conditions" are defined as humidity <22% between observatory altitude and 5km; < 25% above 5km.

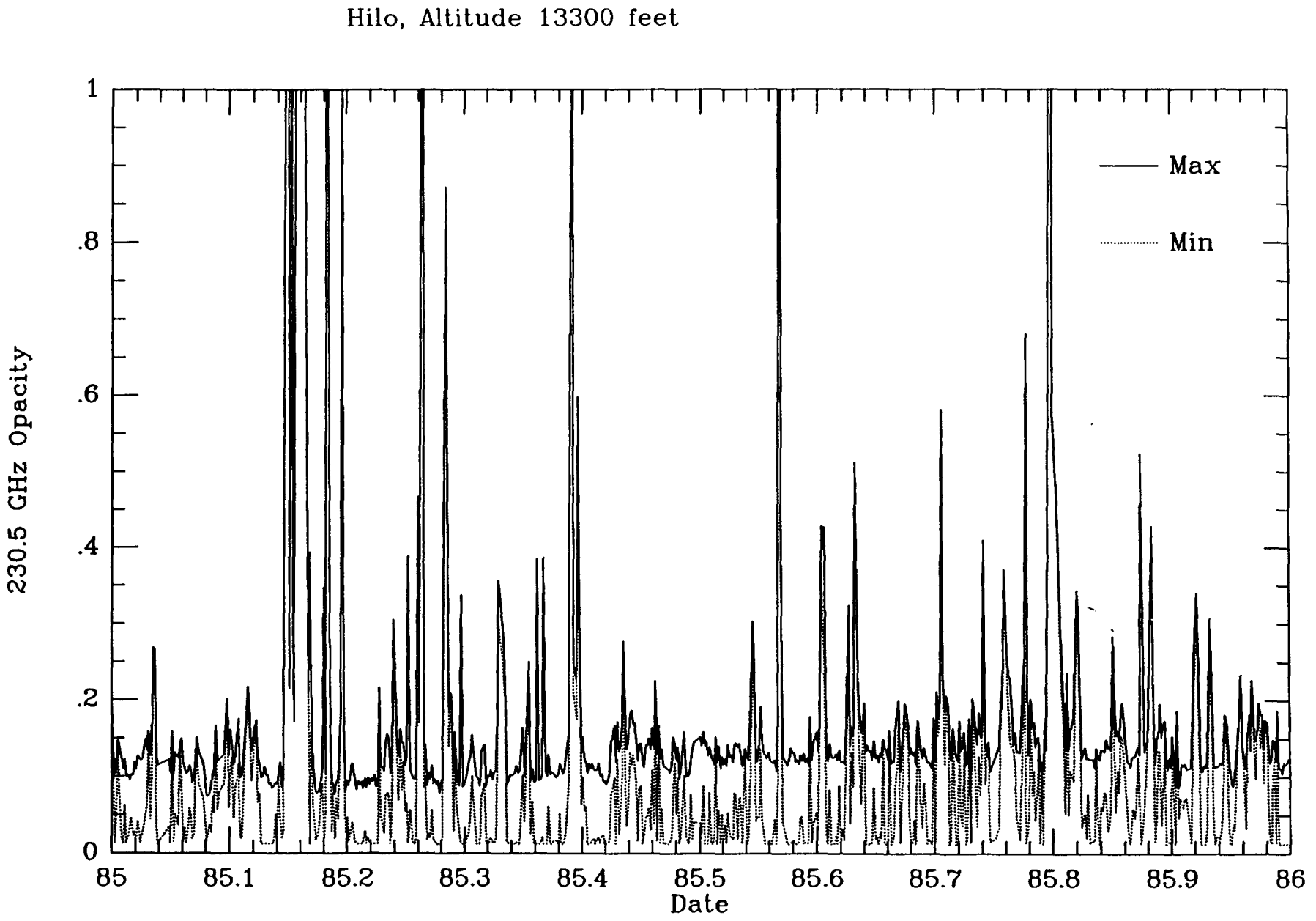

Figure 6(a-b). Computed opacities for year 1985. "Max" values computed using maximum humidities consistent with radiosonde; "Min" using minimum consistent with radiosonde. (a.) Hilo.

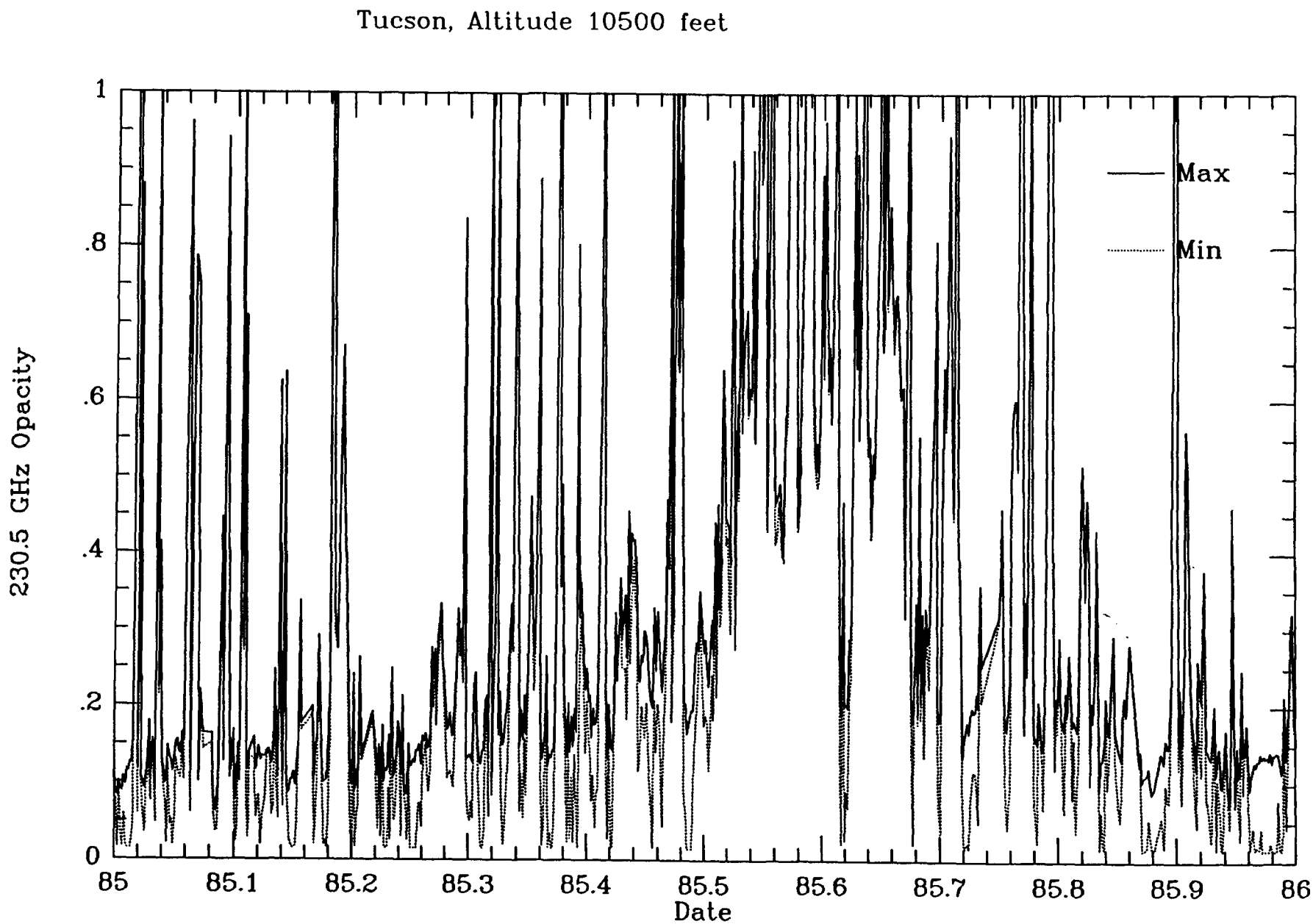

Figure 6(b). Tucson.

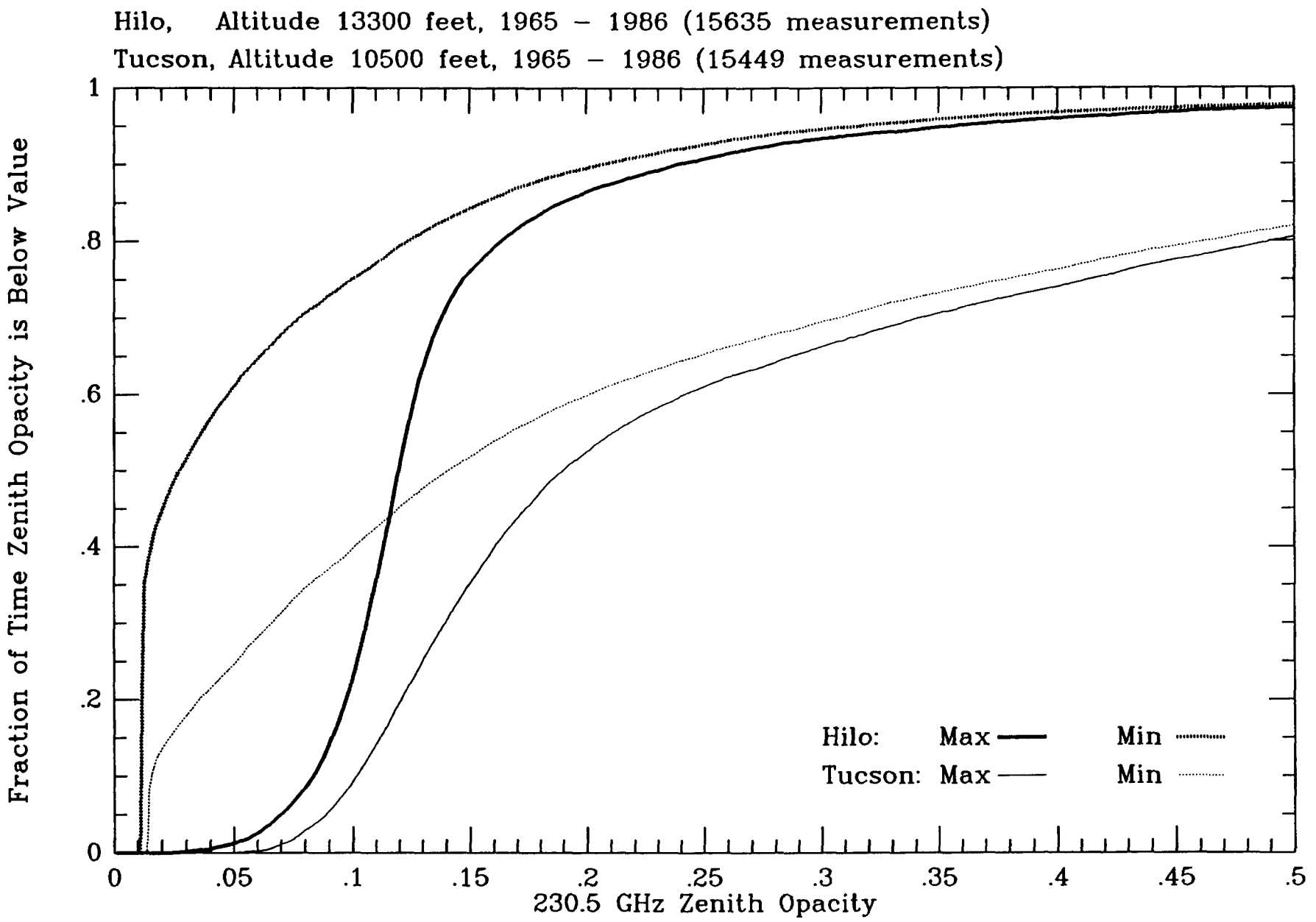

Figure 7. Comparison of cumulative probability distribution of zenith opacities for Hilo (Mauna Kea) and Tucson (Mt. Graham). Data from January 1965 to October 1986. "Max" distribution computed using maximum humidities consistent with radiosonde; "Min" using minimum consistent with radiosonde.

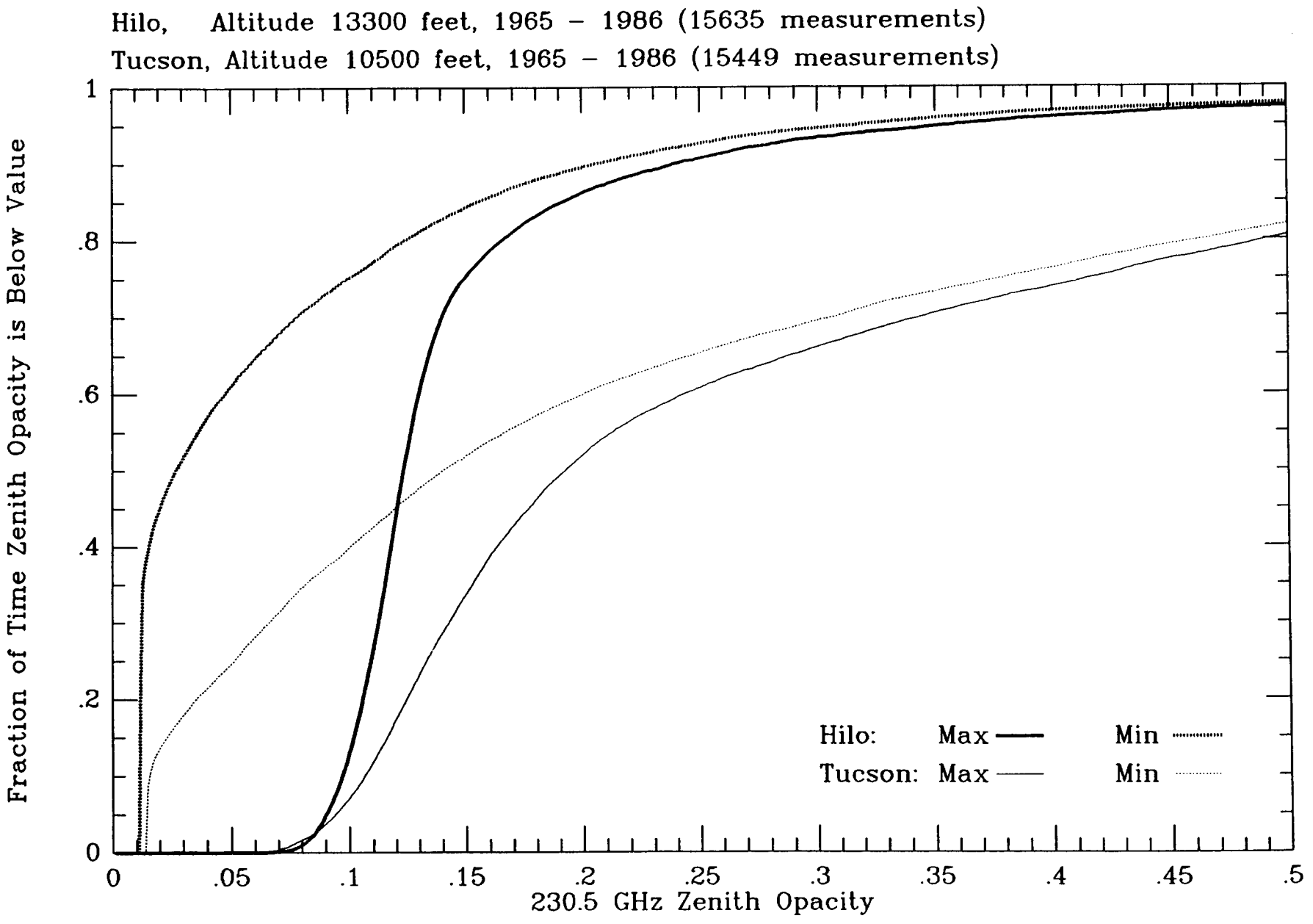

Figure 7.1. Same as Figure 7, but humidities less than 19% have been set to 19% for all the data.

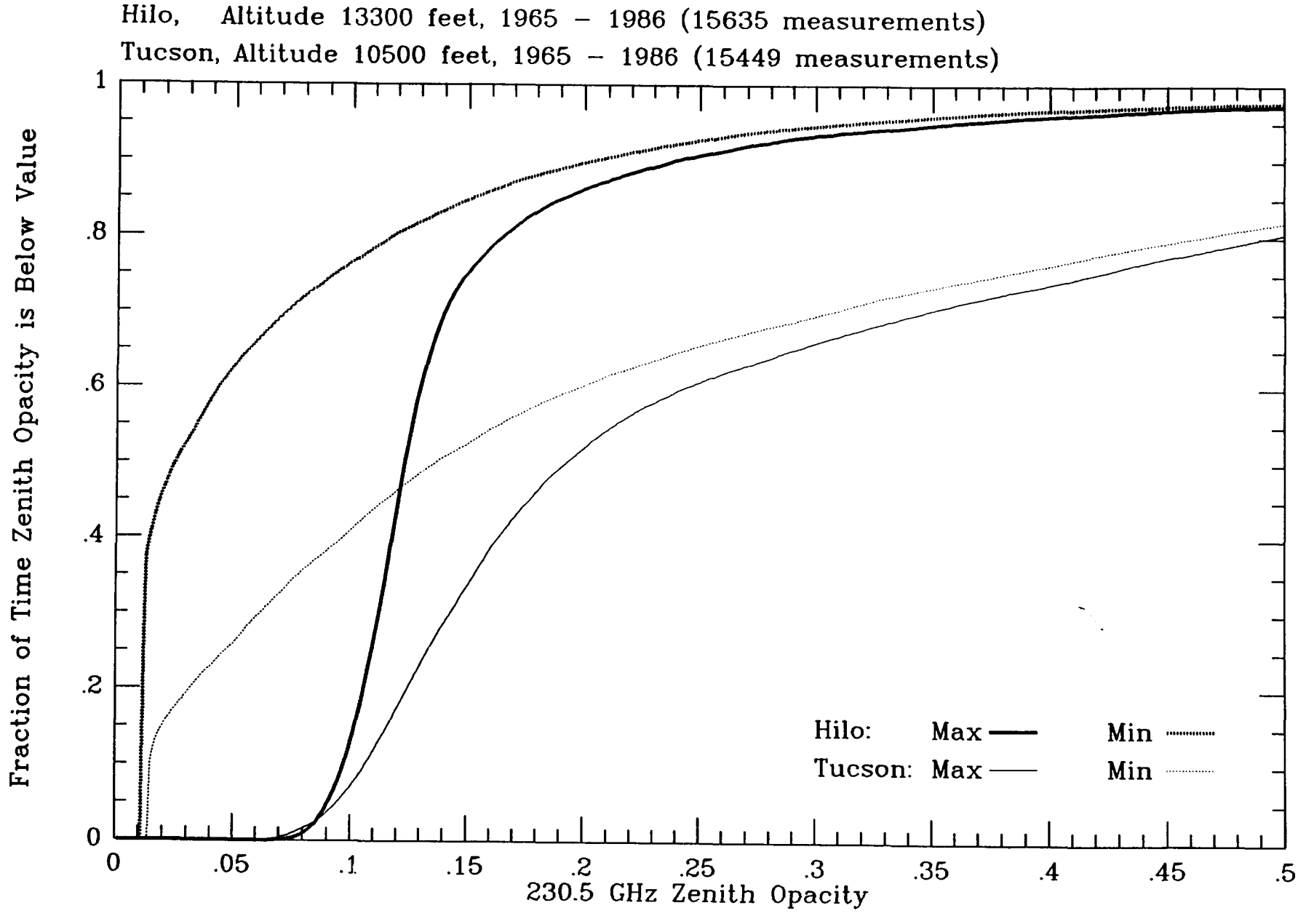

Figure 7.2. Same as Figure 7.1, but minimum opacity computed to allow for variation in lower limit of lithium chloride hygrometer response caused by temperature.

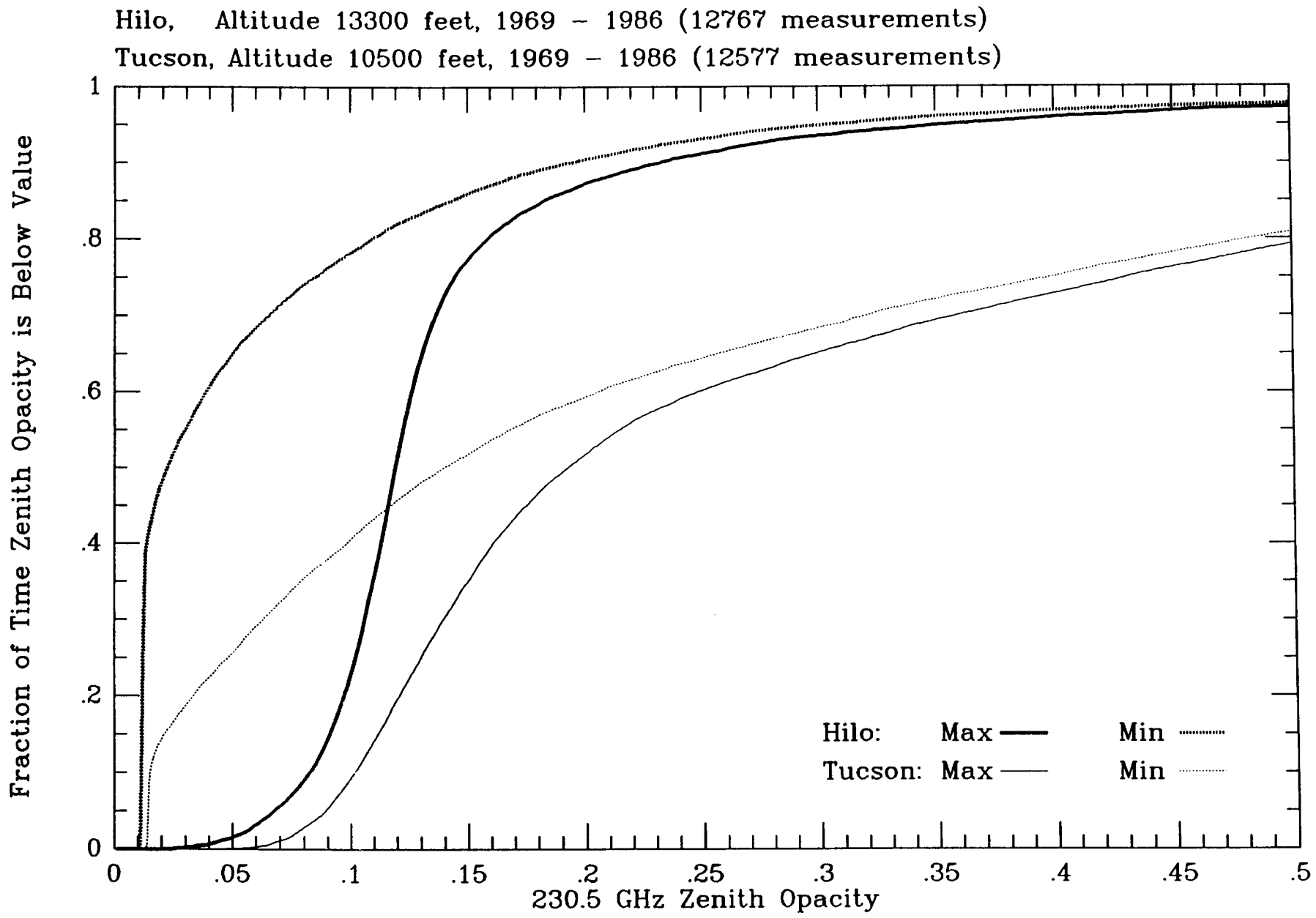

Figure 7.3. Same as Figure 7, but only data for 1969 - 1986 where the lithium chloride hygrometer is not used.

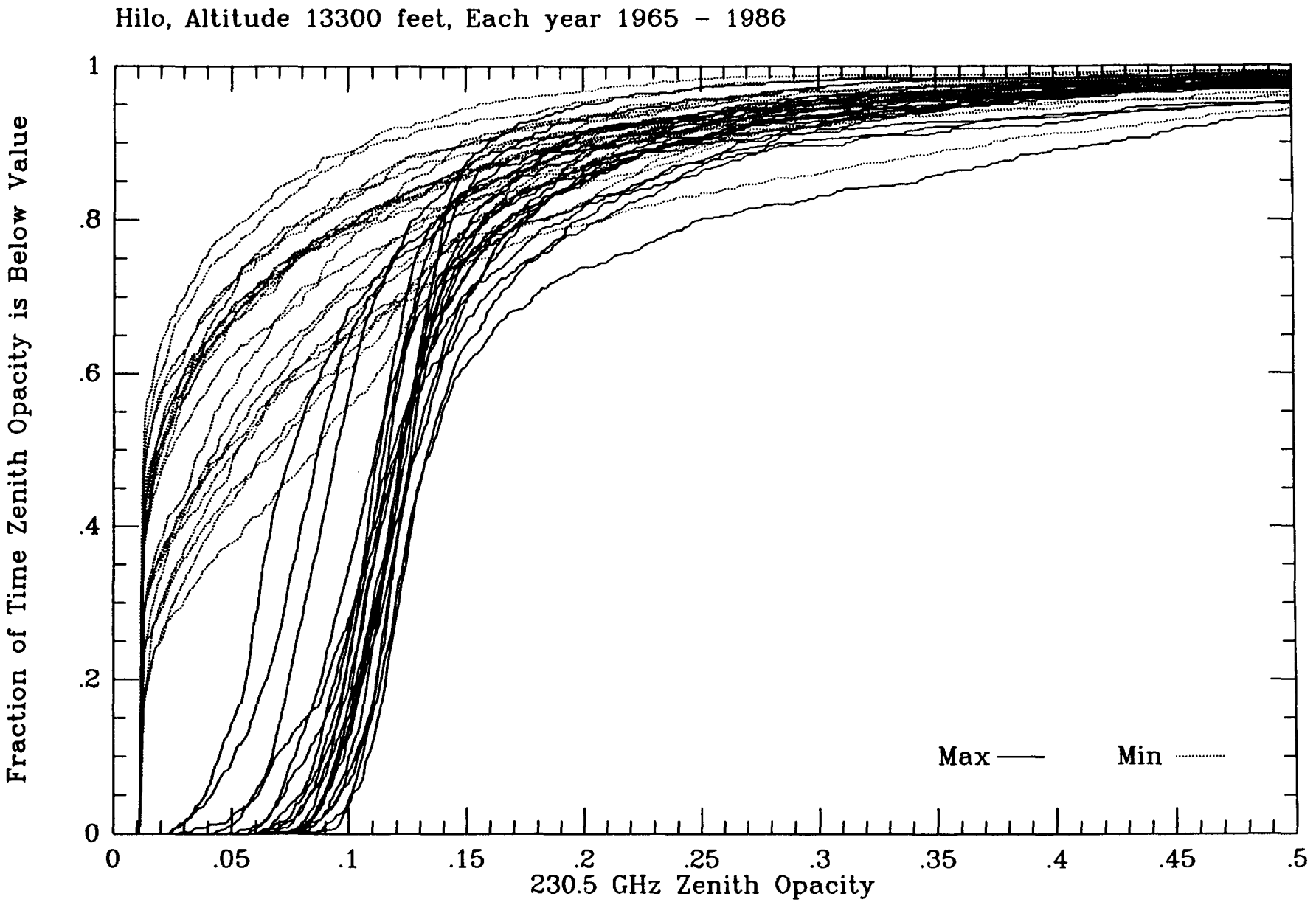

Figure 8(a-b). Same as Figure 7, but each year plotted separately. (a.) Hilo (Mauna Kea).

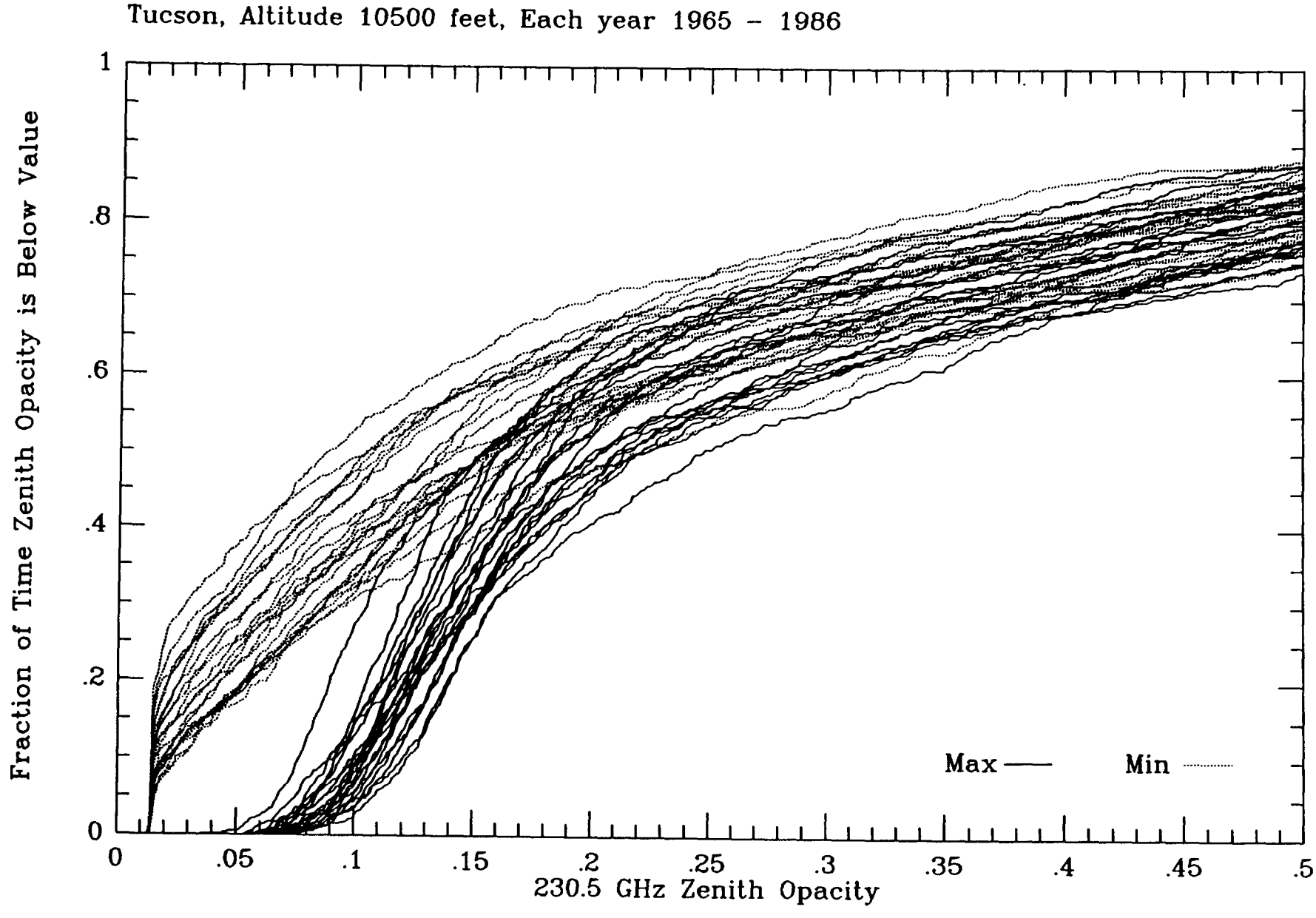

Figure 8(b). Tucson (Mt. Graham).

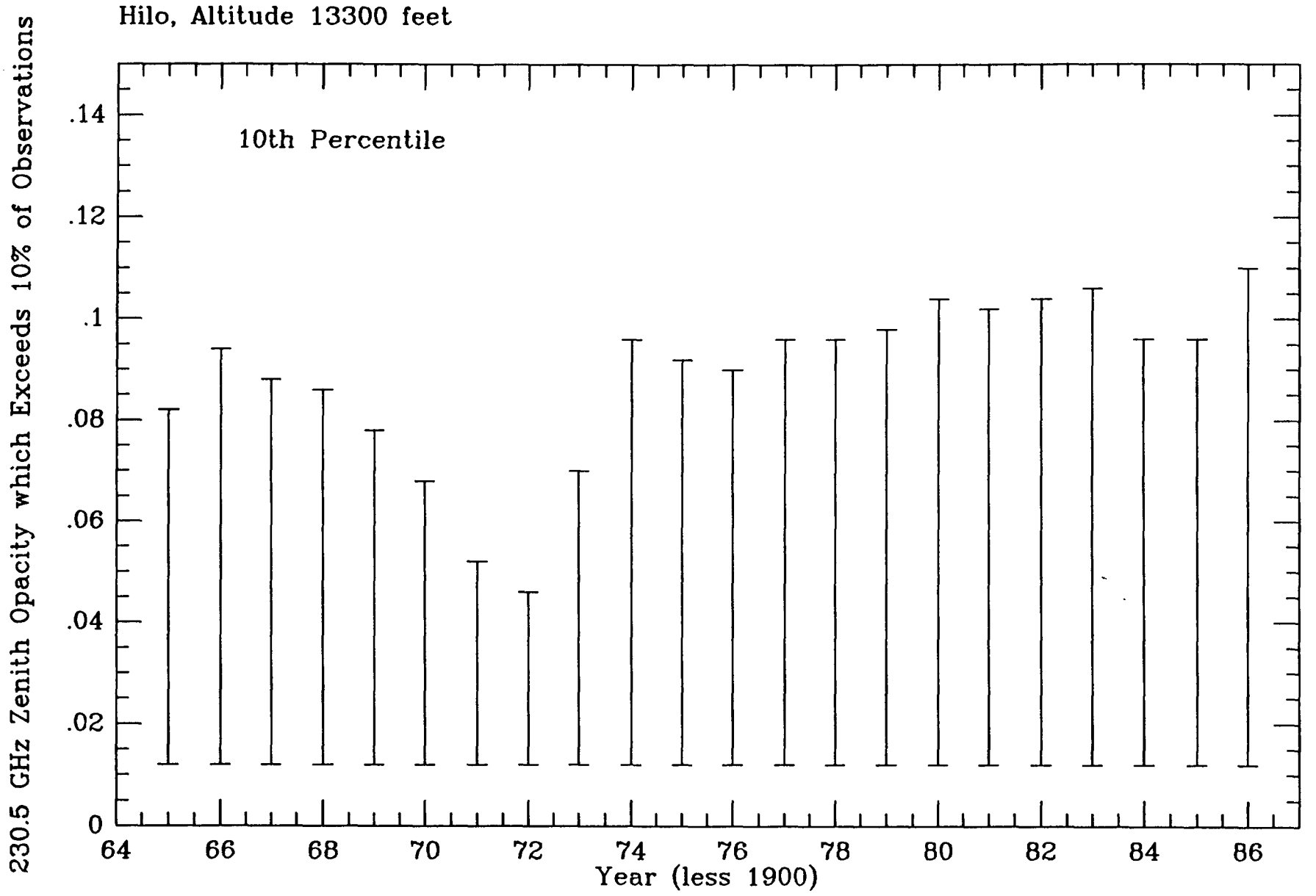

Figure 8.1(a-f). Statistics for Hilo (Mauna Kea) plotted against calendar year. (a.) 230.5 GHz zenith opacity which exceeds 10% of the observations.

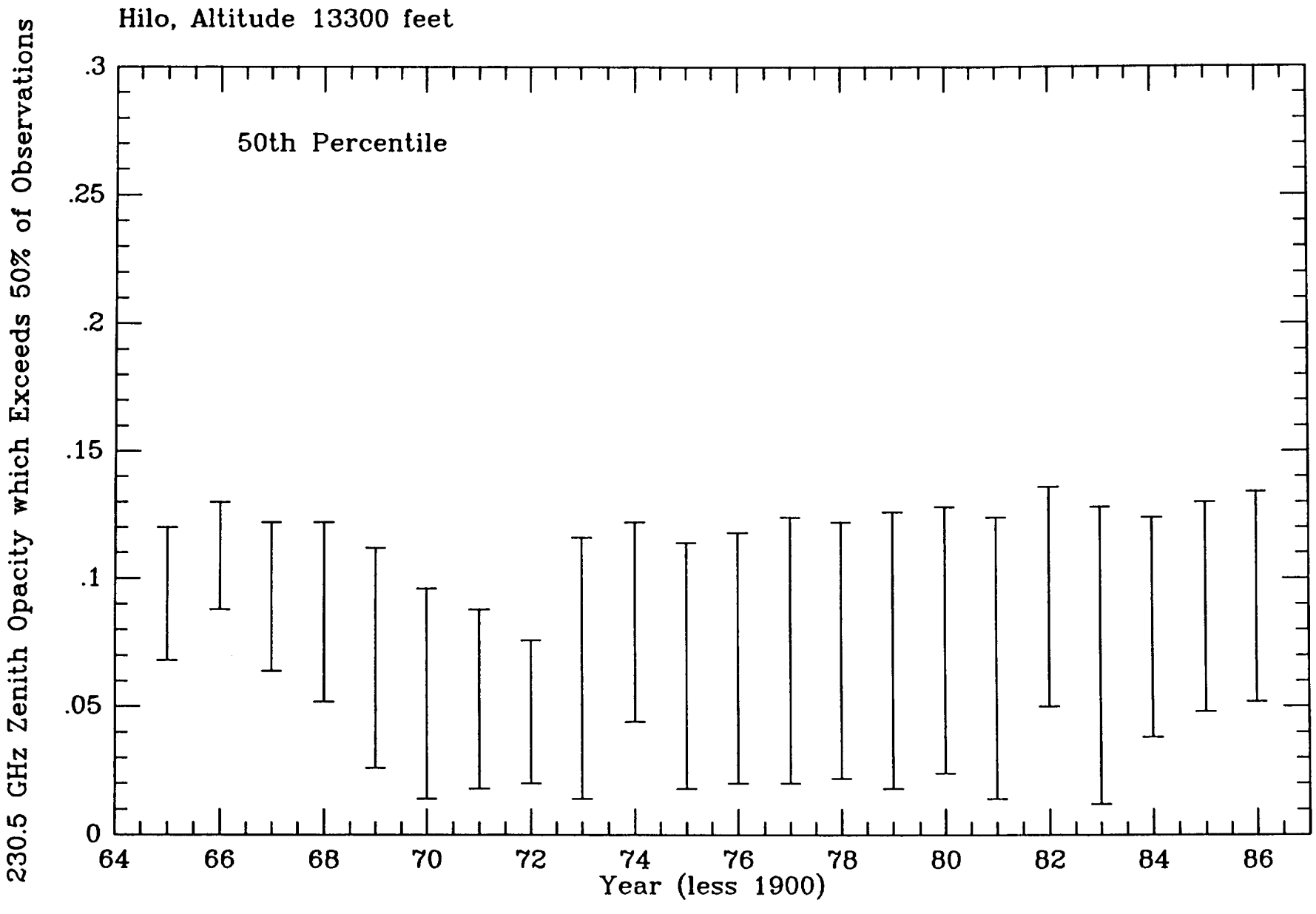

Figure 8.1(b.) 230.5 GHz zenith opacity which exceeds 50% of the observations (median opacity) at Hilo (Mauna Kea) vs. calendar year.

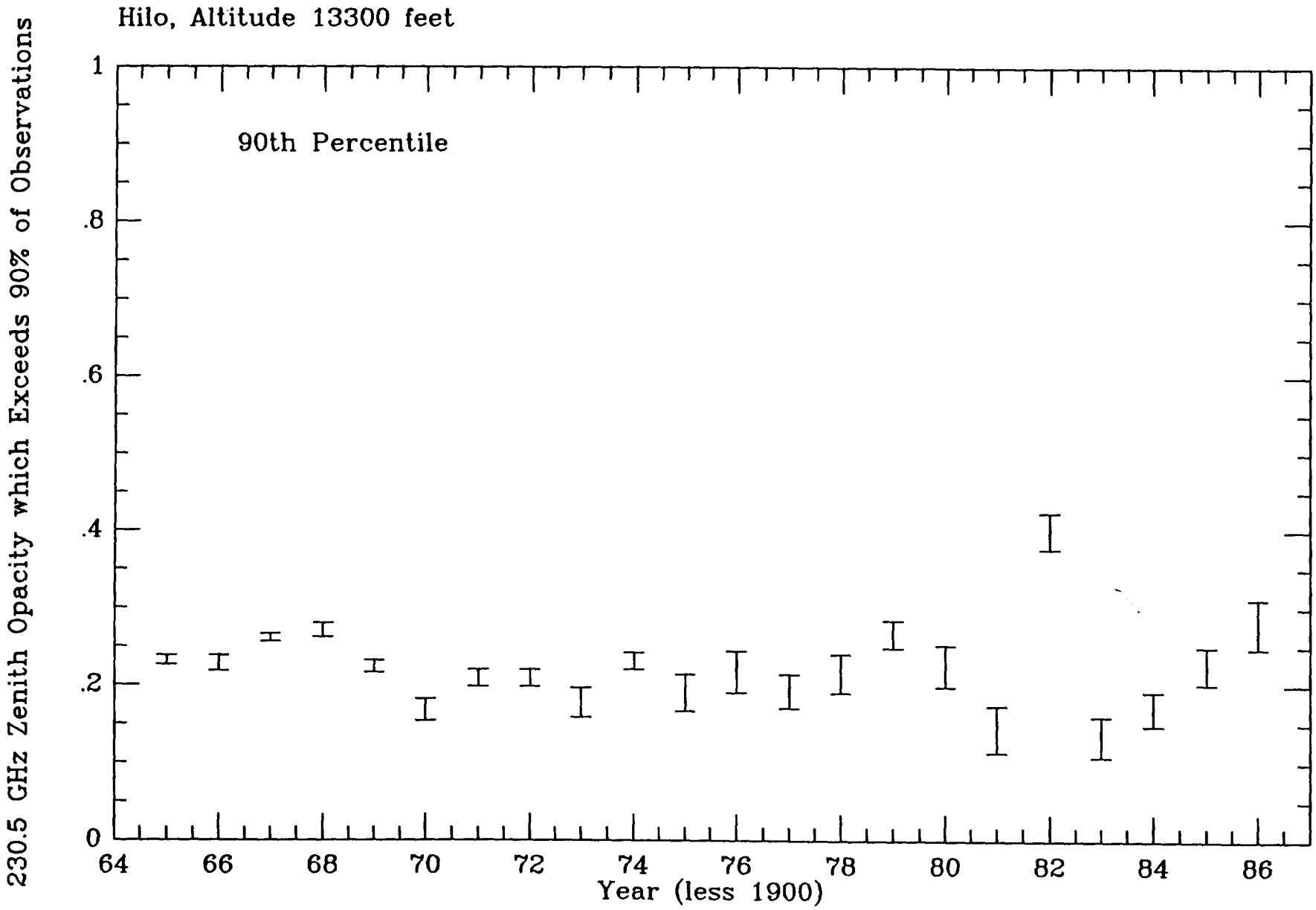

Figure 8.1(c.) 230.5 GHz zenith opacity which exceeds 90% of the observations at Hilo (Mauna Kea) vs. calendar year.

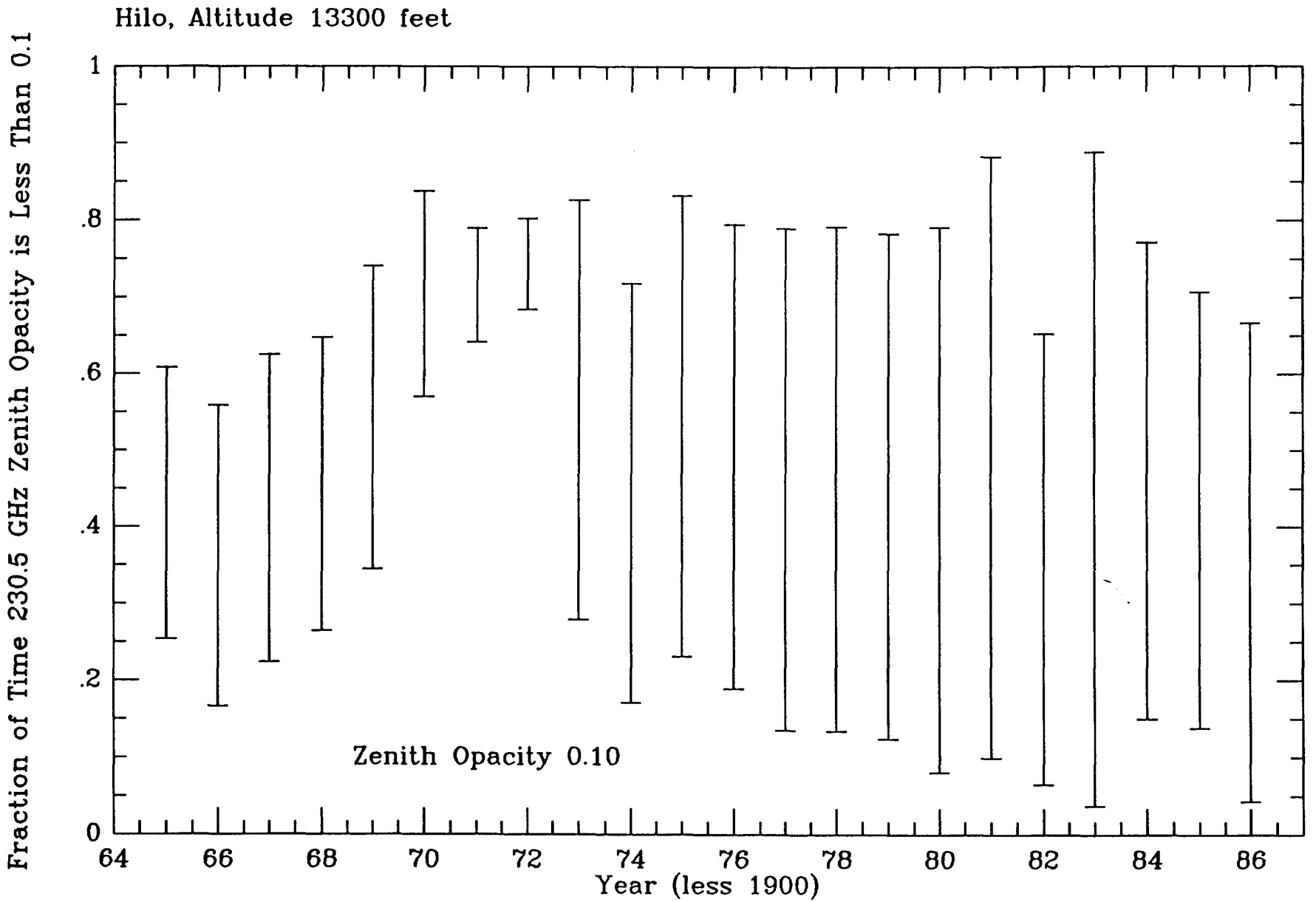

Figure 8.1(d.) Fraction of time 230.5 GHz zenith opacity is less than 0.1 at Hilo (Mauna Kea) vs. calendar year.

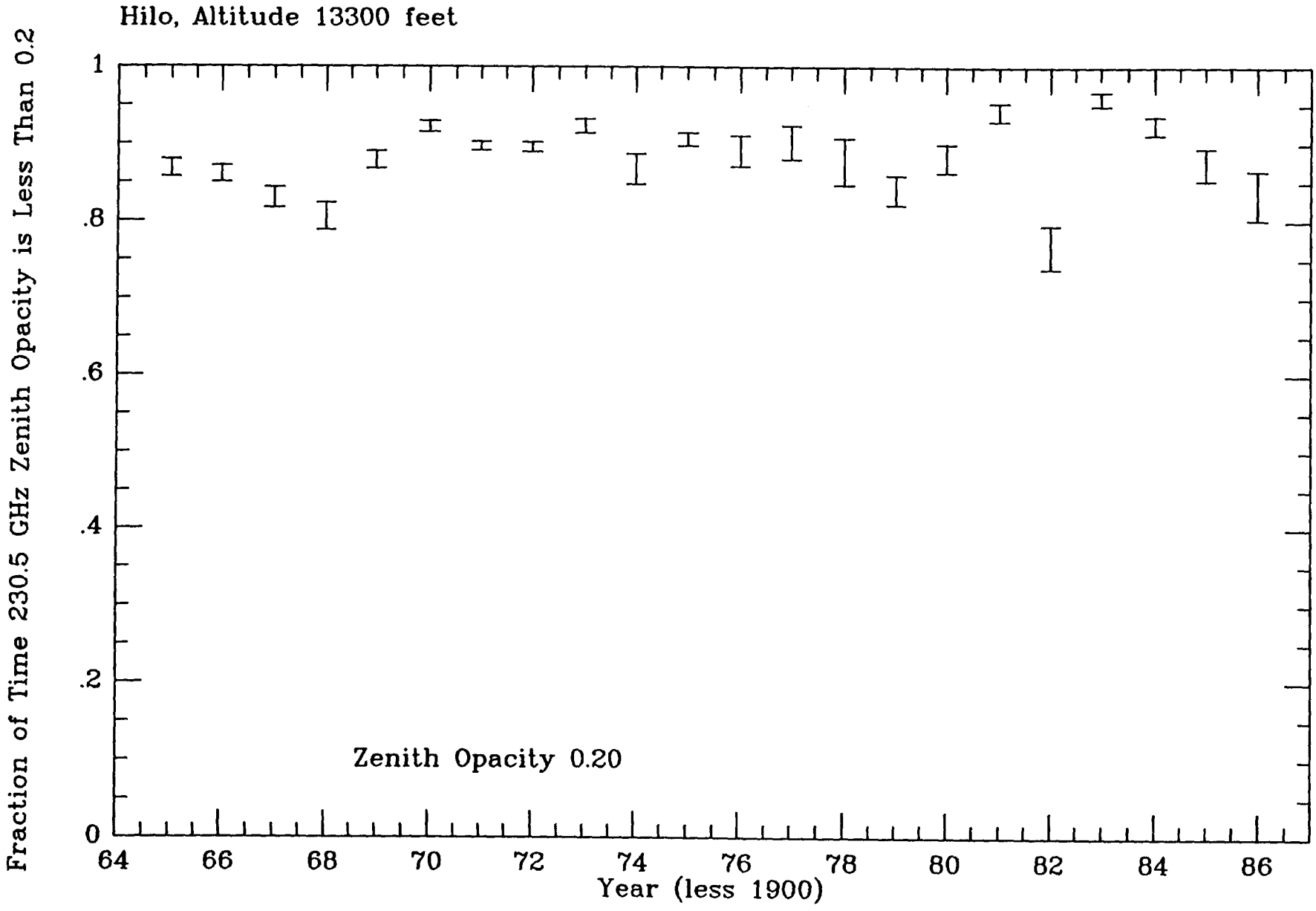

Figure 8.1(e.) Fraction of time 230.5 GHz zenith opacity is less than 0.2 at Hilo (Mauna Kea) vs. calendar year.

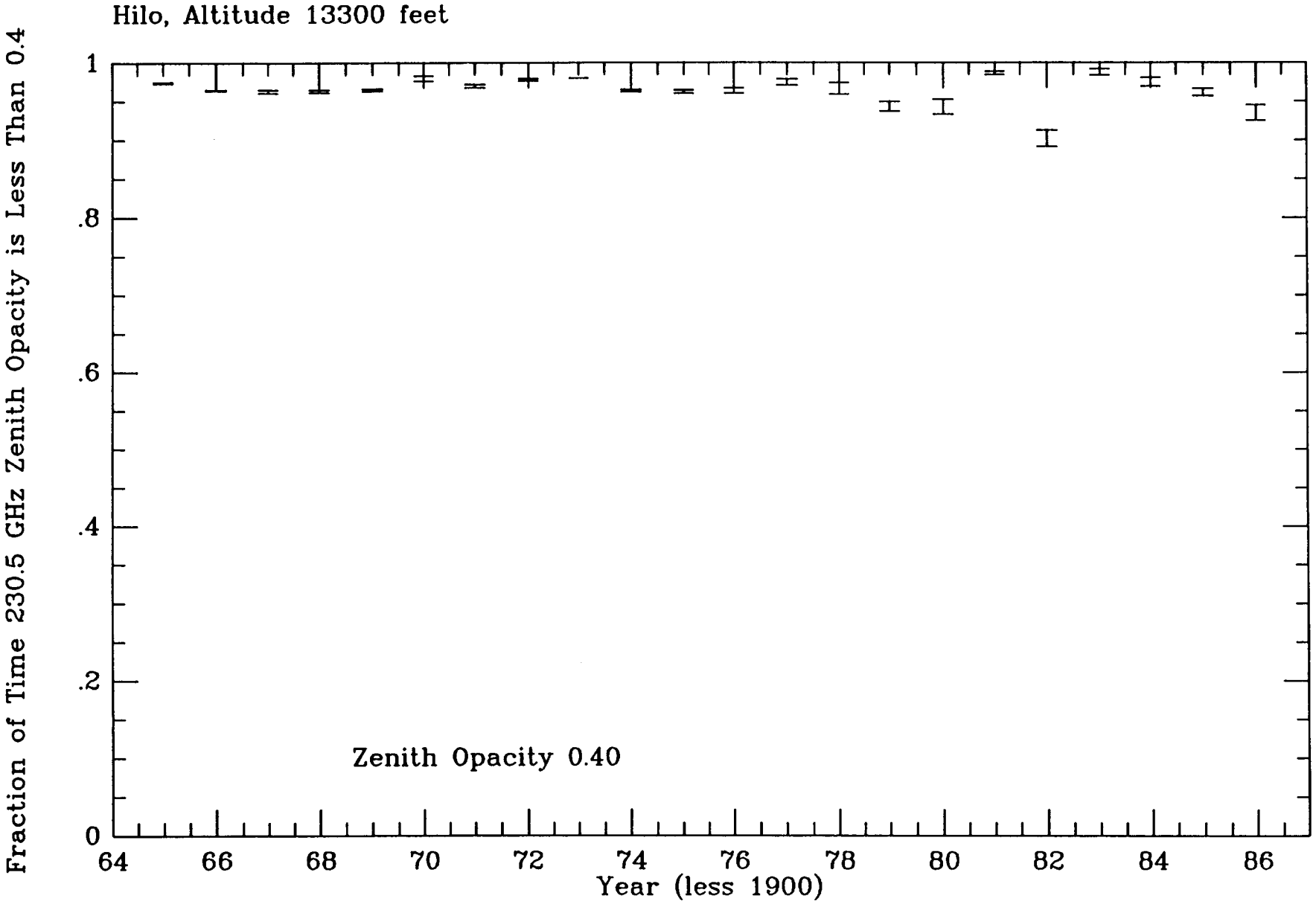

Figure 8.1(f.) Fraction of time 230.5 GHz zenith opacity is less than 0.4 at Hilo (Mauna Kea) vs. calendar year.

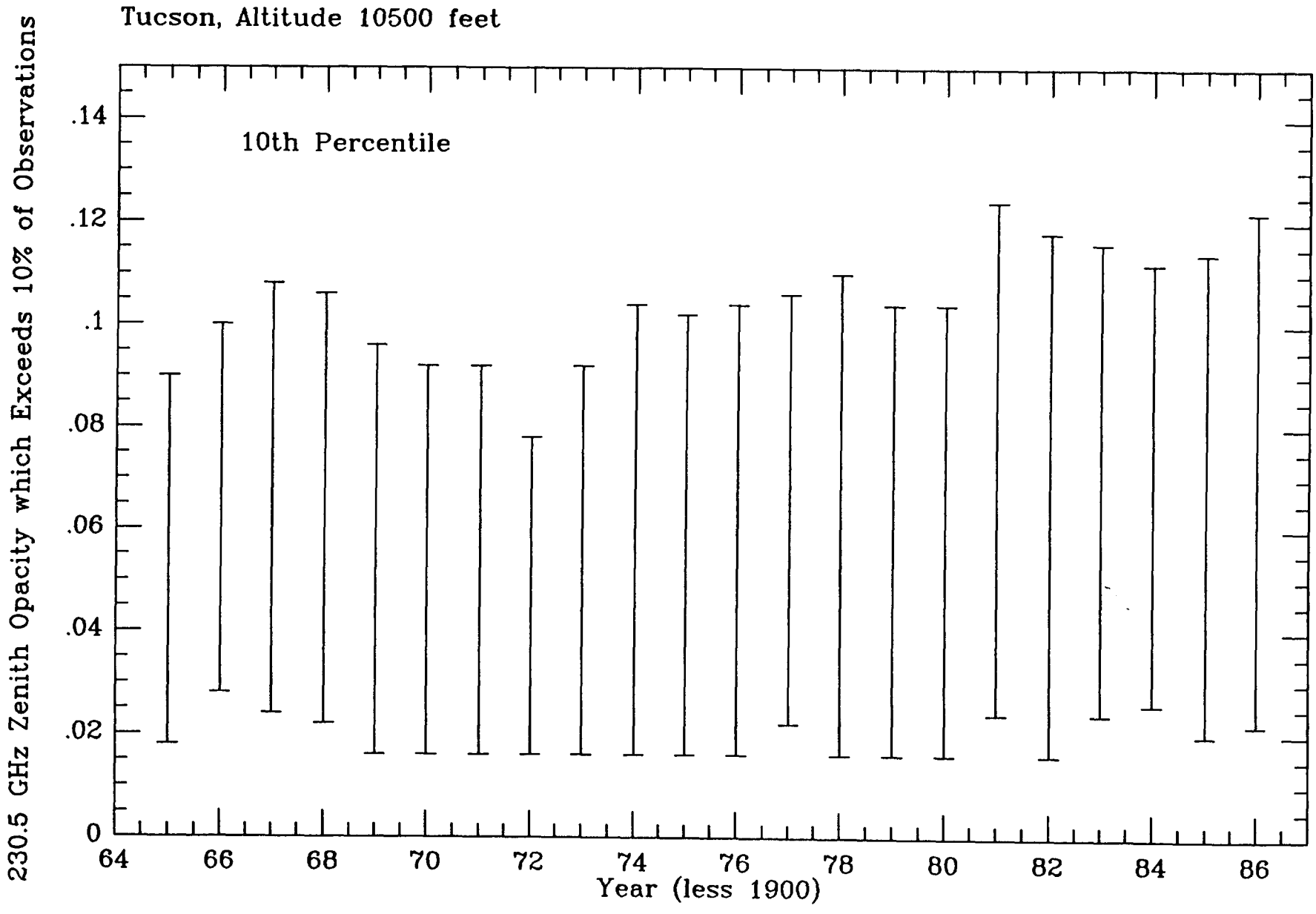

Figure 8.2(a-f). Statistics for Tucson (Mt. Graham) plotted against calendar year.
(a.) 230.5 GHz zenith opacity which exceeds 10% of the observations.

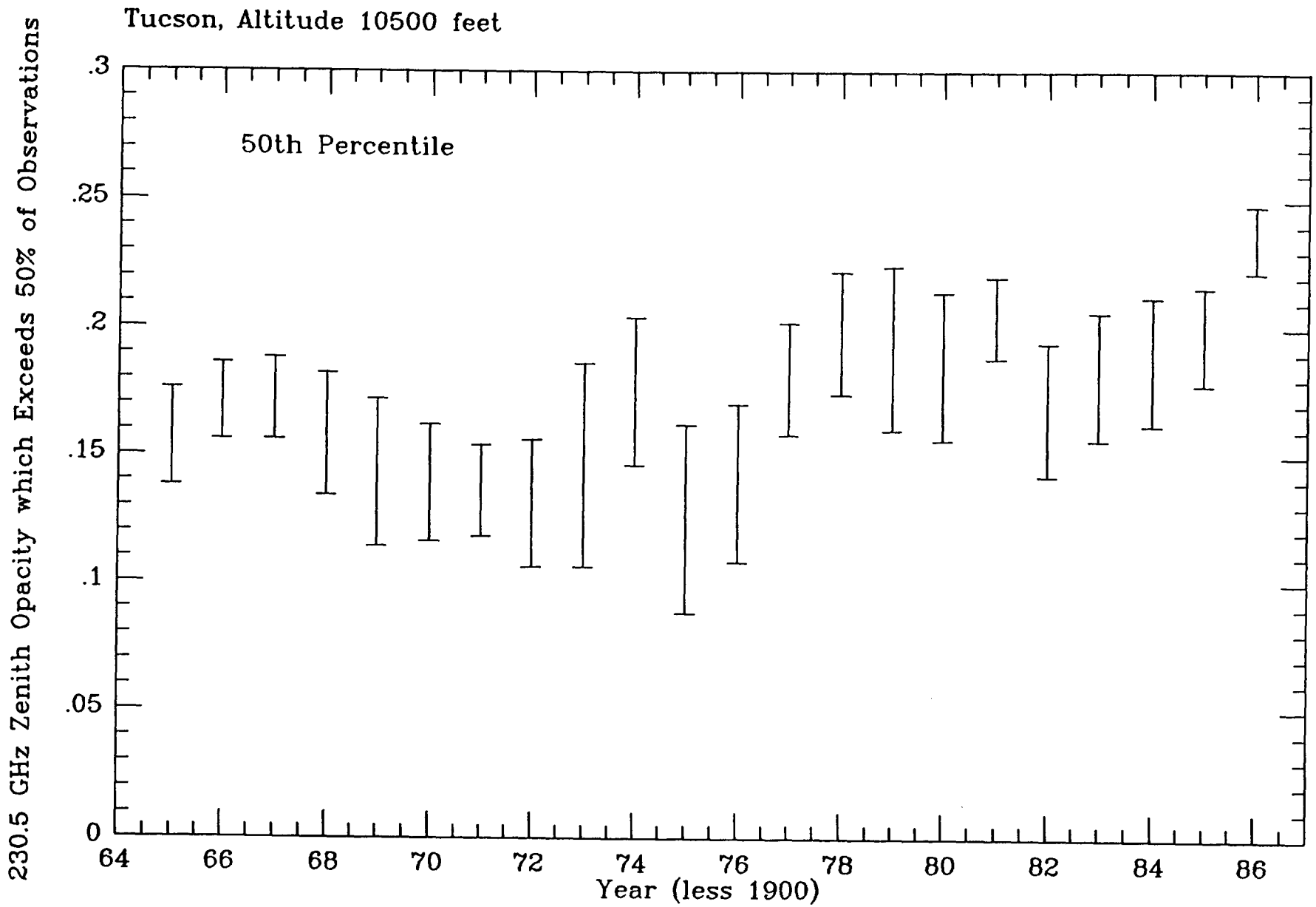

Figure 8.2(b.) 230.5 GHz zenith opacity which exceeds 50% of the observations (median opacity) at Tucson (Mt. Graham) vs. calendar year.

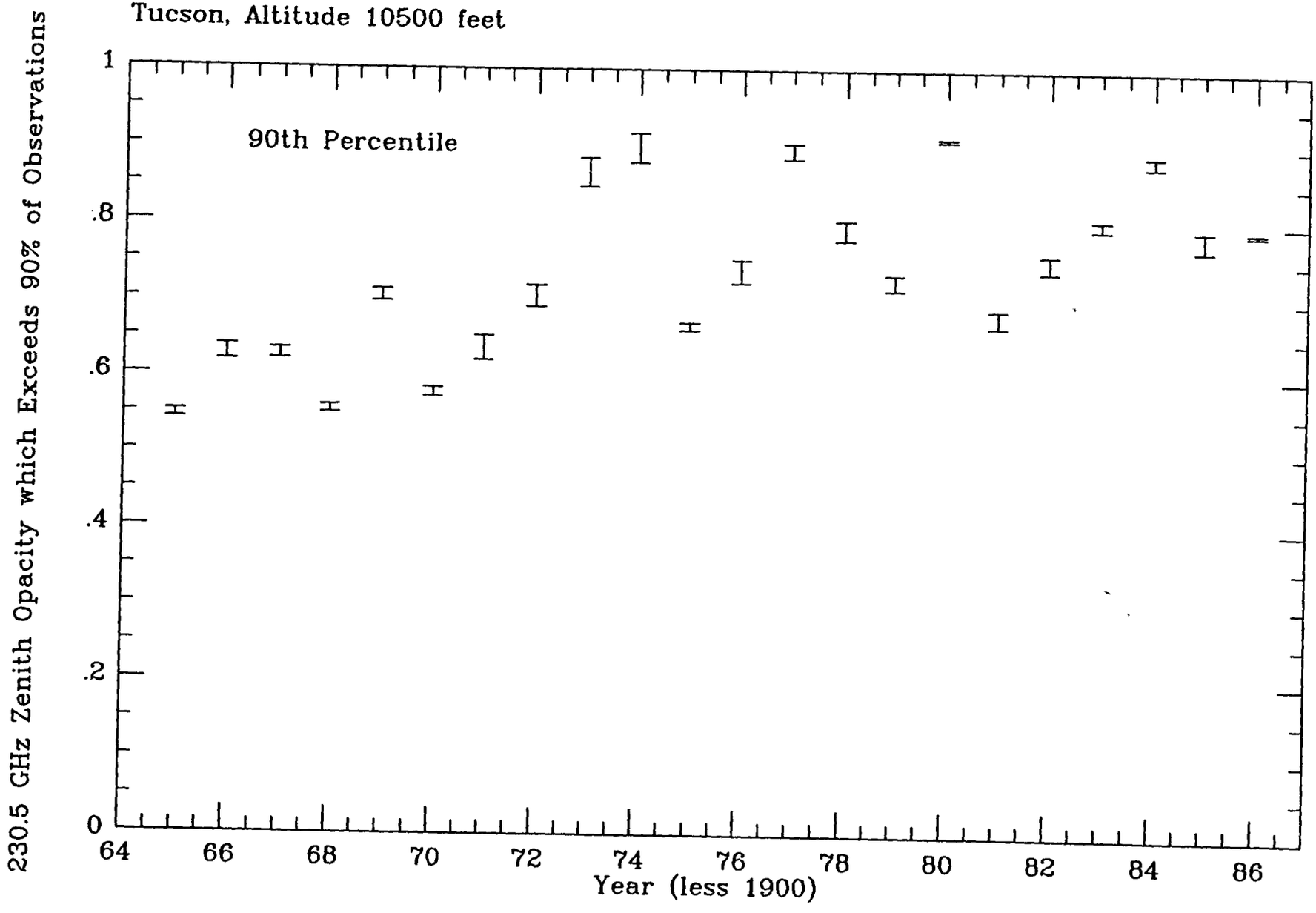

Figure 8.2(c.) 230.5 GHz zenith opacity which exceeds 90% of the observations at Tucson (Mt. Graham) vs. calendar year.

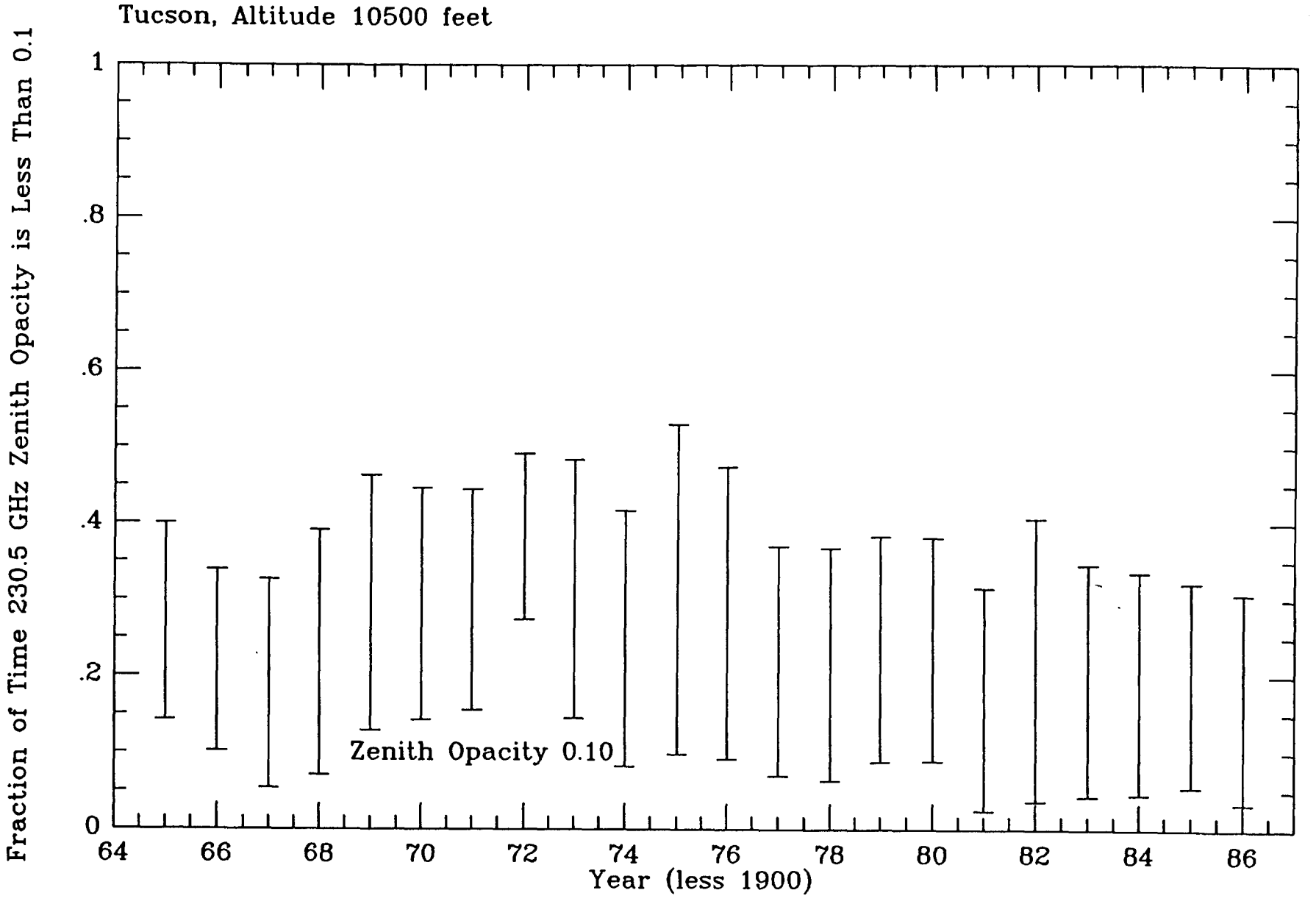

Figure 8.2(d.) Fraction of time 230.5 GHz zenith opacity is less than 0.1 at Tucson (Mt. Graham) vs. calendar year.

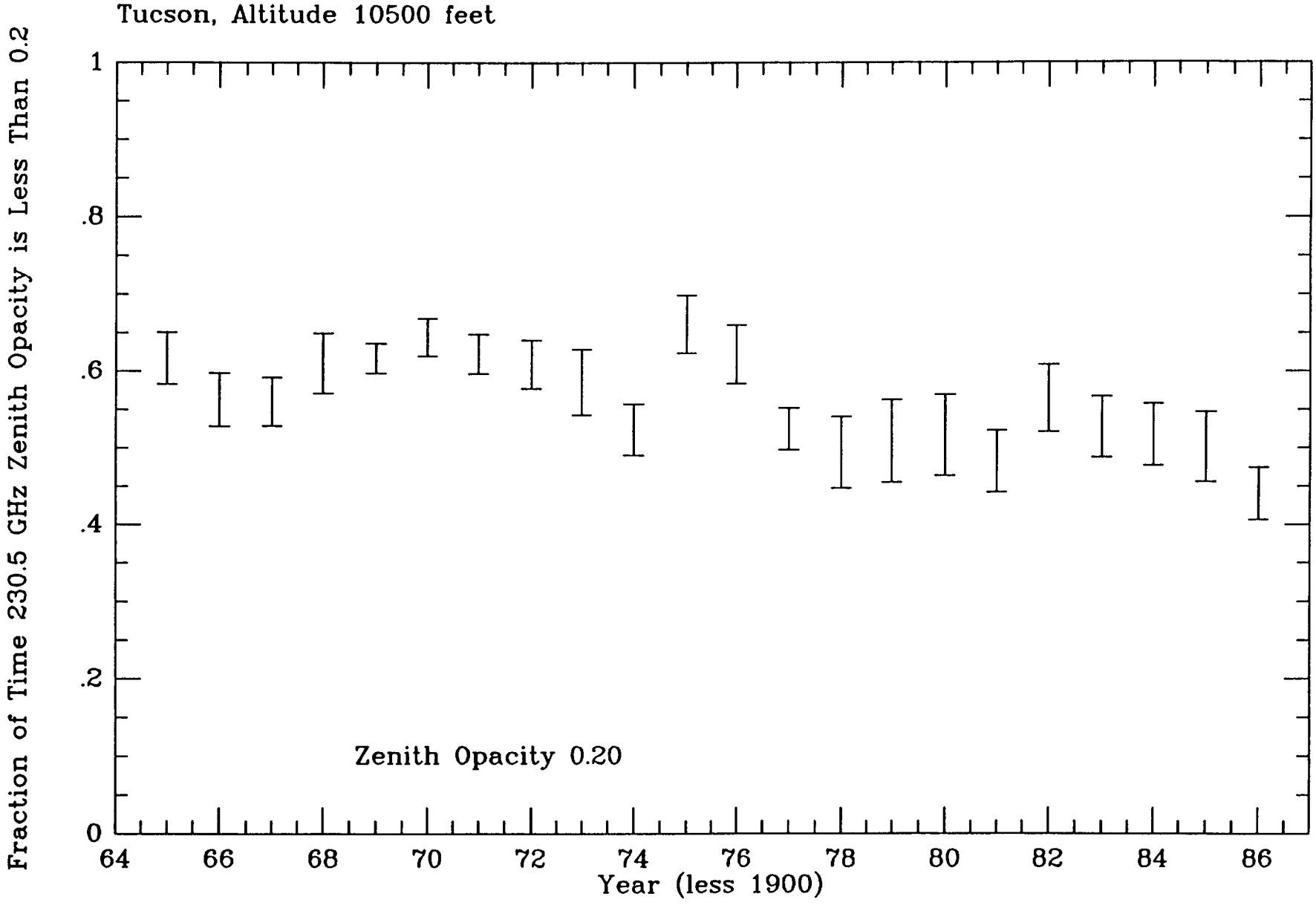

Figure 8.2(e.) Fraction of time 230.5 GHz zenith opacity is less than 0.2 at Tucson (Mt. Graham) vs. calendar year.

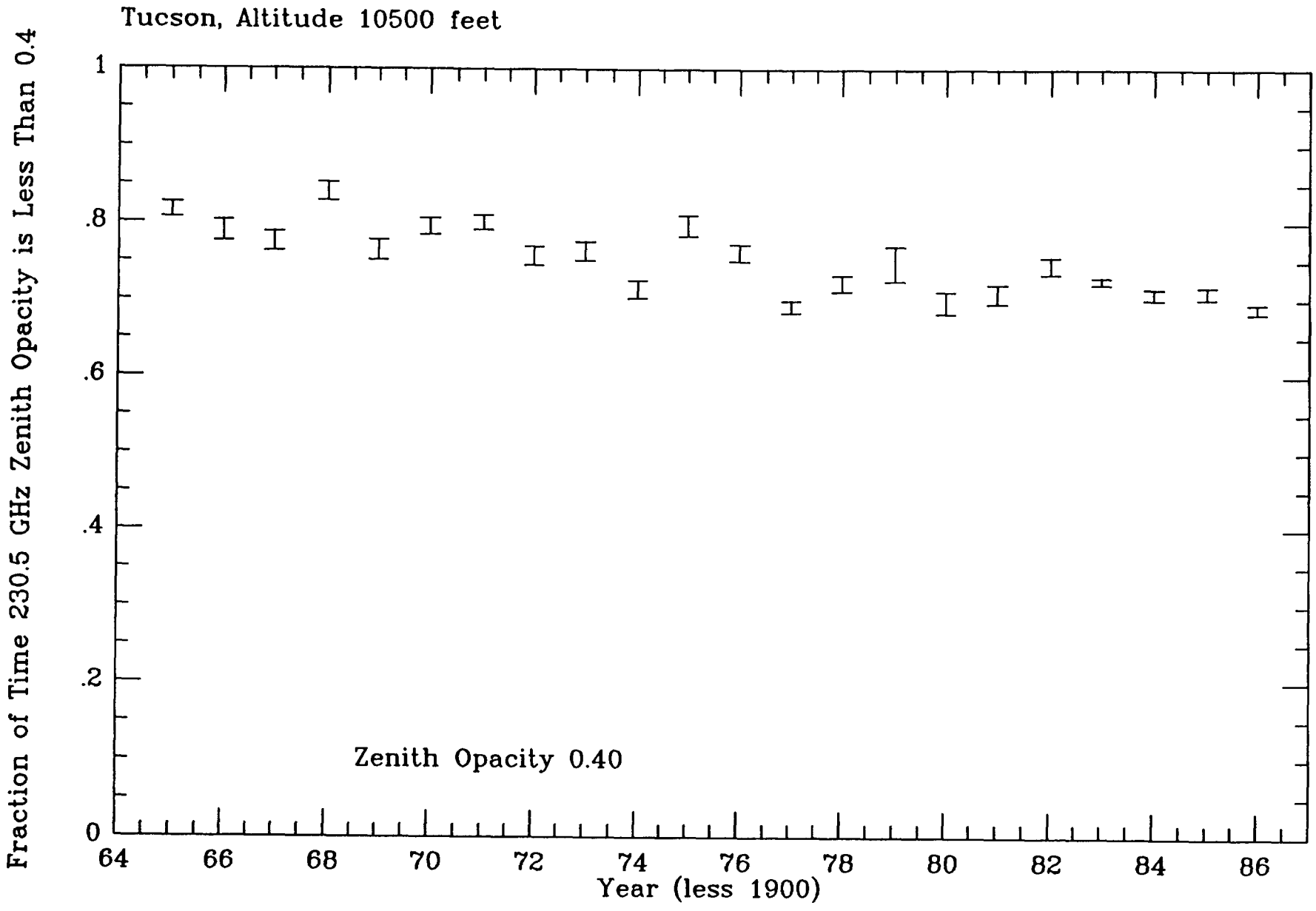

Figure 8.2(f.) Fraction of time 230.5 GHz zenith opacity is less than 0.4 at Tucson (Mt. Graham) vs. calendar year.

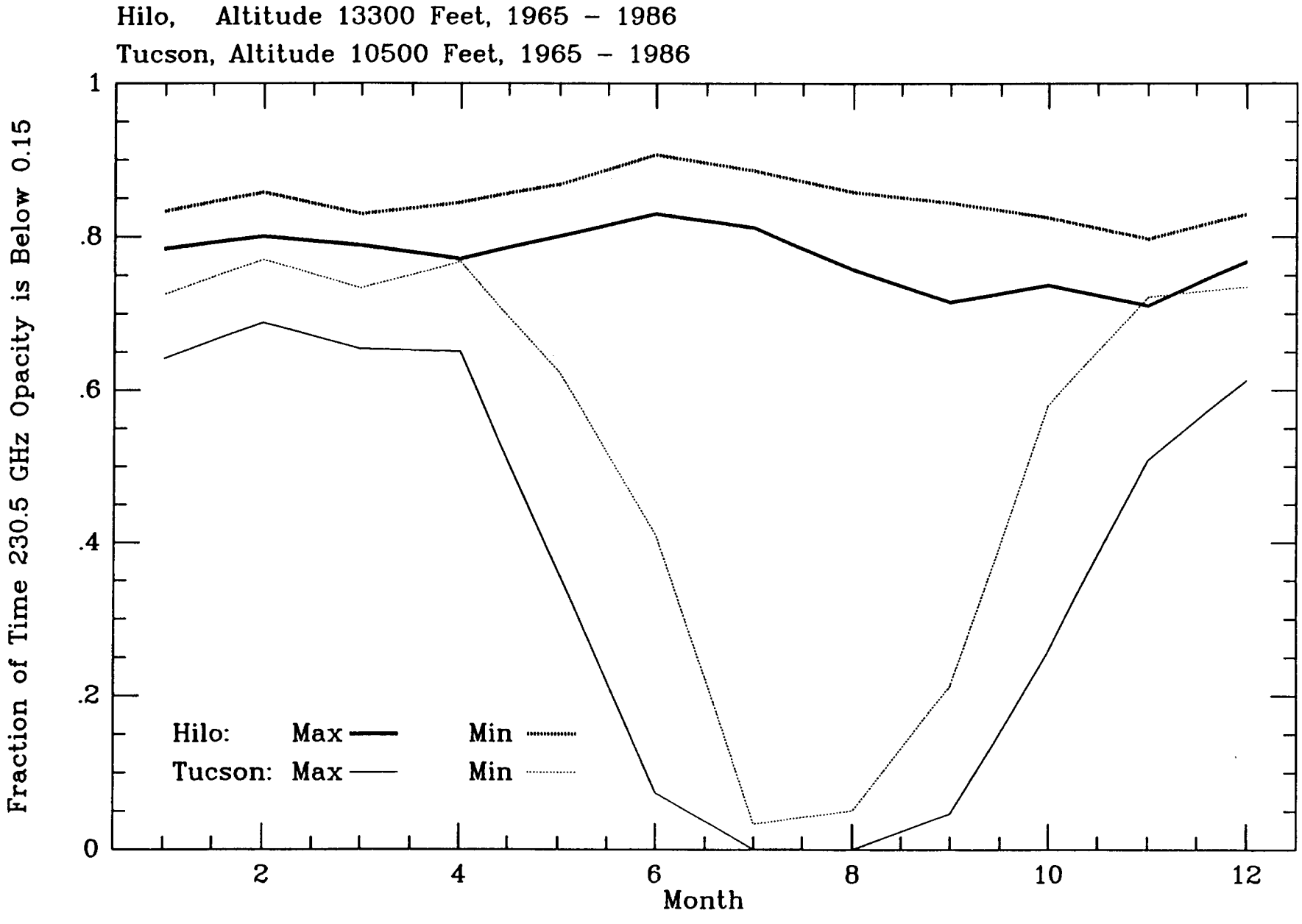

Figure 9. Comparison of cumulative probability of zenith opacity < 0.15 for each month of year for Hilo (Mauna Kea) and Tucson (Mt. Graham). Data from January 1965 to October 1986.

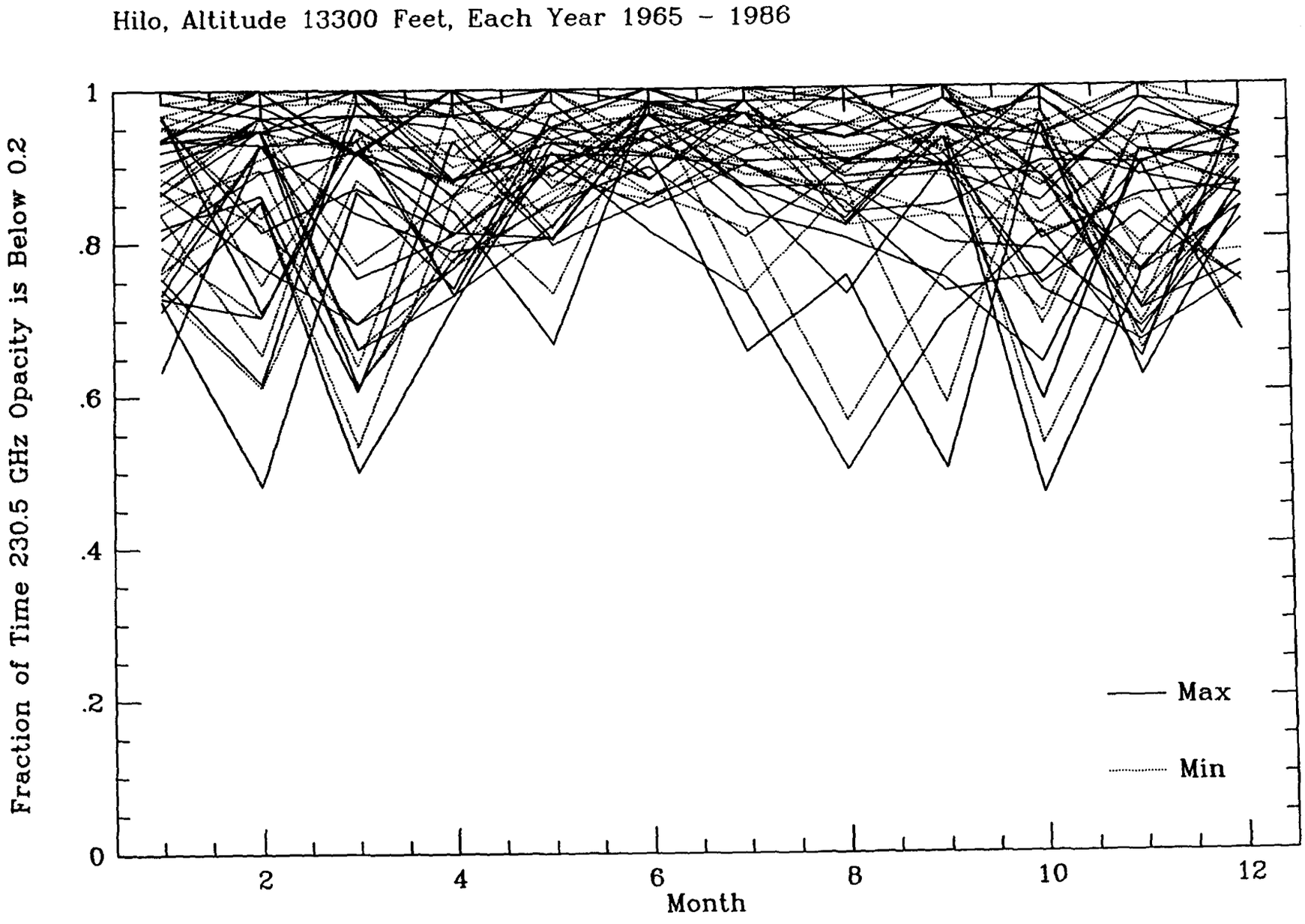

Figure 10(a-b). Same as Figure 9, but each year plotted separately. (a.) Hilo (Mauna Kea).

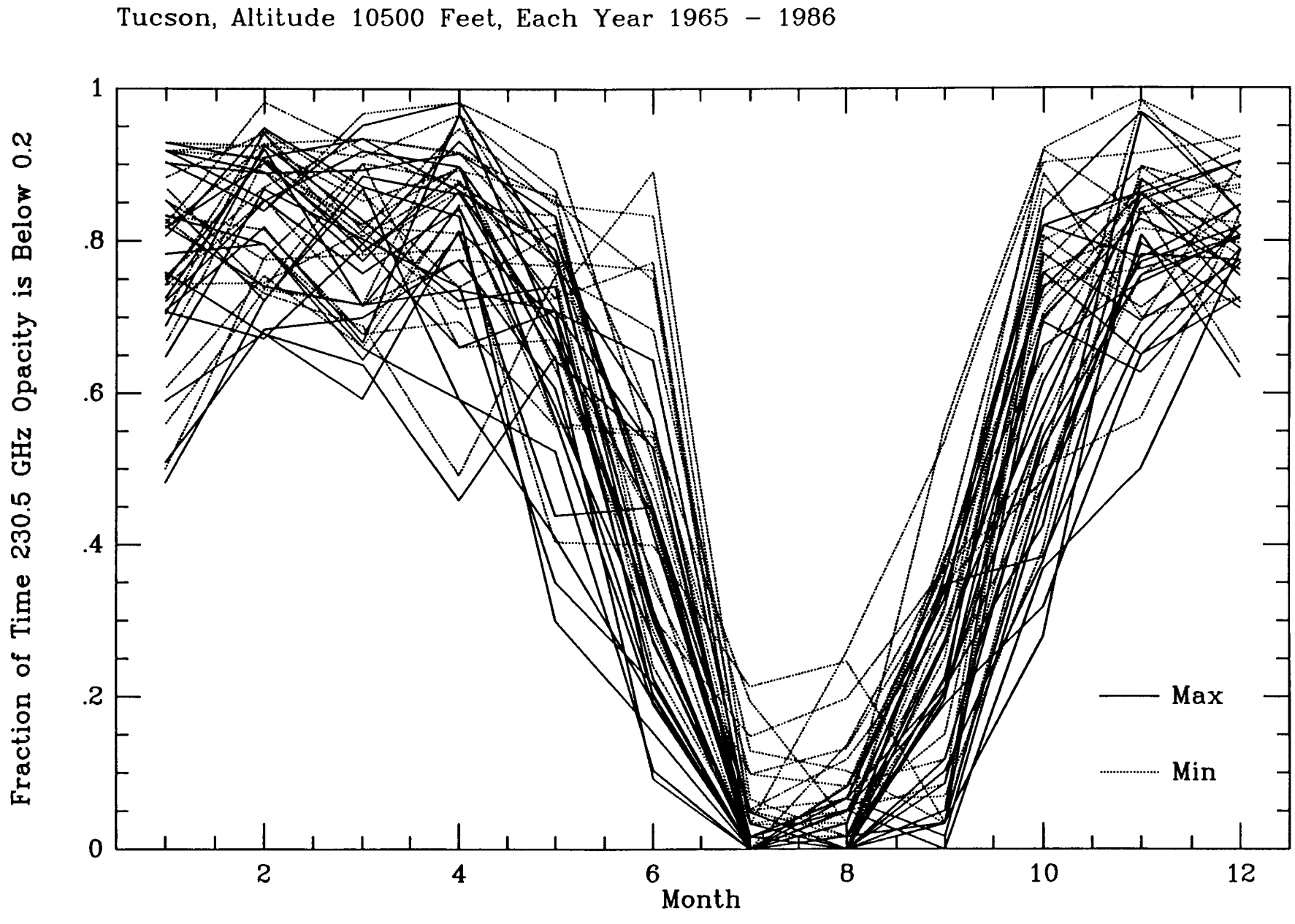

Figure 10(b). Tucson (Mt. Graham).

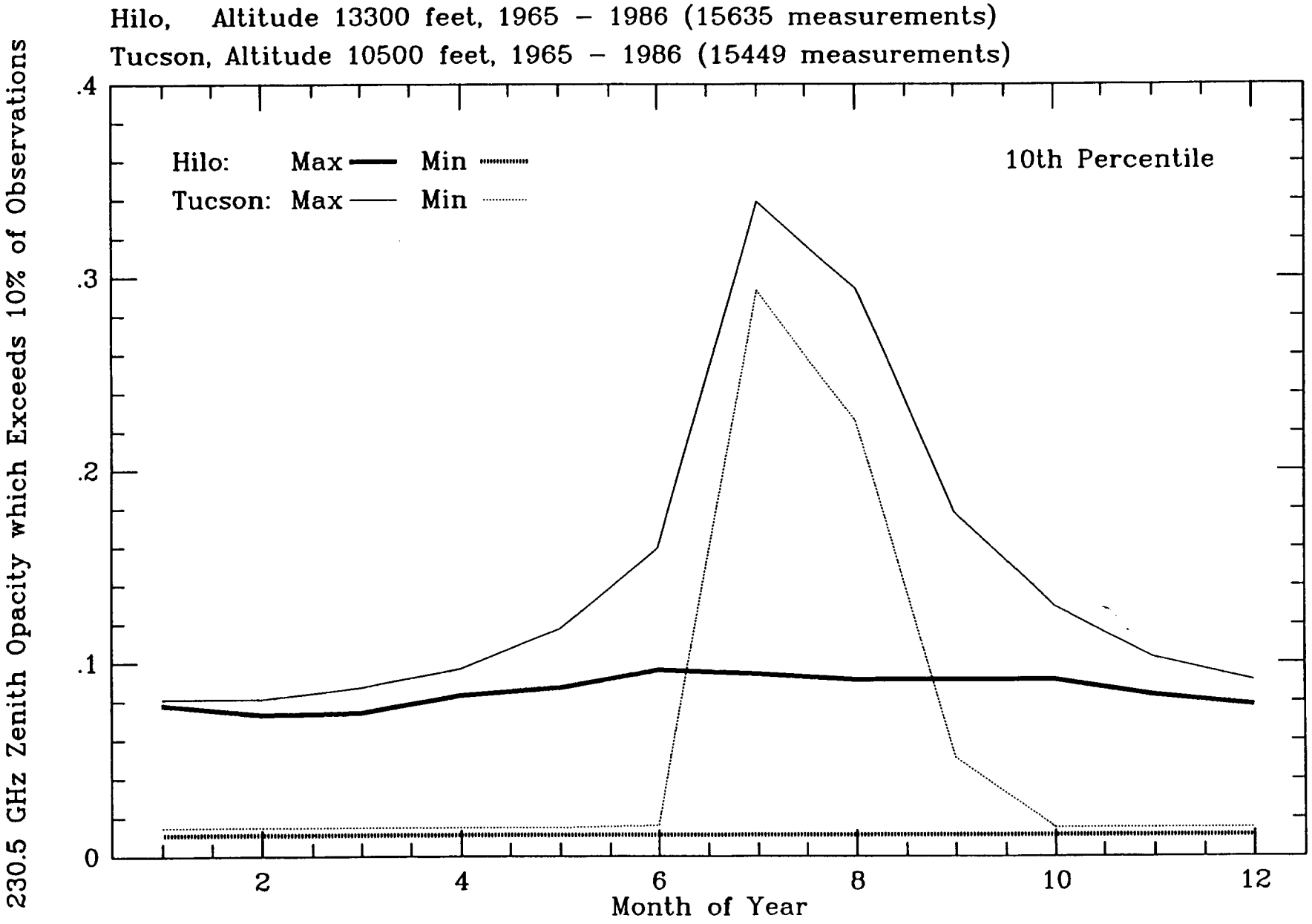

Figure 11(a-c). Opacity value at 10^{th}, 50^{th}, and 90^{th} percentile vs. month of year. Data from January 1965 to October 1986. (a.) 10^{th} percentile.

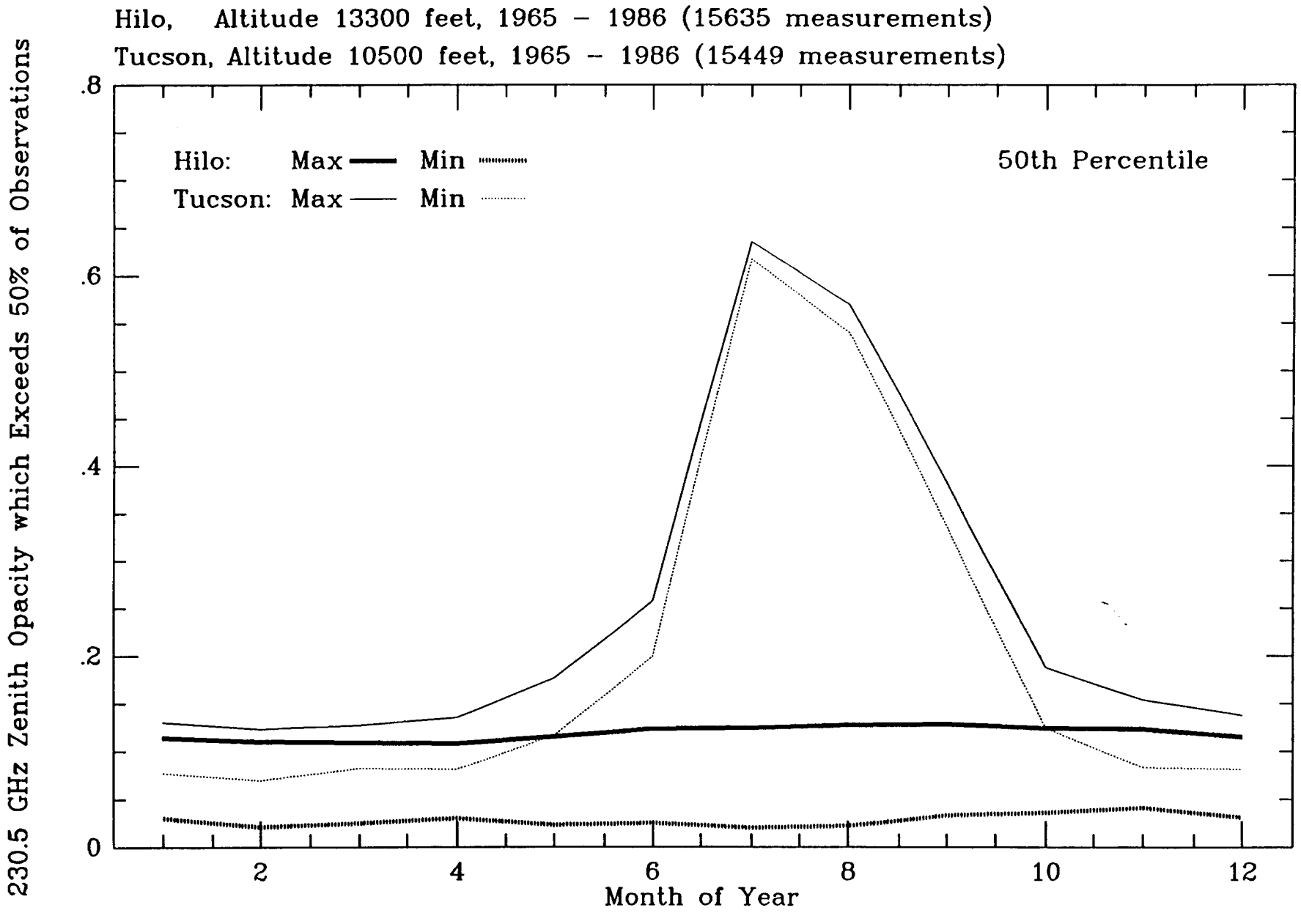

Figure 11(b). 50^{th} percentile (median).

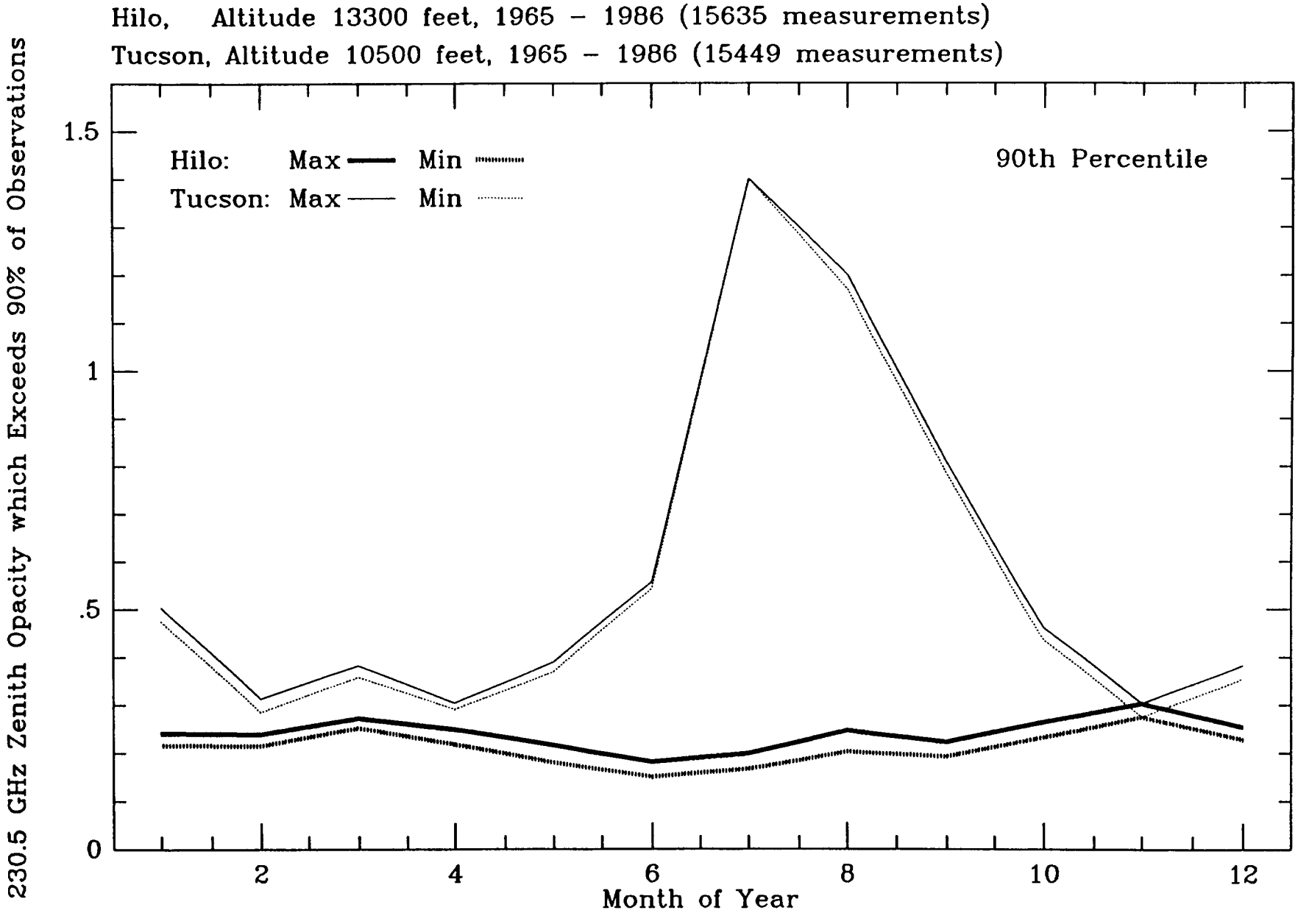

Figure 11(c). 90^{th} percentile.

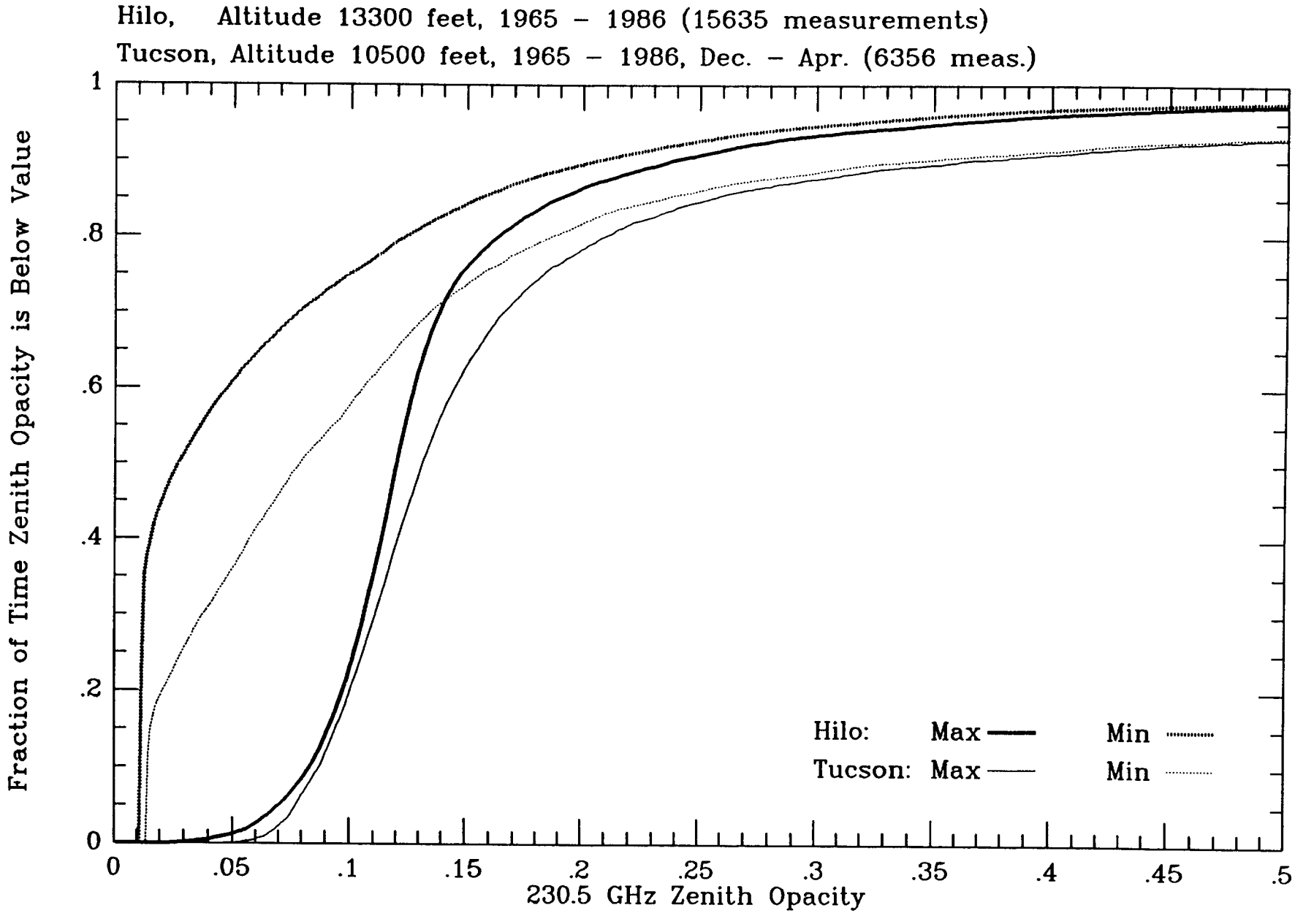

Figure 12. Comparison of best months (December to April) at Tucson (Mt. Graham) with year round data for Hilo (Mauna Kea). Curves show cumulative probability distributions of zenith opacities. Data fr[redacted]period January 1965 to October 1986.

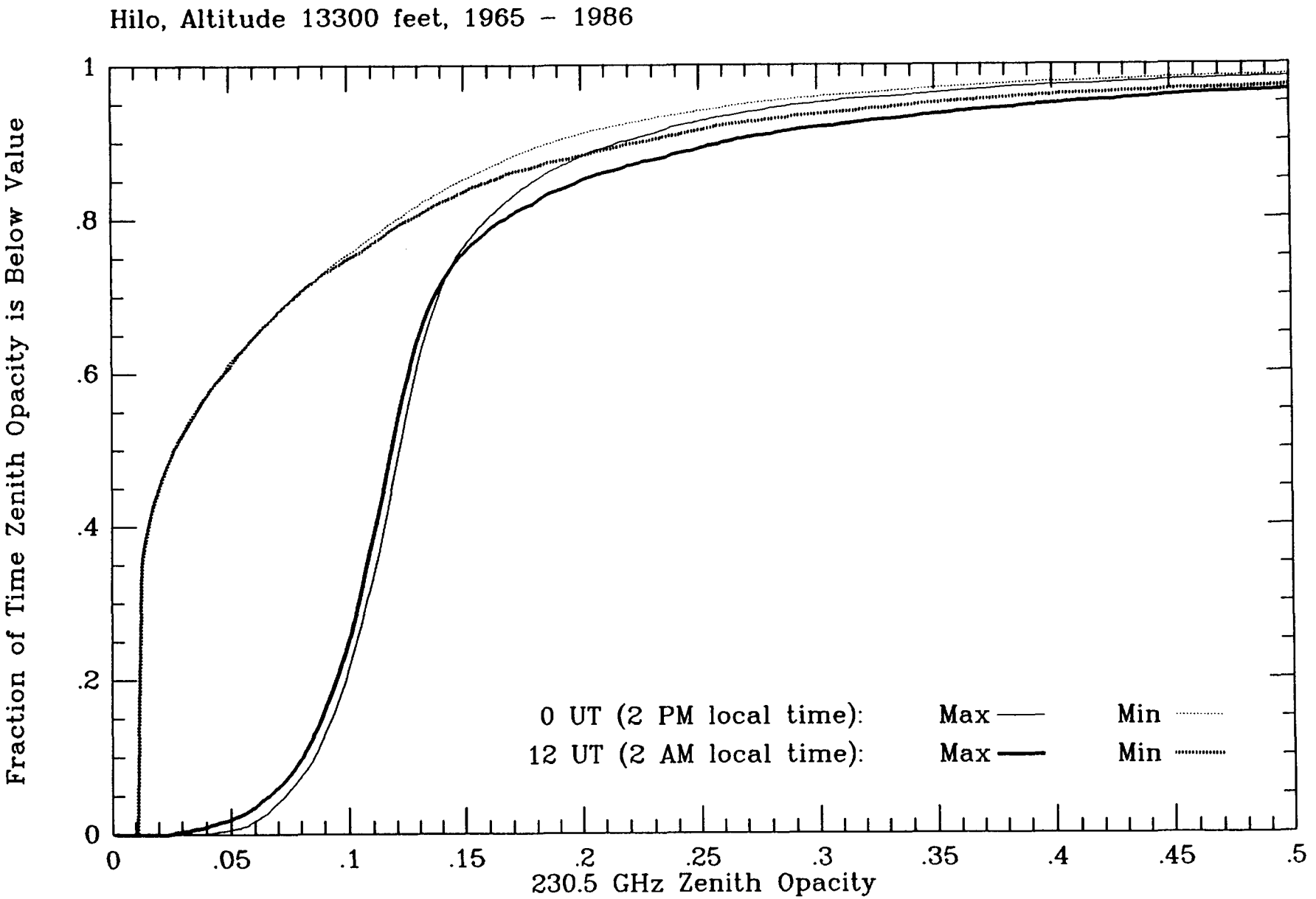

Figure 13(a-b). Comparison of 0 and 12 UT opacities. Curves show cumulative probability distribution of zenith opacities. Data from period January 1965 to October 1986. (a.) Hilo (Mauna Kea).

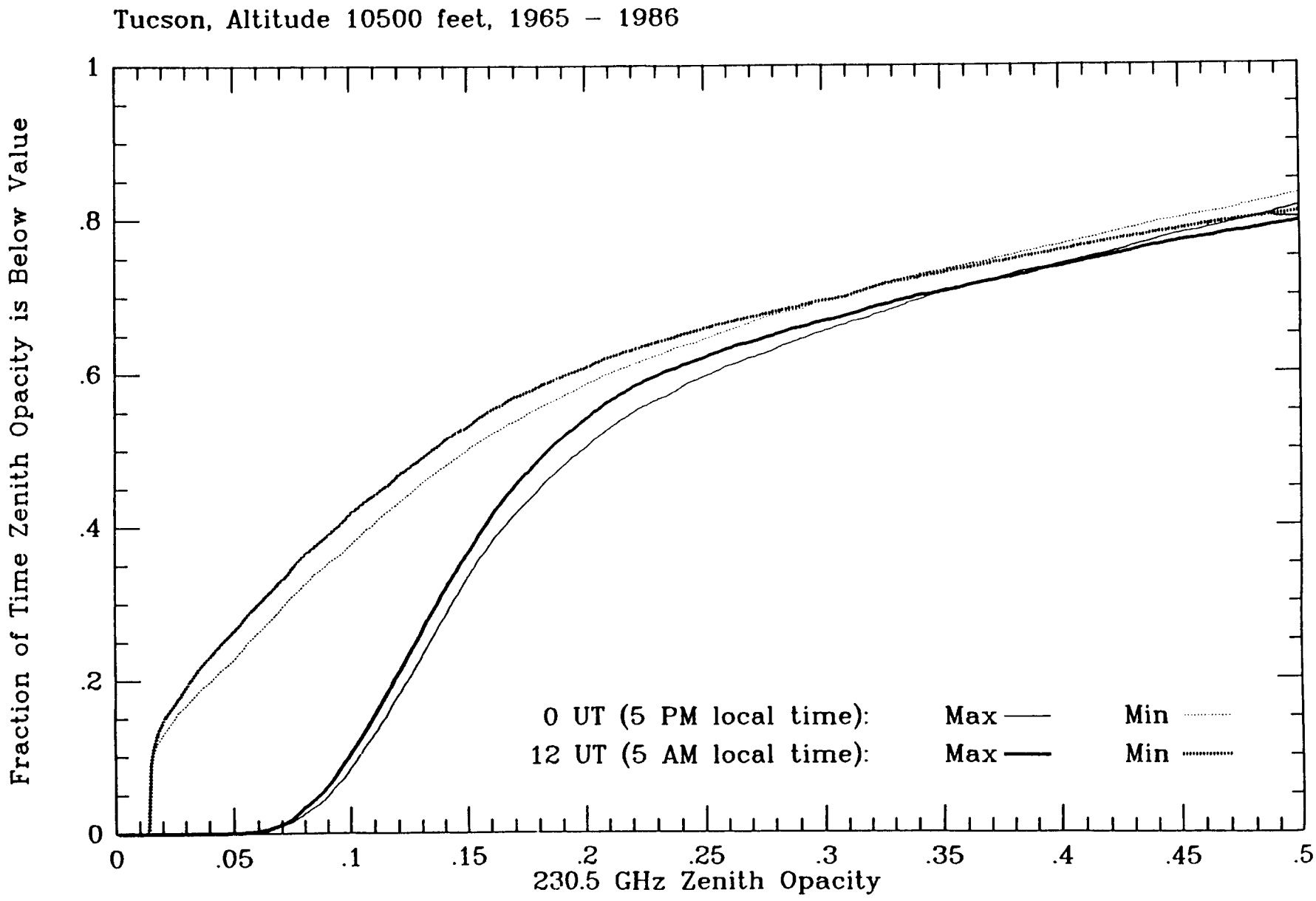

Figure 13(b). Tucson (Mt. Graham).

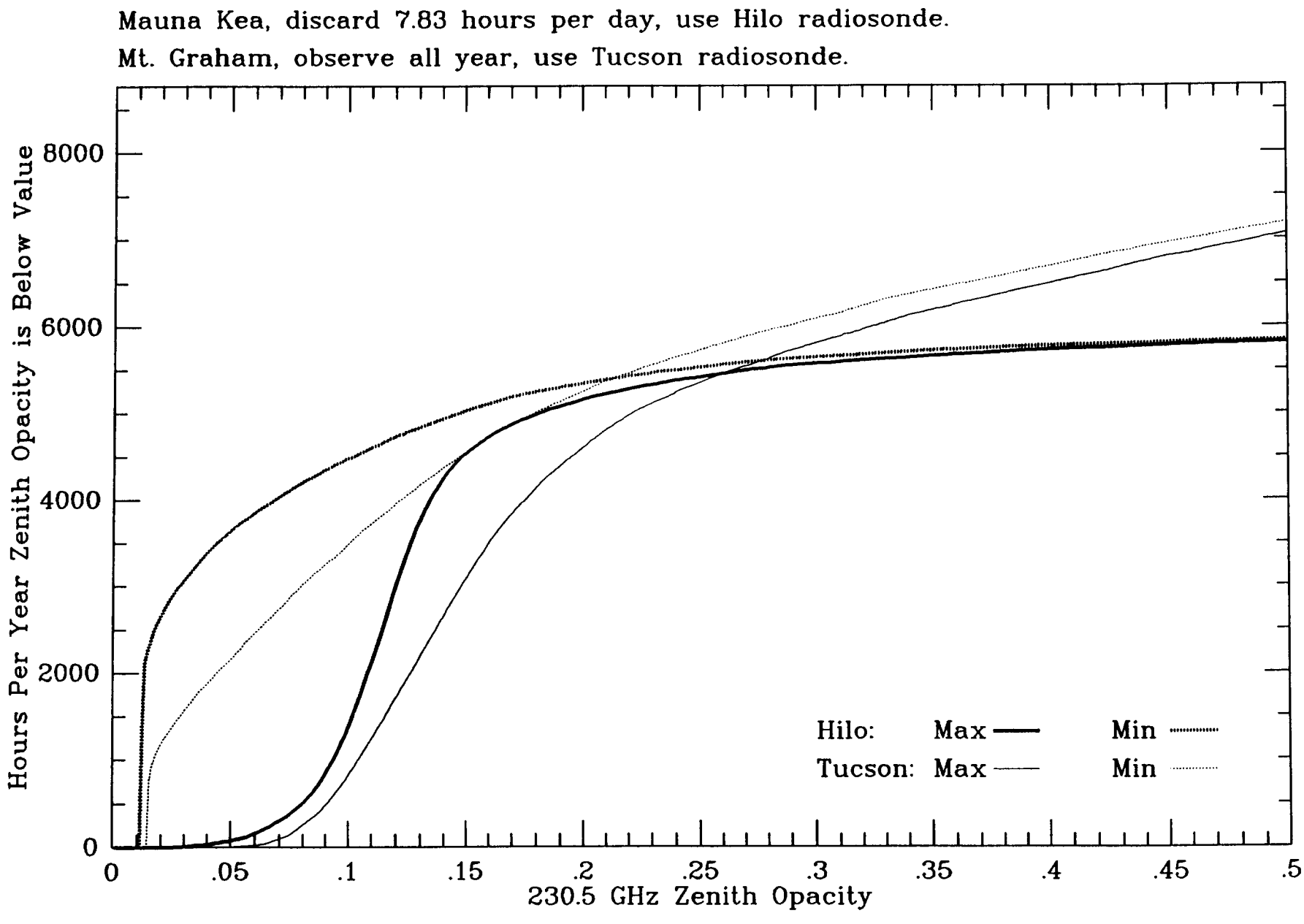

Figure 14(a-b). Effect of losing time at Mauna Kea due to diurnal (afternoon) opacity increase. Curves show hours per year opacity is below value. (a.) Both sites have same number of hours per year (up to $\tau \sim 0.2$ when >7.83 hrs day^{-1} lost at Mauna Kea.

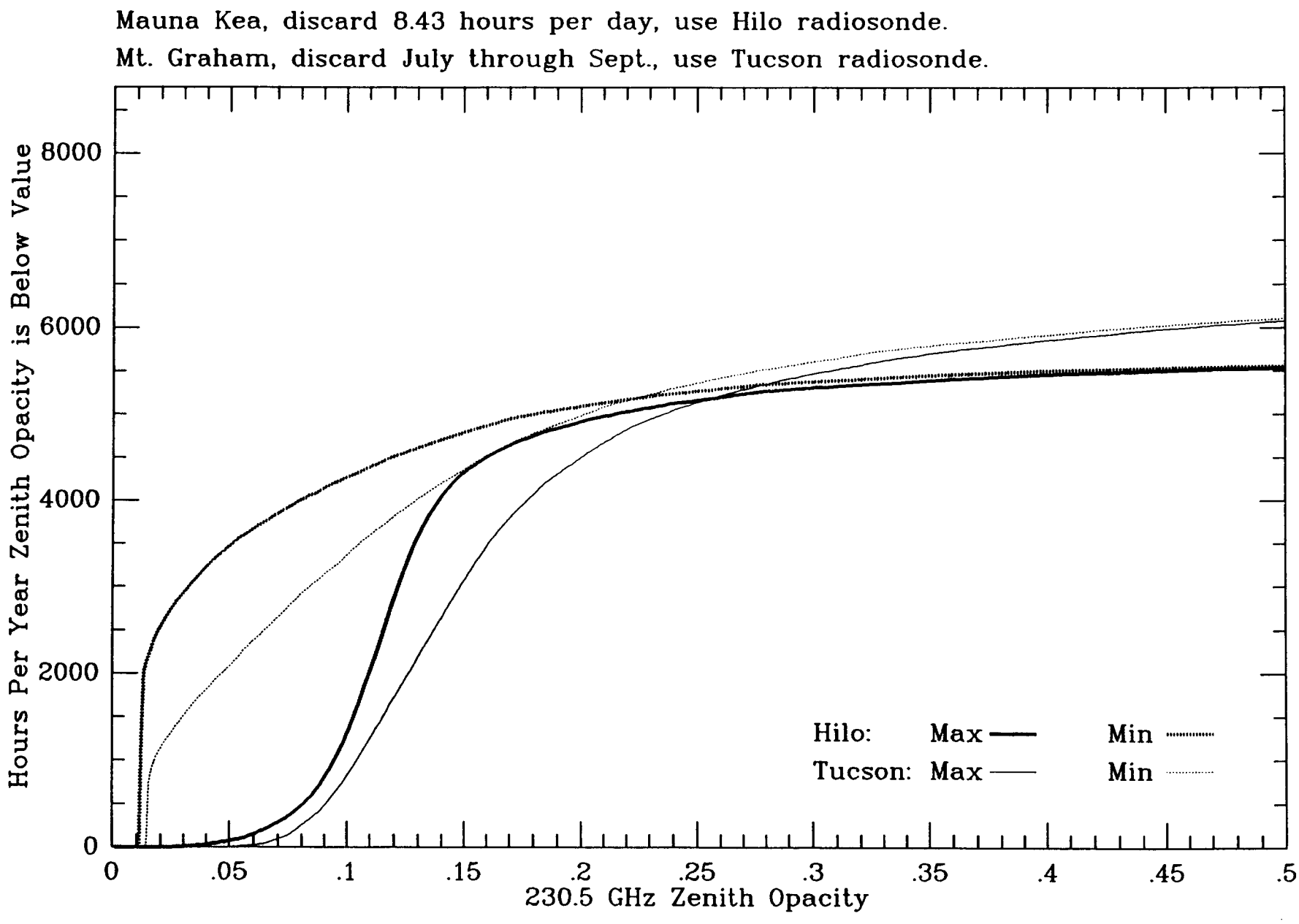

Figure 14(b). Both sites have same hours per year (up to $\tau \sim 0.28$) when >8.43 hrs day^{-1} lost at Mauna Kea, and summer months discarded at Mt. Graham.

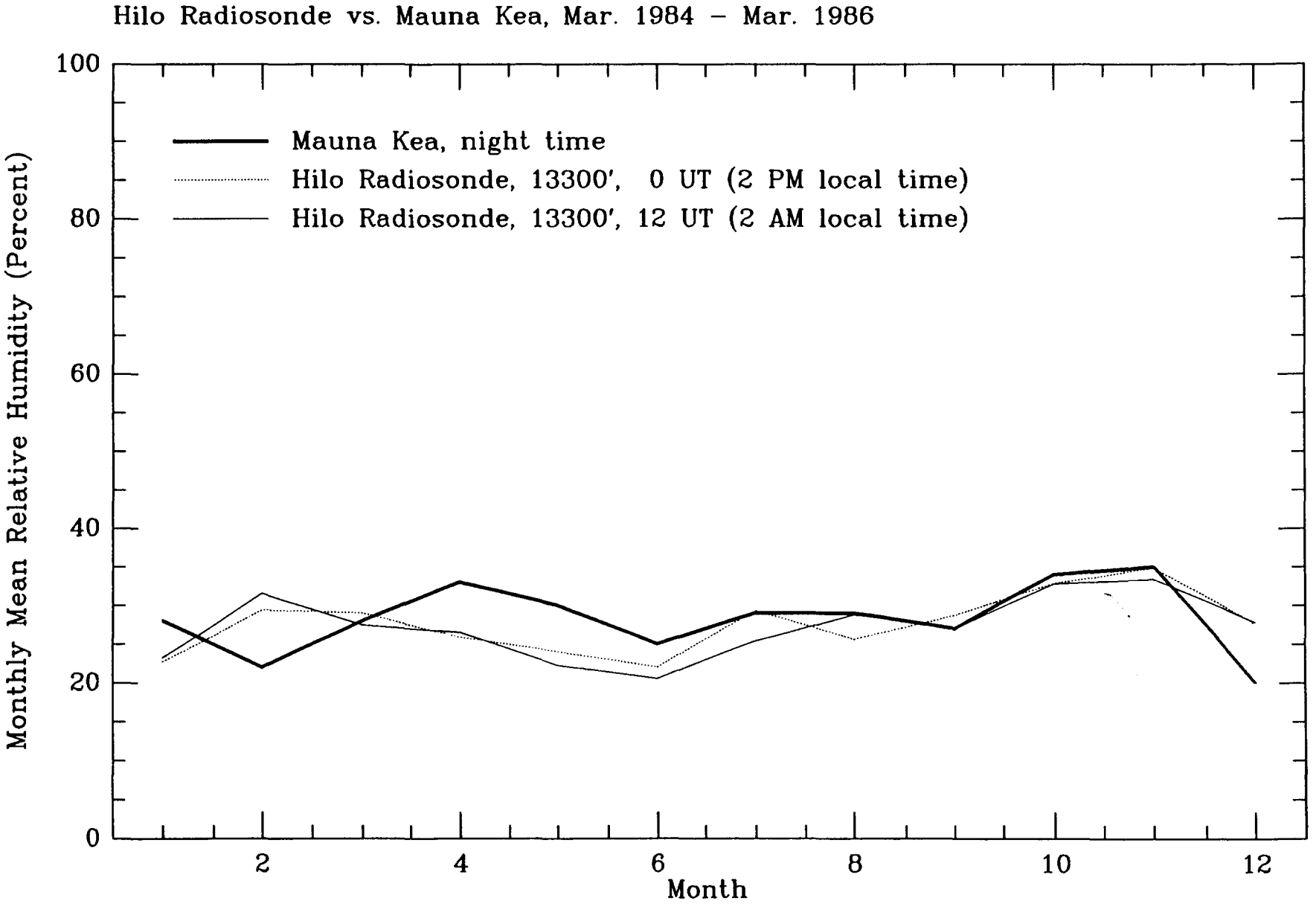

Figure 15(a-b). Comparison of radiosonde and local humidity measurements. Local humidity data from Merrill, *et al.* (1987) for March 1984 to March 1986. (a.) Hilo vs. Mauna Kea.

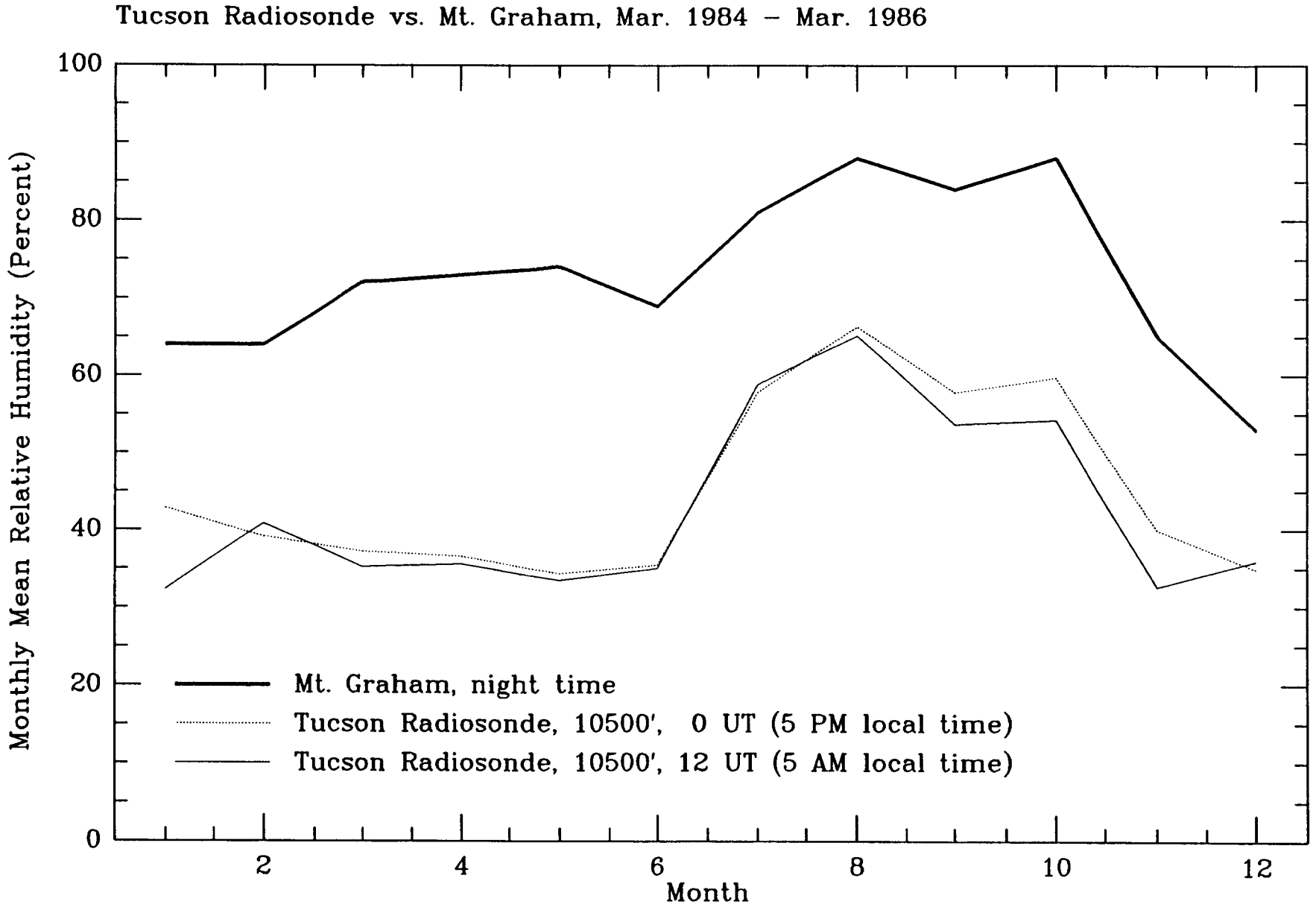

Figure 15(b). Tucson vs. Mt. Graham.

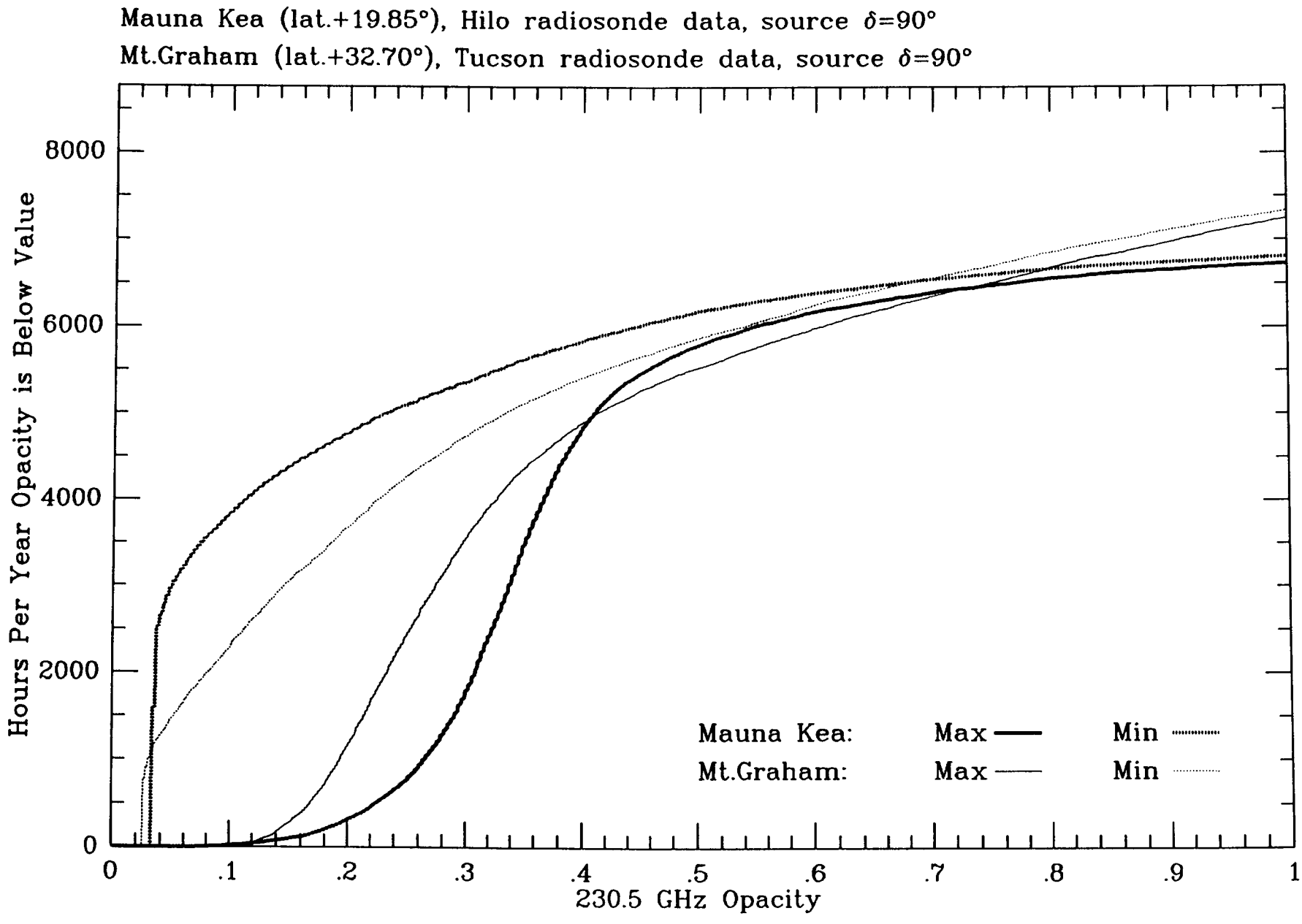

Figure 16(a-e). Effect of observatory latitude on cumulative distribution of opacities. Curves show hours per year opacity is less than value for a given source. (a.) For source at δ=90°.

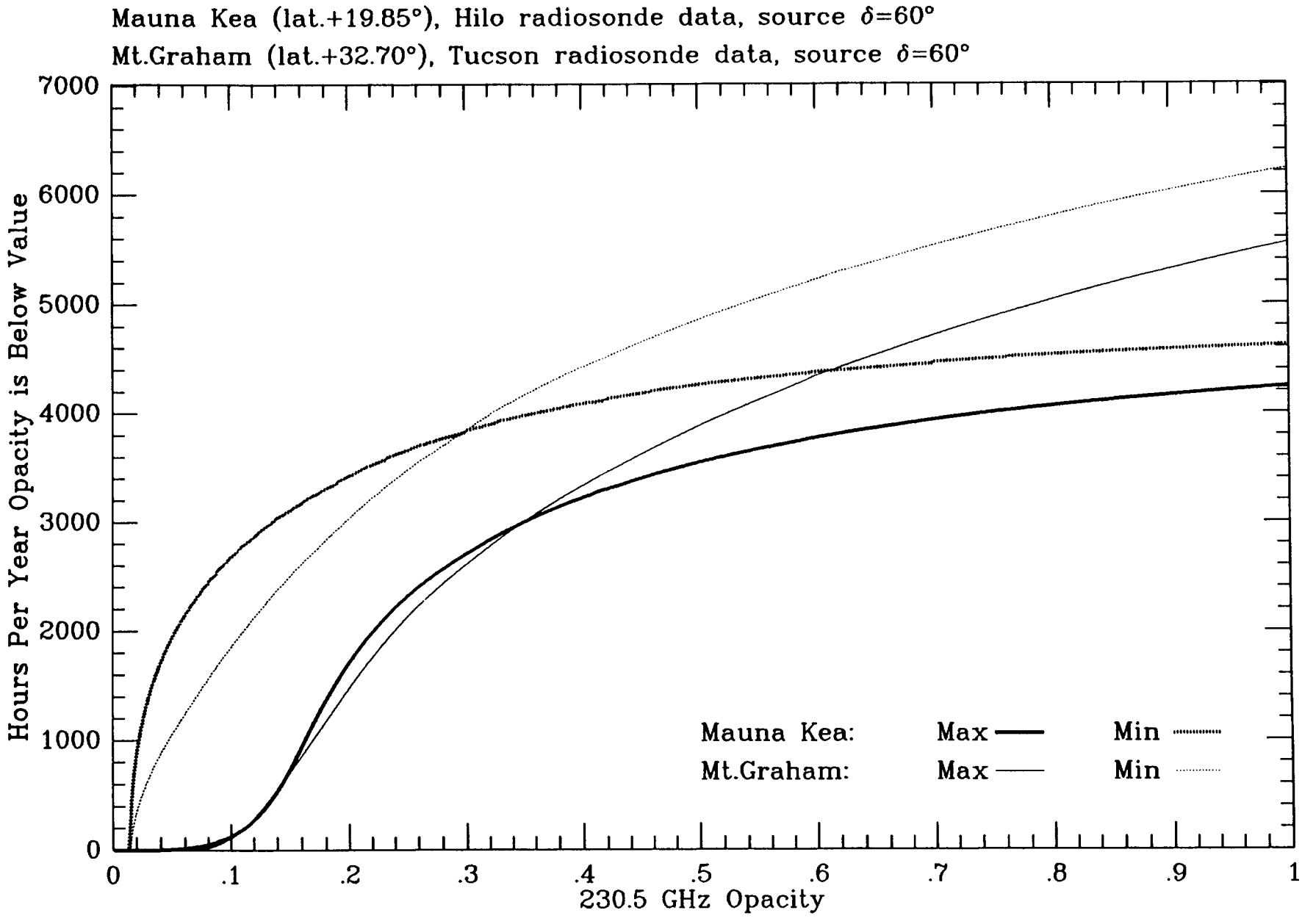

Figure 16(b). δ=60°.

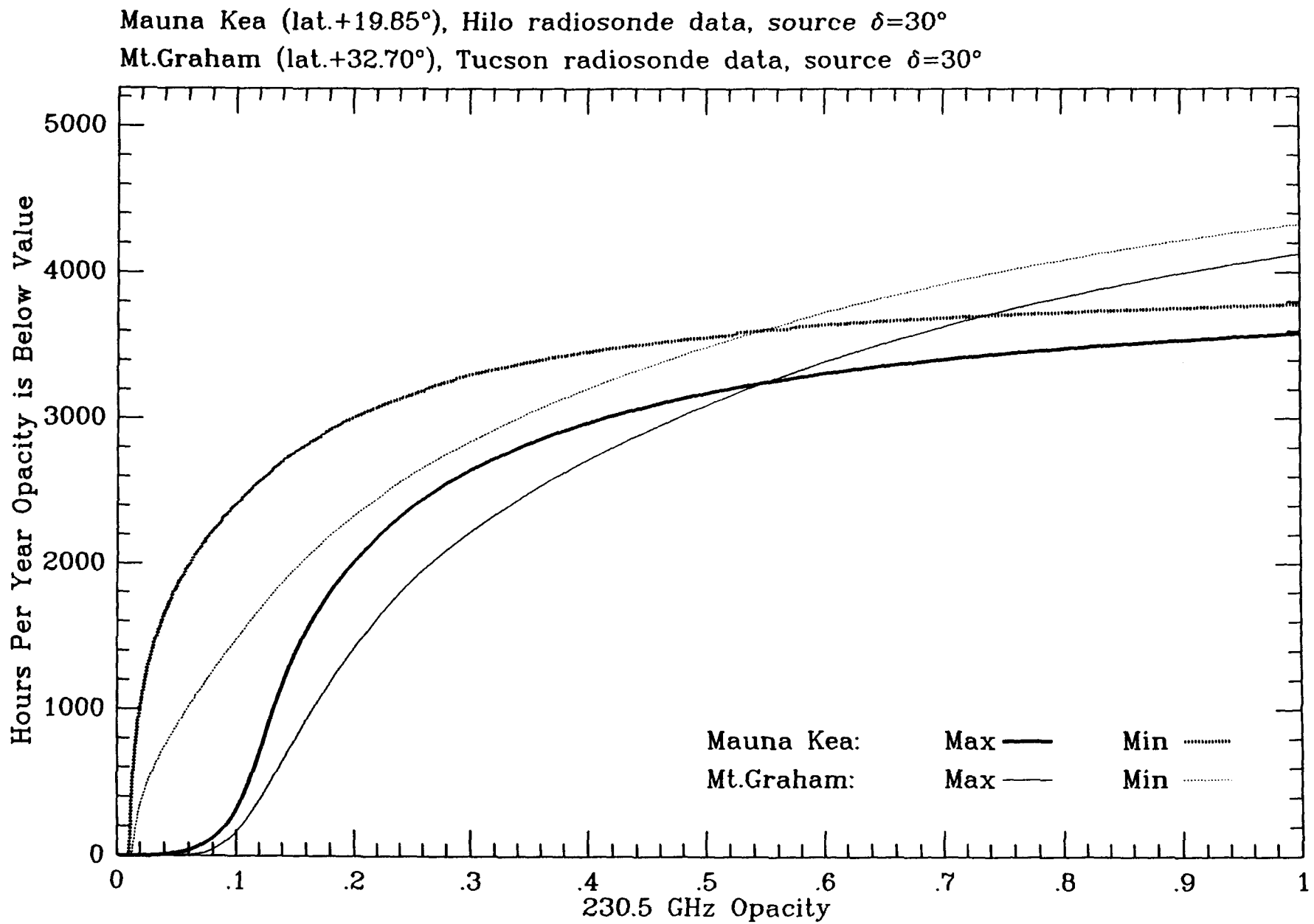

Figure 16(c). δ=30°.

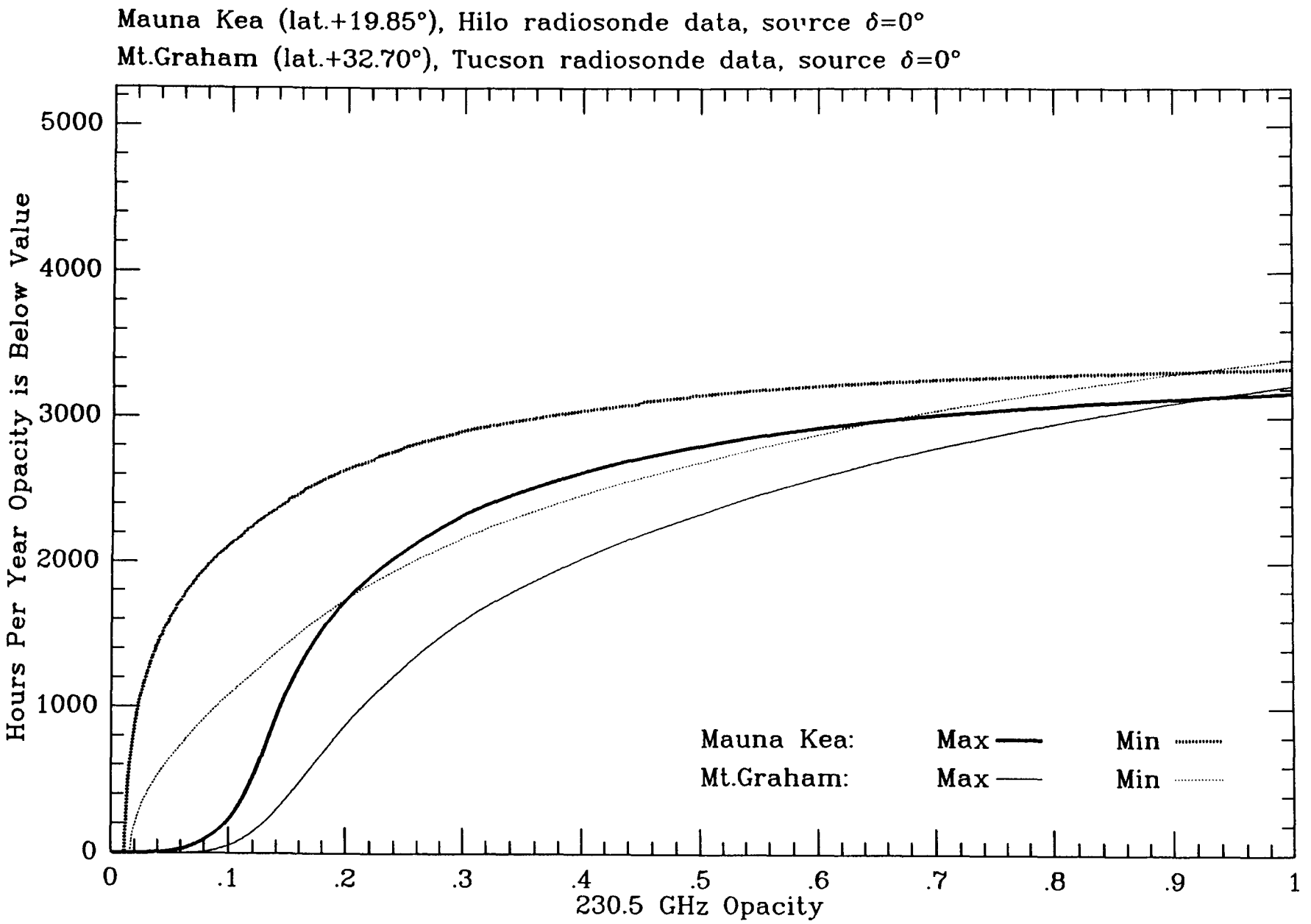

Figure 16(d). δ=0°.

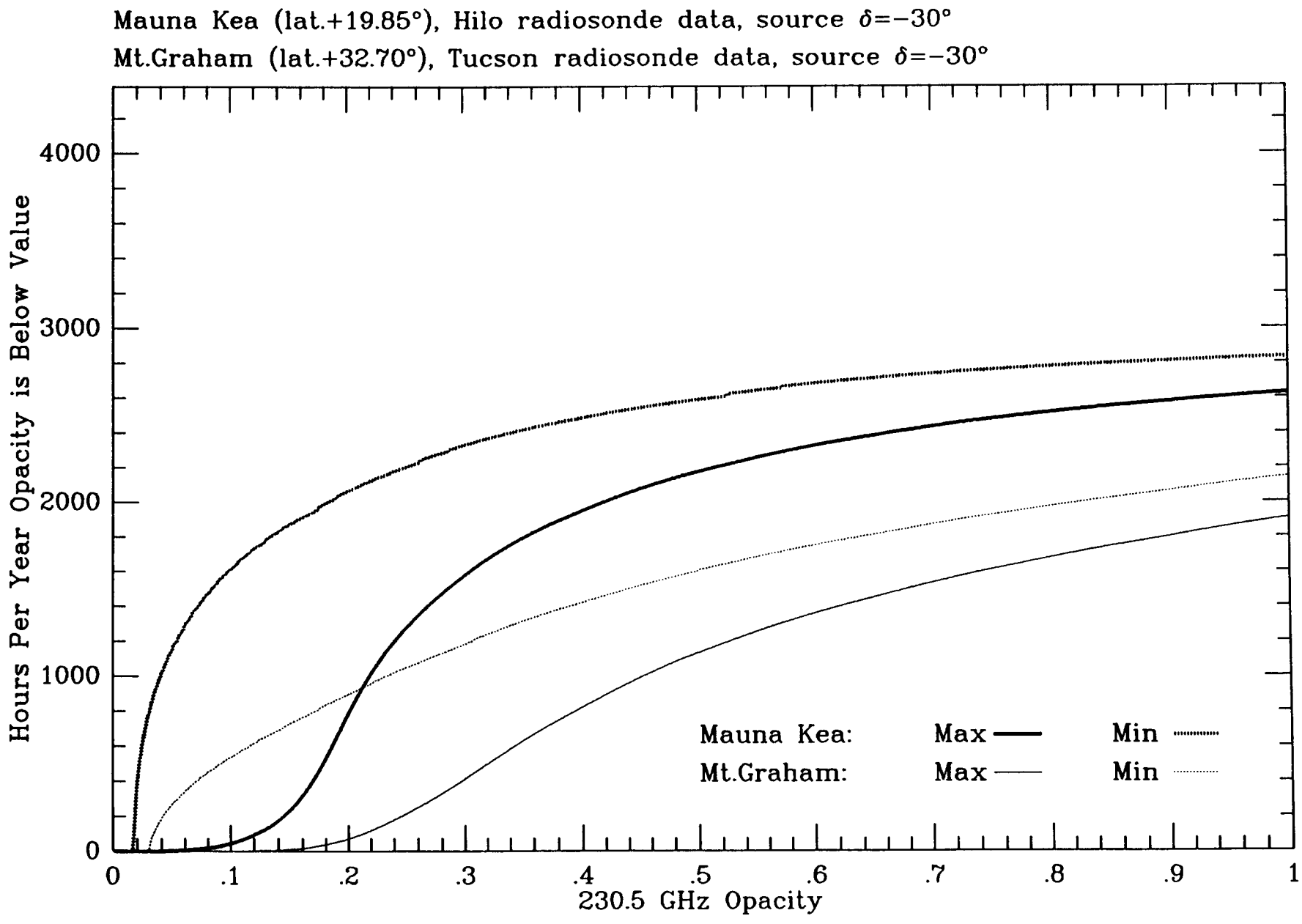

Figure 16(e). δ=-30°.

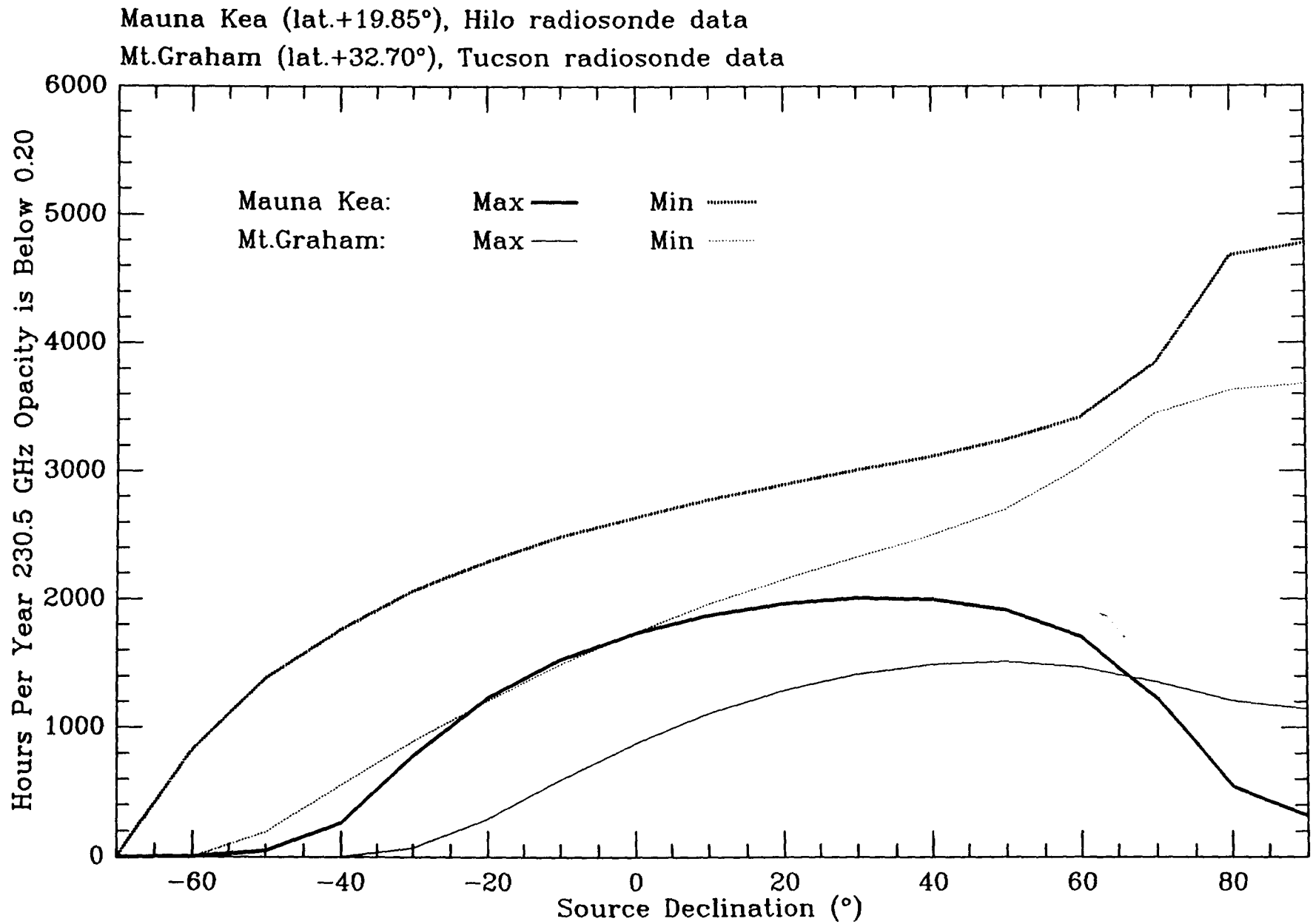

Figure 17(a-b). Effect of observatory latitude. Curves show hours per year opacity is less than value vs. source declination. (a.) For opacity <0.20.

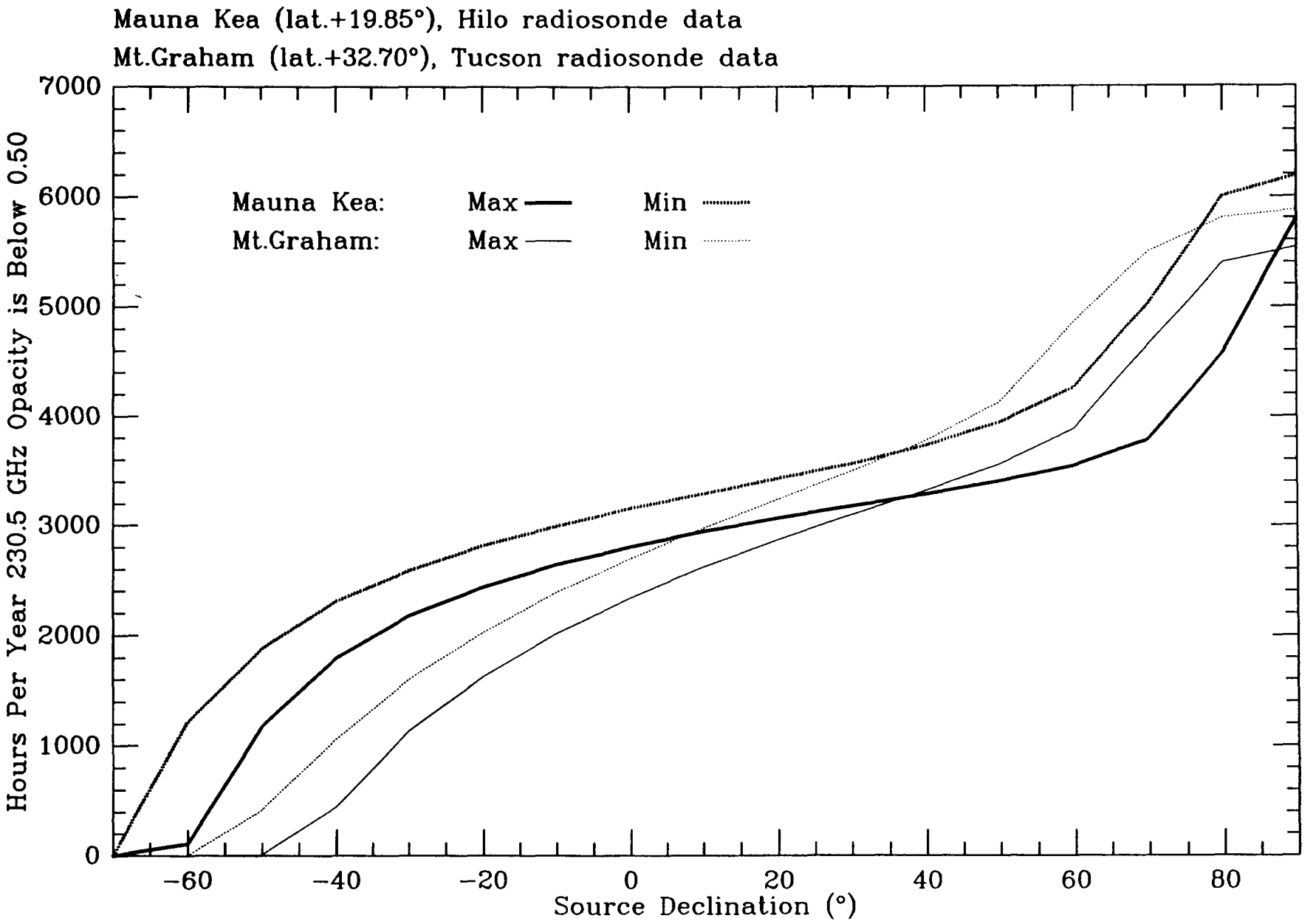

Figure 17(b). For opacity <0.50.

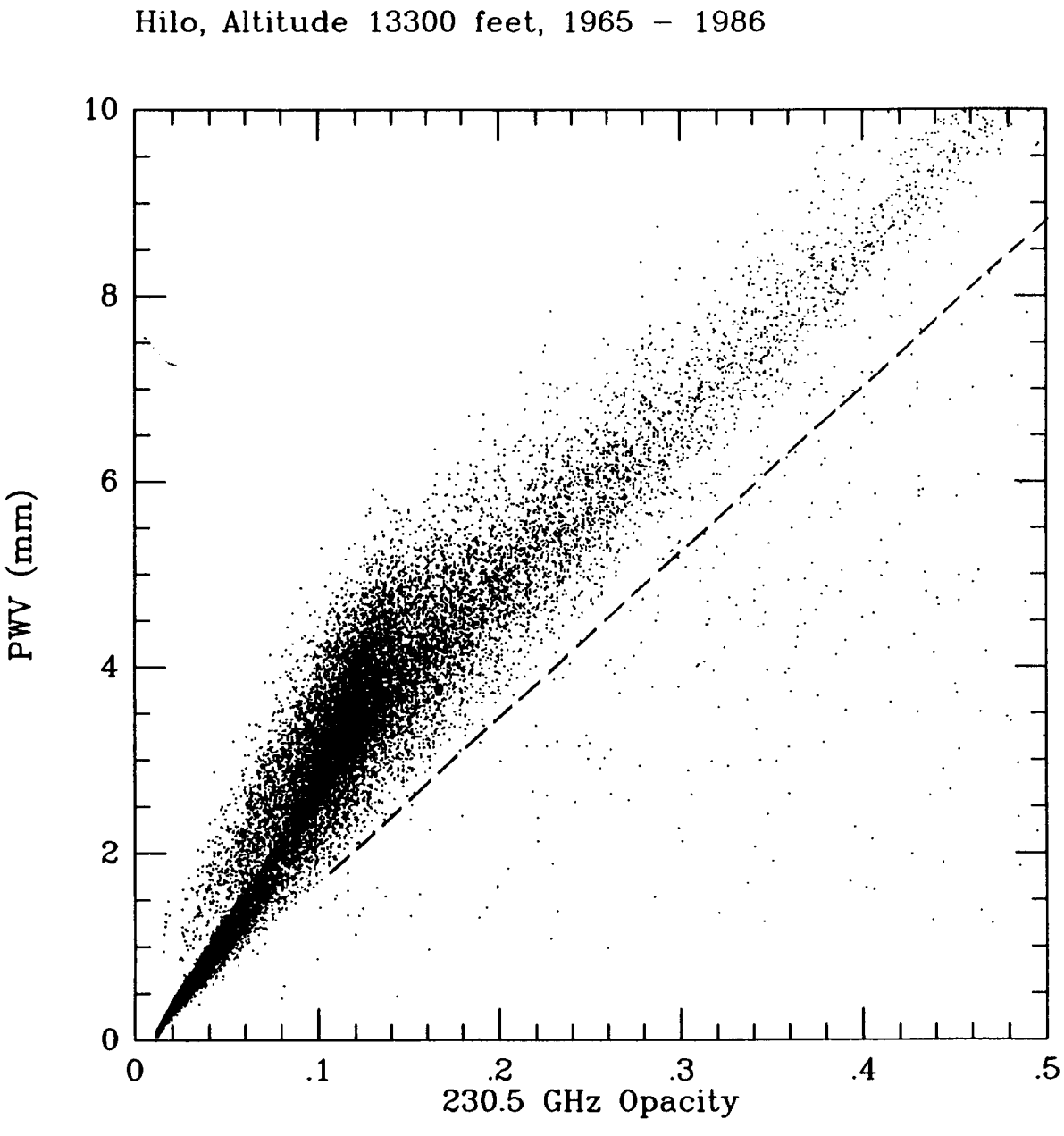

Figure 18(a). PWV (mm) vs. 230.5 GHz opacity. Dashed line gives empirical slope found by Zammit and Ade (1981) for PWV>4mm. Data for 1965 to 1986 used.

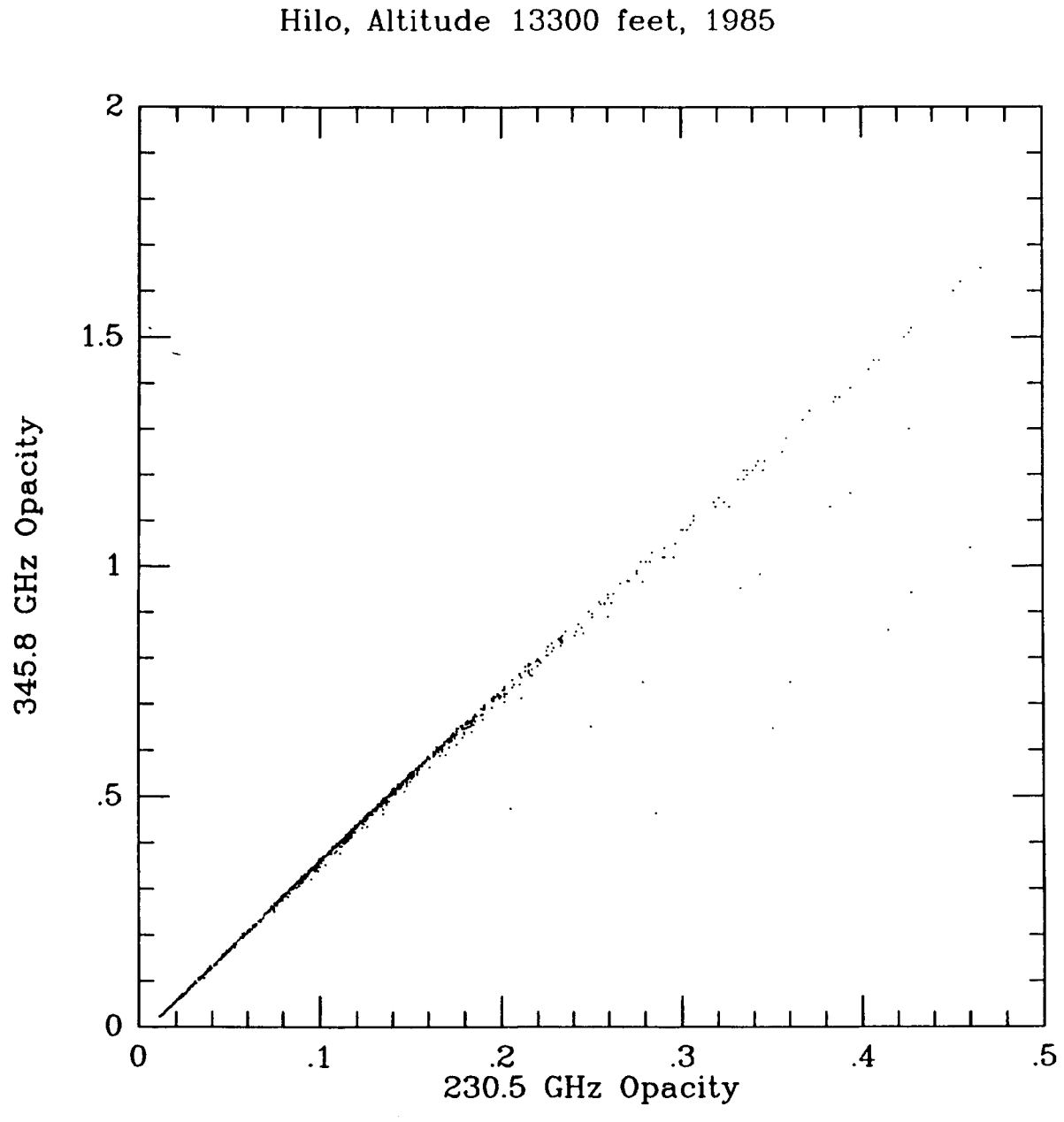

Figure 18(b-e). Opacity at specified frequency vs 230.5 GHz opacity. Data for 1985 only. (b.) 345.8 GHz vs. 230.5 GHz.

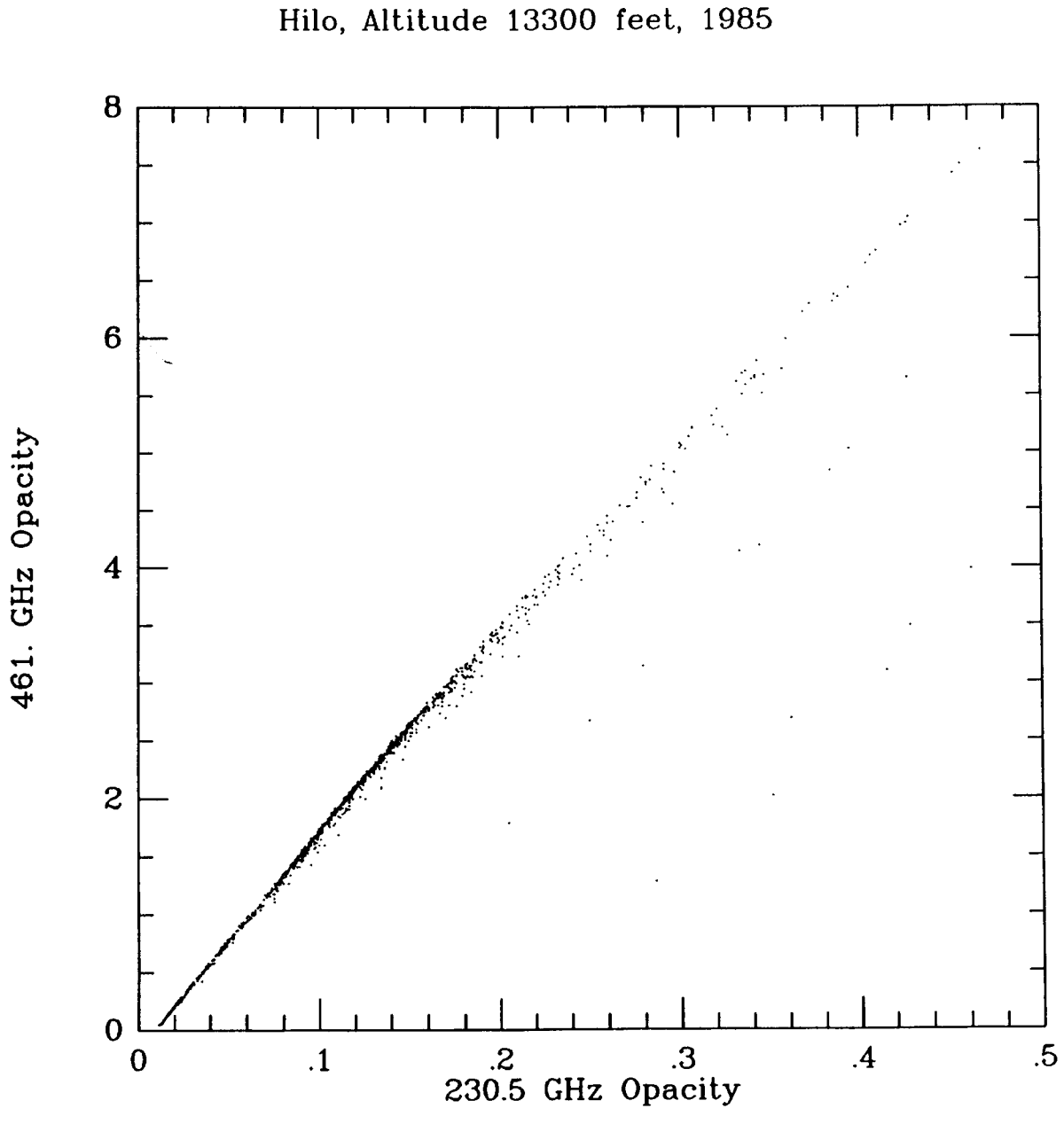

Figure 18(c). 461 GHz vs. 230.5 GHz.

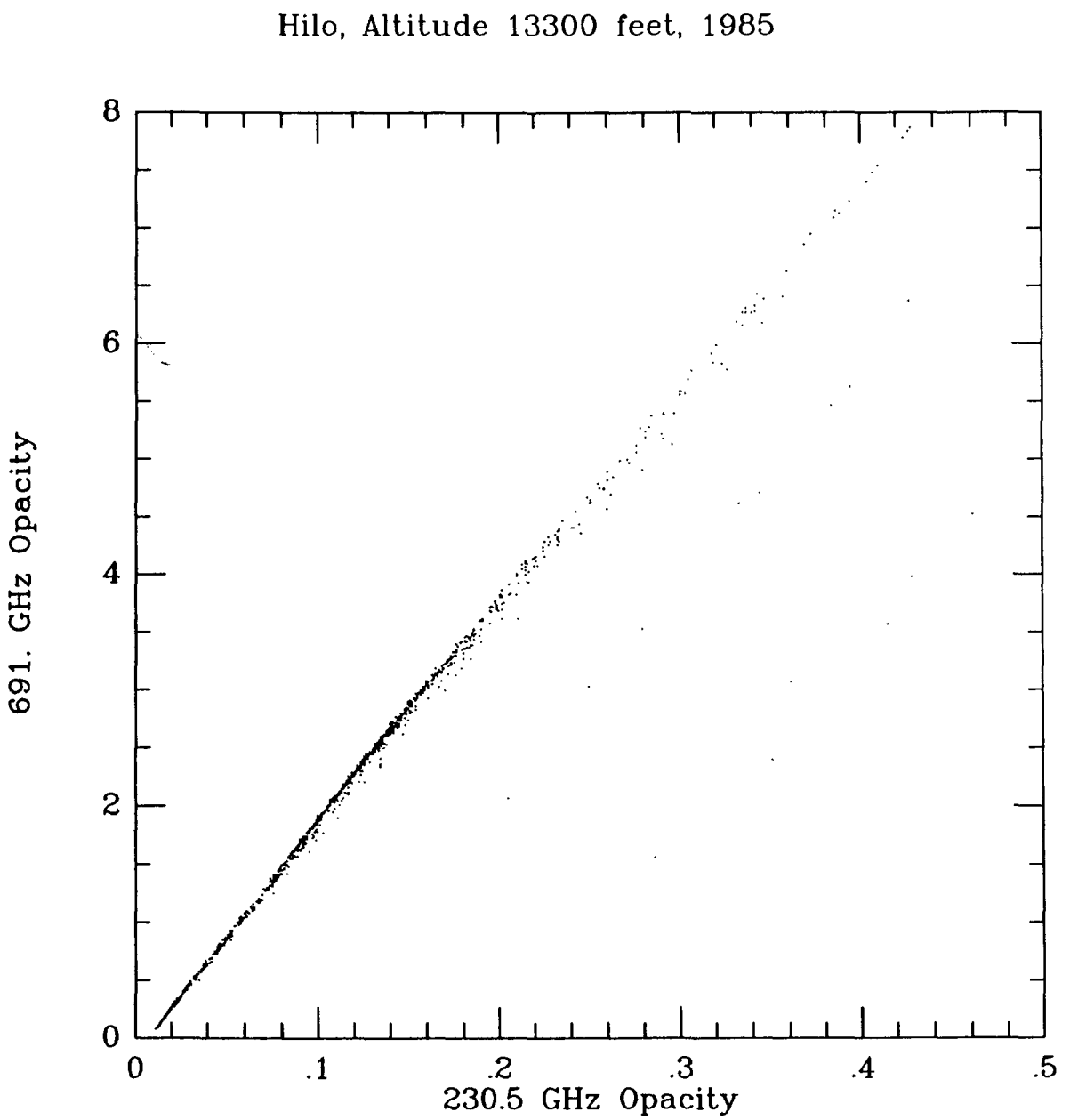

Figure 18(d). 691 GHz vs. 230.5 GHz.

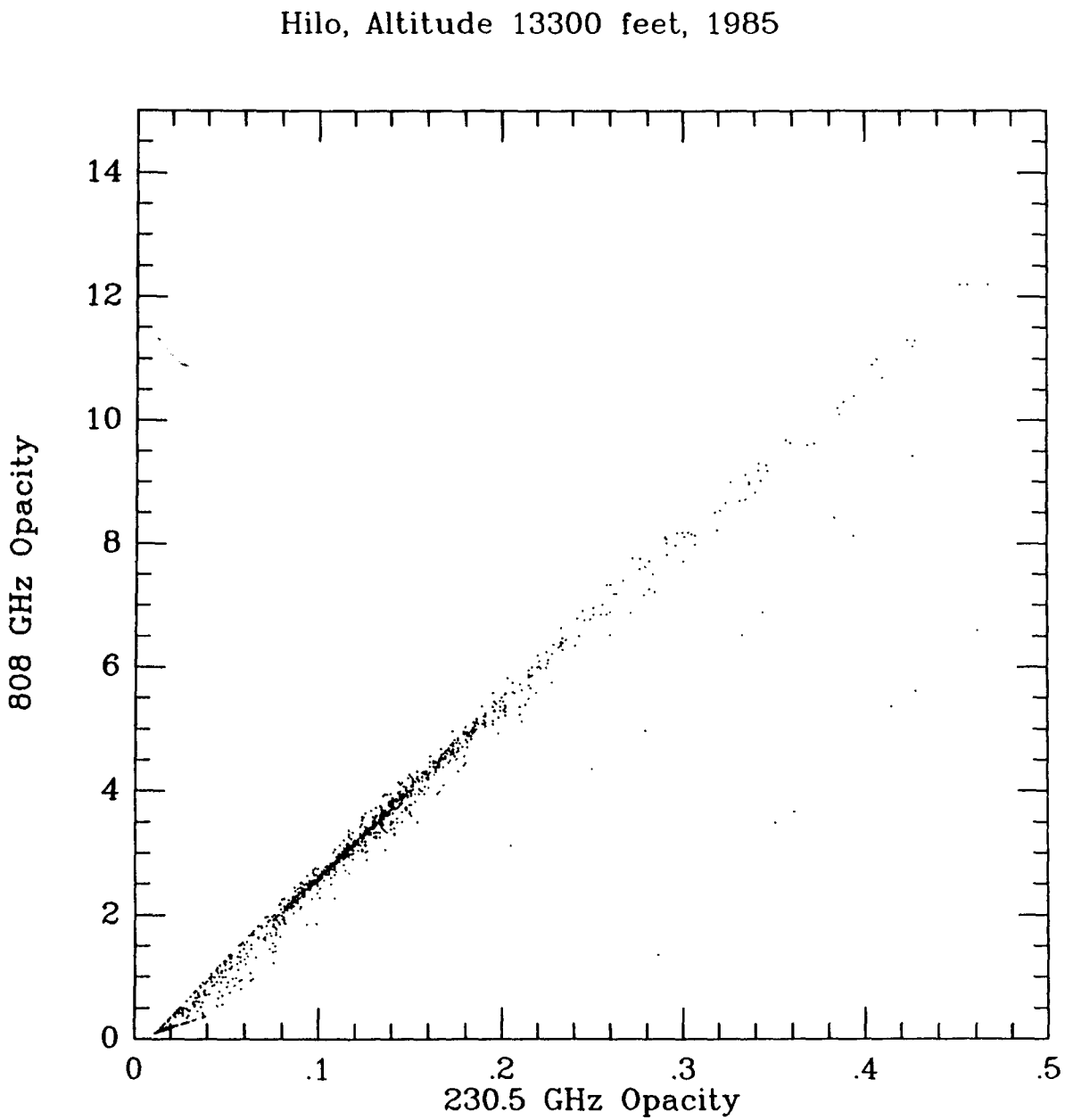

Figure 18(e). 808 GHz vs. 230.5 GHz.

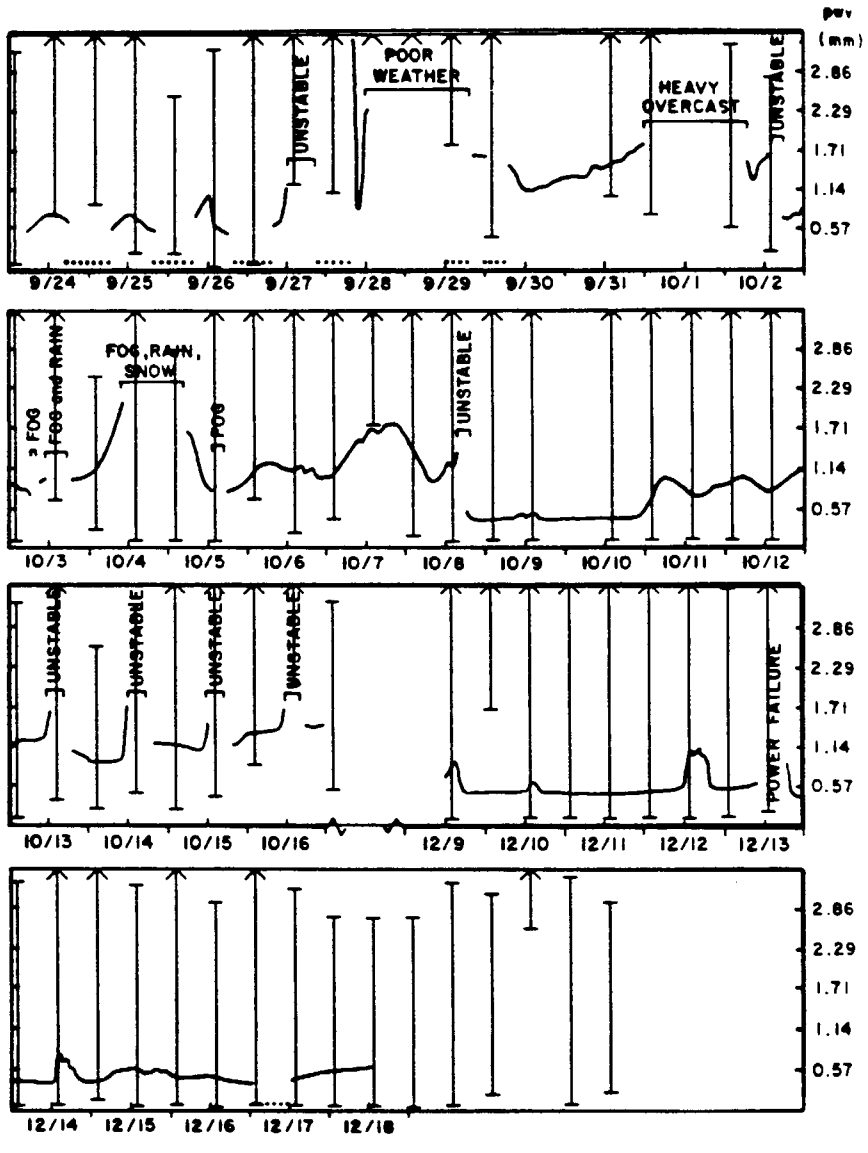

Figure 19. Comparison of Hilo radiosonde data and Mauna Kea 270 GHz radiometer data for 1982. Radiometer data shown by undulating line; radiosonde data shown by vertical bars at 12 hour spacing. Length of bars give range of PWV consistent with radiosonde; up arrows indicate values above top of plot. Month/day indicated along horizontal axis; upper tick marks at noon local time. Radiometer data from de Zafra, *et al.* (1983).

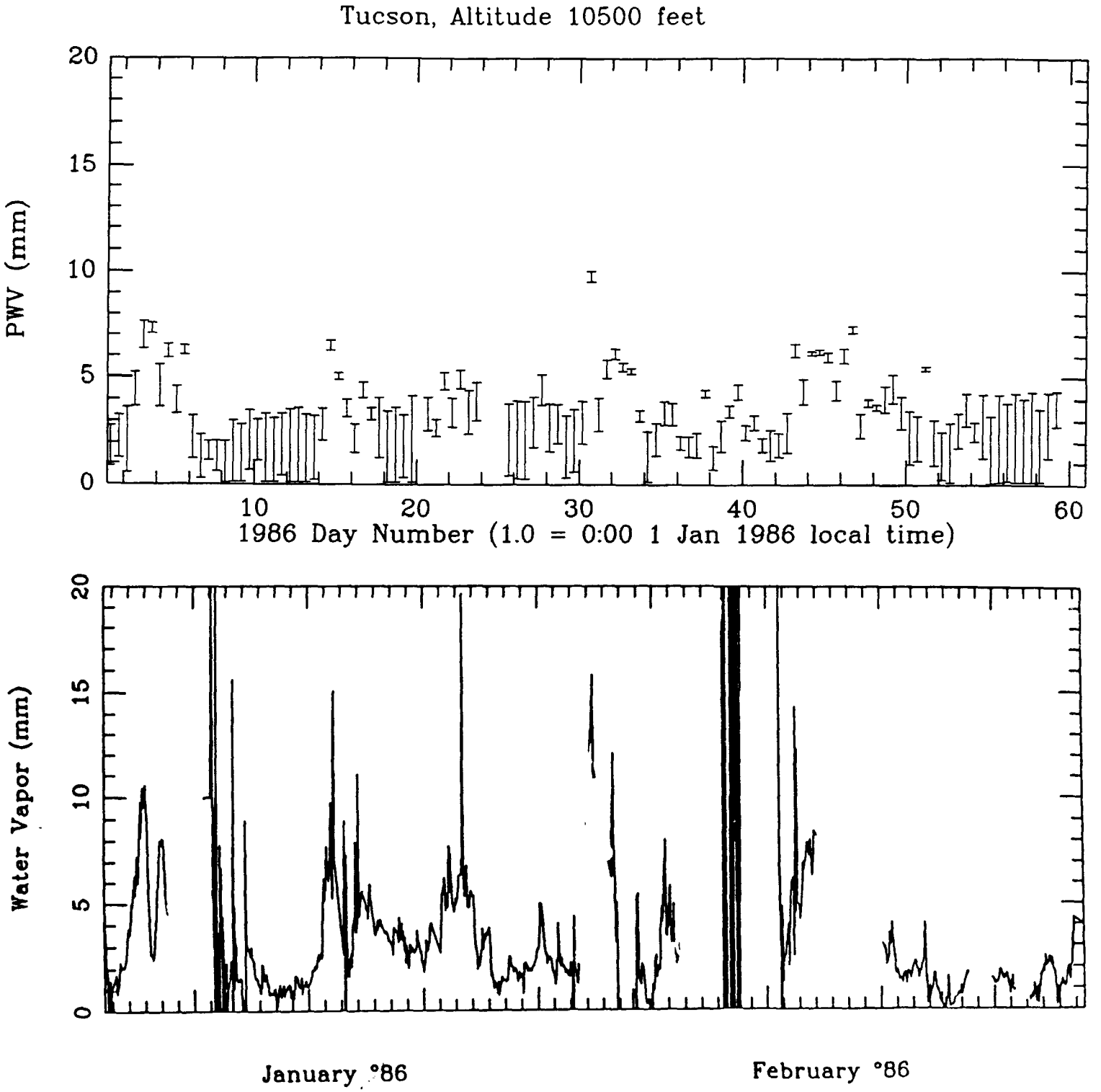

Figure 20(a-c). Comparison of Tucson radiosonde with Mt. Graham 22 GHz radiometer data. Undulating line shows radiometer data. Vertical bars with 12 hour spacing give radiosonde result; length of bar indicates range of PWV consistent with radiosonde. Radiometer data from R. Martin (private communication, 1989). (a.) Radiosonde upper panel; radiometer lower panel.

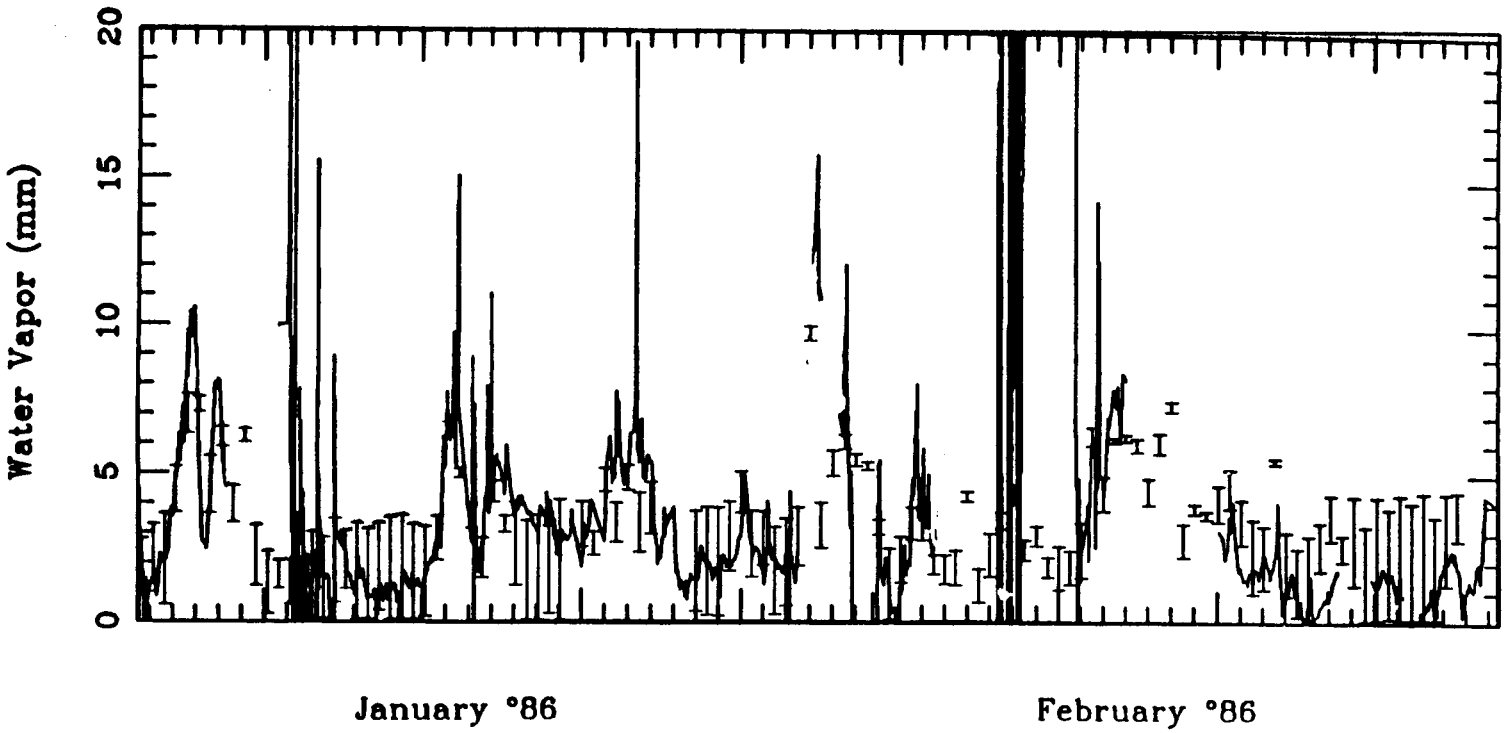

Figure 20(b). Plotted together. Tick marks at local noon.

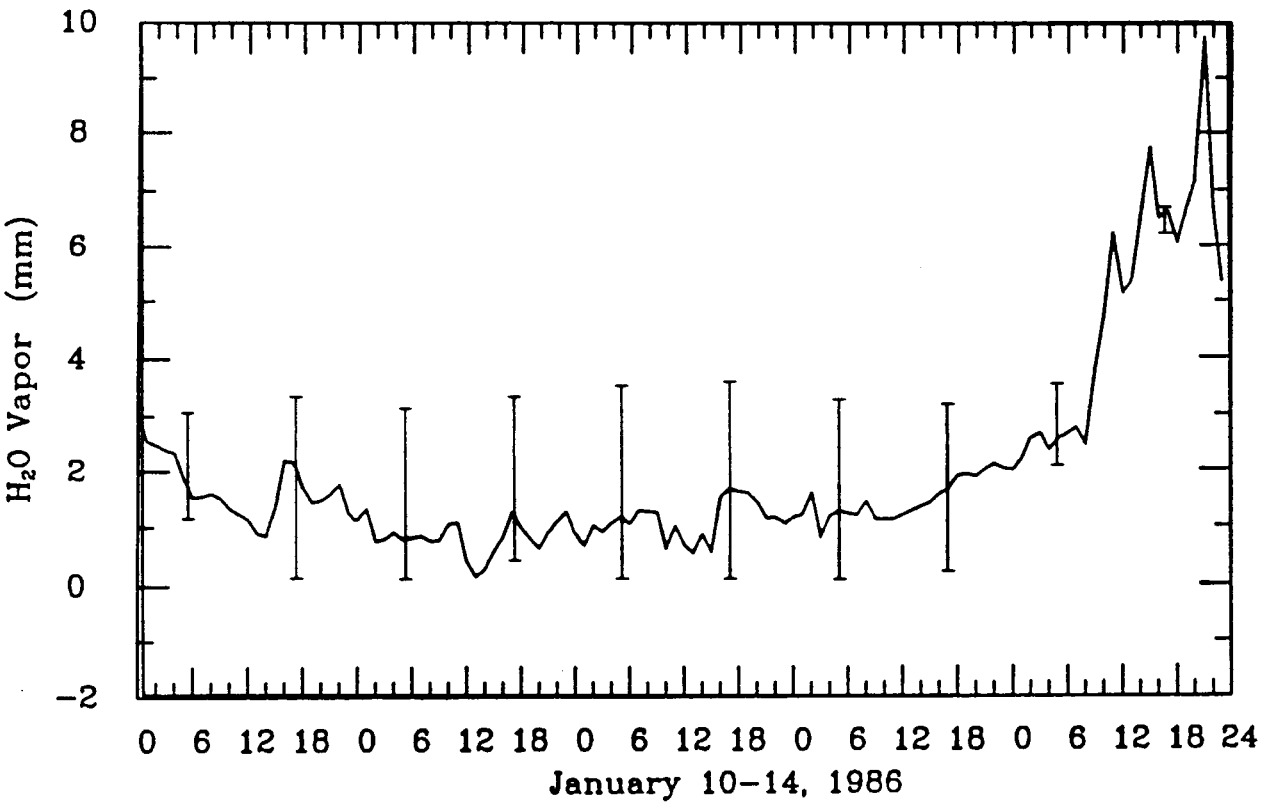

Figure 20(c). Detail.